EXPERIMENTAL AND NUMERICAL INVESTIGATION OF COAXIAL PRESSURE SWIRL INJECTORS

A THESIS SUBMITTED TO
THE GRADUATE SCHOOL OF NATURAL AND APPLIED SCIENCES
OF
MIDDLE EAST TECHNICAL UNIVERSITY

BY

ONUR BARAN

IN PARTIAL FULFILLMENT OF THE REQUIREMENTS
FOR
THE DEGREE OF MASTER OF SCIENCE
IN
AEROSPACE ENGINEERING

JUNE 2019

Approval of the thesis:

EXPERIMENTAL AND NUMERICAL INVESTIGATION OF COAXIAL PRESSURE SWIRL INJECTORS

submitted by **ONUR BARAN** in partial fulfillment of the requirements for the degree of **Master of Science in Aerospace Engineering Department, Middle East Technical University** by,

Prof. Dr. Halil Kalıpçılar
Dean, Graduate School of **Natural and Applied Sciences** _____

Prof. Dr. İsmail Hakkı Tuncer
Head of Department, **Aerospace Engineering** _____

Prof. Dr. Yusuf Özyörük
Supervisor, **Aerospace Engineering, METU** _____

Examining Committee Members:

Prof. Dr. Oğuz Uzol
Aerospace Engineering, METU _____

Prof. Dr. Yusuf Özyörük
Aerospace Engineering, METU _____

Assoc. Prof. Dr. Sinan Eyi
Aerospace Engineering, METU _____

Assist. Prof. Dr. Sıtkı Uslu
Mechanical Engineering, TOBB ETU _____

Assist. Prof. Dr. Mustafa Kaya
Aerospace Engineering, AYBU _____

Date: 11.06.2019

I hereby declare that all information in this document has been obtained and presented in accordance with academic rules and ethical conduct. I also declare that, as required by these rules and conduct, I have fully cited and referenced all material and results that are not original to this work.

Name, Surname: Onur Baran

Signature:

ABSTRACT

EXPERIMENTAL AND NUMERICAL INVESTIGATION OF COAXIAL PRESSURE SWIRL INJECTORS

BARAN, ONUR
Master of Science, Aerospace Engineering
Supervisor: Prof. Dr. Yusuf Özyörük

June 2019, 98 pages

Experimental and numerical investigations were carried out for determining spray characteristics of a liquid-liquid coaxial injector in this work. As a baseline injector, the RD-0110 rocket engine injector was chosen which consists of two coaxial atomizers. The inner atomizer is an open-end type pressure swirl atomizer which supplies oxidizer, whereas the outer one is a closed-end type pressure swirl atomizer which supplies fuel. Tests were carried out for two different recess lengths and various mass flow rates. A high-speed camera was used to determine the spray cone angles, while a phase Doppler particle analyzer (PDPA) was employed to characterize the distributions of various parameters. More specifically two-dimensional velocity profiles and Sauter mean diameters (SMD) were obtained for both inner atomizer and the coaxial injector, but PDPA measurements could not be performed for the outer one due to the high spray cone angle. Also, 2D axisymmetric swirl and 3D CFD analyses were carried out for the inner and outer atomizers at different mass flow rates. Experimental and numerical results are compared in detail. Results show that big spray droplets move with the same velocity as that of the liquid film, whereas small droplets move with the air. When the inner and outer atomizers operate together, their spray cone angles change from those observed from standalone operations. Spray cone angle of the outer atomizer decreases, while that for the inner one increases, but they later

merge at some point and forms a single spray. It was observed that the inner atomizer has more effect on this spray than the outer atomizer. Comparing the two different recess length reveals that recess length is significant parameter which affects spray properties. Lastly, comparing the experimental and numerical results proved that numerical analyses match well with test results. Therefore, numerical analyses can be used to find the velocity profile of the spray prior to detailed measurements.

Keywords: Coaxial Pressure Swirl Injector, PDPA, Pressure Swirl Atomizer, VOF

ÖZ

EŞ MERKEZLİ BASINÇLI GİRDAP ENJEKTÖRLERİN DENEYSEL VE SAYISAL OLARAK İNCELENMESİ

BARAN, ONUR
Yüksek Lisans, Havacılık ve Uzay Mühendisliği
Tez Danışmanı: Prof. Dr. Yusuf Özyörük

Haziran 2019, 98 sayfa

Bu çalışmada sıvı-sıvı tipi eş merkezli basınçlı girdap enjektörler deneysel ve sayısal olarak incelenmiştir. Temel enjektör geometrisi olarak, eş merkezli iki atomizörden oluşan RD-0110 motorunun enjektörü seçilmiştir. Bu enjektörü oluşturan iç atomizör oksitleyici sağlayan kapalı uçlu atomizer tipi iken, dış atomizör yakıt sağlayan açık uçlu atomizördür. Testler iki farklı girinti uzunluğunda ve farklı debilerde gerçekleştirilmiştir. Sprey açısı hızlı kamera yardımıyla ölçülmüştür. Spreyin, iki boyutlu hız profili ve Sauter ortalama çapları Faz Doppler parçacık analizcisi ile eş merkezli enjektör ve iç atomizör için elde edilmiştir. Ancak, Faz Doppler parçacık analizcisi ölçümleri dış atomizör için, dış atomizörün sprey açısının yüksek olması nedeniyle gerçekleştirilememiştir. Ölçümlere ek olarak, 2 boyutlu eksenel simetrik döngülü ve üç boyutlu sayısal analizler iç ve dış atomizörler için farklı debilerde gerçekleştirilmiştir. Deneysel ve sayısal sonuçlar detaylı olarak karşılaştırılmıştır. Sonuçlar spreydeki büyük parçacıkların sıvı filmi ile aynı hızda hareket ettiklerini, küçük taneciklerin ise havayla birlikte hareket ettiğini göstermiştir. İç ve dış atomizörler birlikte çalıştıklarında, sprey açılarının tek çalıştıkları duruma göre değiştiği gözlemlenmiştir. Birlikte çalıştıkları durumda dış atomizörün spray açısı azalırken, iç atomizörün artmış ve iki sprey bir noktada birleşerek tek bir sprey oluşturmuştur. İç atomizör, eş merkezli enjektörün spreyinin özeliklerinde dış

atomizörden daha fazla etkiye sahip olduğu tespit edilmiştir. İki farklı girinti uzunluğunun karşılaştırılması, girinti uzunluğunun spreyin özelliklerini etkileyen kritik bir parametre olduğu gözlemlenmiştir. Son olarak, deneysel ve sayısal sonuçların karşılaştırılması ile sayısal analizlerin, test sonuçlarına oldukça yakın sonuçlar verdiği görülmüştür. Bu nedenle, sayısal analizlerin, detaylı deneysel incelemeden sprey açısını belirleme ve spreyin hız profilini belirlemede kullanılabileceği görülmüştür.

Anahtar Kelimeler: Eşmerkezli Basınçlı Girdap Enjektör, Sprey Hızı, Sprey Tanecik Boyutu

To my family

ACKNOWLEDGMENTS

Firstly, I wish to express my deepest gratitude to my supervisor Prof. Dr. Yusuf Özyörük for his guidance, understanding, and insight throughout the research.

I would also like to thank to my thesis committee members, Prof. Dr. Oğuz Uzol, Assoc. Prof. Dr. Sinan Eyi, Assit. Prof. Dr. Sıtkı Uslu and Assit. Prof. Dr. Mustafa Kaya for their valuable comments on the research.

Furthermore, I am grateful to my fellow colleagues Berksu Erkal and Tolga Tokgöz for their precious help, and Dr. Bülent SÜMER, Chief of Propulsion Systems Division for his support on research. Also, I would like to thank my dear friends Ali Tevfik Büyükkoçak, Zeynep İdil Seçkin, Mehmet Anıl Eldemir, and Özgür Serin, who have motivated me with their most valuable friendship.

I cannot thank my beloved mother and father enough for their continuous support and encouragement through my life.

Finally, I would like to thank to my beloved Melike Aslı As for her understanding, support and love.

TABLE OF CONTENTS

LIST OF TABLES

TABLES

LIST OF FIGURES

FIGURES

CHAPTER 1

INTRODUCTION

Atomization is a breaking process of the bulk liquid into the smaller droplets. It is extensively used in many areas, such as combustion, coating, and medicine. To design an effective and efficient atomizer, one should understand the physics of the process. However, the atomization process is a highly complex phenomenon which involves multiphase flow, the break of the droplets, the interaction of droplets with the ambient gas as well as the interaction of droplets with each other.

Atomization is required in combustion applications to break up the propellants into the smaller droplets so that droplets participate in the chemical reaction with lower activation energy. In this research, atomization in the combustion chamber of a liquid rocket engine is the main area of interest and in liquid rocket engines atomization is provided through the devices called injectors.

Therefore, the spray characteristics of the injector have a significant impact on propulsion efficiency and combustion stability. Thus, to design a liquid rocket engine, spray characteristics of the injector needs to be examined first. To characterize the spray of the injector, numerous tests need to be performed, and these tests are expensive and time-consuming. A validated numerical model which can approximately estimates major properties of the spray such as cone angle, the pressure drop through the injector and velocity of the spray droplets would greatly help to reduce the number of required tests for designing or choosing appropriate injector for an application. For these reasons atomization process of coaxial pressure swirl injector was investigated numerically and experimentally, and then the results were compared in this study.

1.1. Background to the Research

Liquid rocket engines (LREs) are extensively used in missiles and launch vehicle systems because it has significant advantages over solid propellant rockets. Firstly, they have higher energy density than solid propellant rockets, and their thrust can be controlled. Moreover, unlike solid propellant rocket engines, they are reusable. These advantages make LREs preferable, especially in ballistic missiles and space launch applications [1] and coaxial pressure swirl injectors have been widely used in LREs for decades.

In LREs, oxidizer and fuel are stored at different tanks. They are fed into the combustion chamber by pumps. In the combustion chamber, oxidizer and fuel are mixed, and they chemically react. As a result of this chemical reaction, a great amount of exhaust gas is produced at high temperature and pressure. This high temperature and pressure exhaust gas are passed through a converging-diverging nozzle which accelerates the flow and creates the thrust. Schematic of LRE is showed in Figure 1.1.

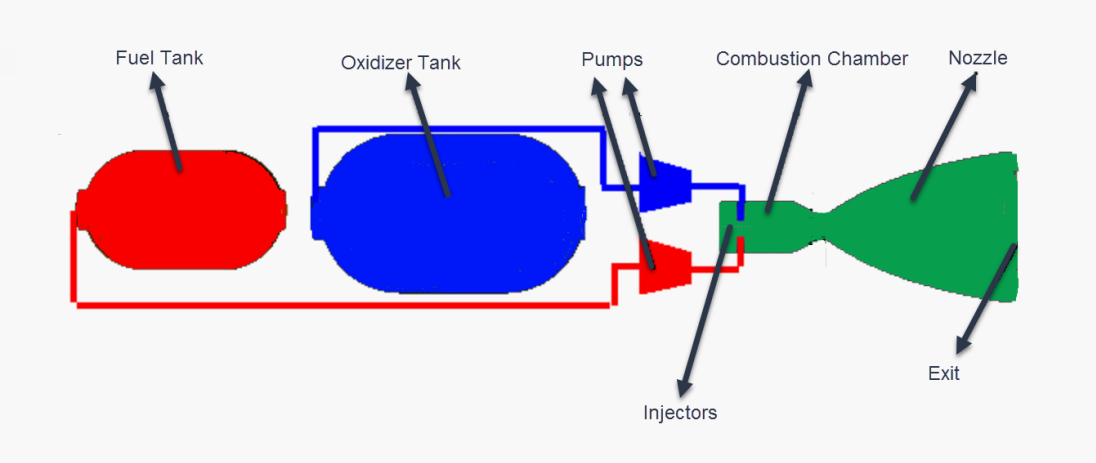

Figure 1.1: Schematic of LRE [2].

There are several types of LRE, and these types may contain some different components but most of the LREs composed of a combustion chamber, injectors, pumps, valves, fuel tanks, gas generator, and a nozzle. Among these components, the nozzle and the combustion chamber are the main ones.

The performance of LREs strongly depends on the properties of exhaust gas, and the exhaust gas properties strongly depend on the combustion process. Combustion takes place in a combustion chamber, and injectors were employed to atomize the oxidizer and the fuel. They are vital elements of the combustion chamber, which directly affect stability and the efficiency of combustion. Thus, designing a good injector is essential to develop high-performance LRE. Since poor injection design not only reduces the performance of LRE, it even may lead to a catastrophic failure of the engine due to acoustic instability [3].

To design a high-performance injector physics of the atomization needs to be examined. Atomization is a complex process, and so far, an analytical model could not be developed to define the process entirely.

Injectors must fulfill three main tasks in LREs [4]. Firstly, they have to provide fine spray atomization for both the fuel and the oxidizer. Secondly, they have to mix the fuel and the oxidizer rapidly. Finally, they should deliver propellants into the combustion chamber with minimum pressure losses at desired mass flow rates. Similarly, Lefebvre [5], stated that the high-performance injector should have a low response time to the changes in flow rates, it should be capable of creating uniform spray field over the wide range of fuel rates and it should be free of instabilities.

A variety of injectors are used in LREs such as shear coaxial, pressure injectors, pintle injectors, and impinging jets. Pressure injectors are widely used ones among these options because their simple design reduces weight and increases reliability [6]. Pressure swirl atomizers use pressure drop through the atomizer to convert liquid bulk into the droplets. During the process, a significant portion of the energy is spent on increasing droplet velocity instead of overcoming surface tension to forming droplets

and results with relatively low energy efficiency. However, despite the energy efficiencies of these devices, they are commonly used in LRE [7]. Coaxial pressure swirl injector is a type of pressure injectors, and Russian LREs RD-0110 and RD 170/180 were employed these type of injectors [8],[9]. Coaxial pressure swirl injectors were chosen for these engines by virtue of high-quality mixing and stability to combustion over a wide range of injection pressure and oxidizer/fuel ratio [10]. Moreover, they have the advantage of costing less than the other injectors owing to their simple geometry [11].

Coaxial pressure swirl injector is comprised of two concentric pressure swirl atomizers. The inner one is a closed-end type atomizer, while the outer one is an open-end type atomizer. The difference between tips of the atomizers is named as recess length and, it has a critical effect on the performance of the injector and generally. Possible recess configurations were shown in Figure 1.2.

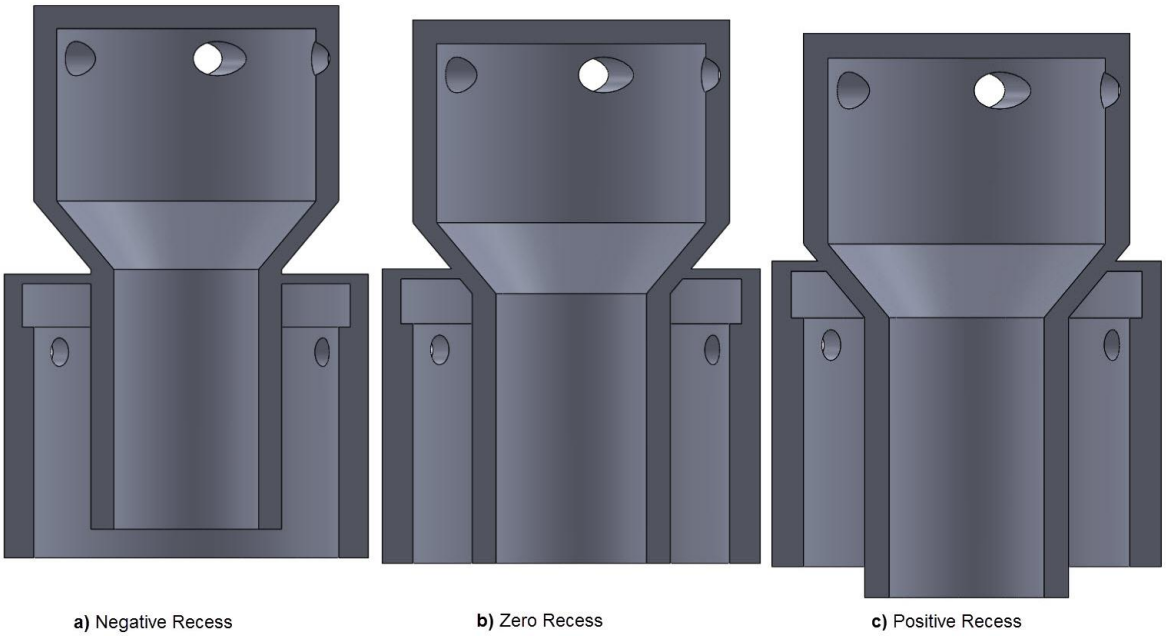

Figure 1.2: Different Recess Configurations.

Generally, the internal recess length configuration is used in coaxial injectors to increase atomization and mixing efficiencies [12]. Cross section sketch of coaxial pressure swirl injector with negative recess and, its comprising atomizers were shown in Figure 1.3.

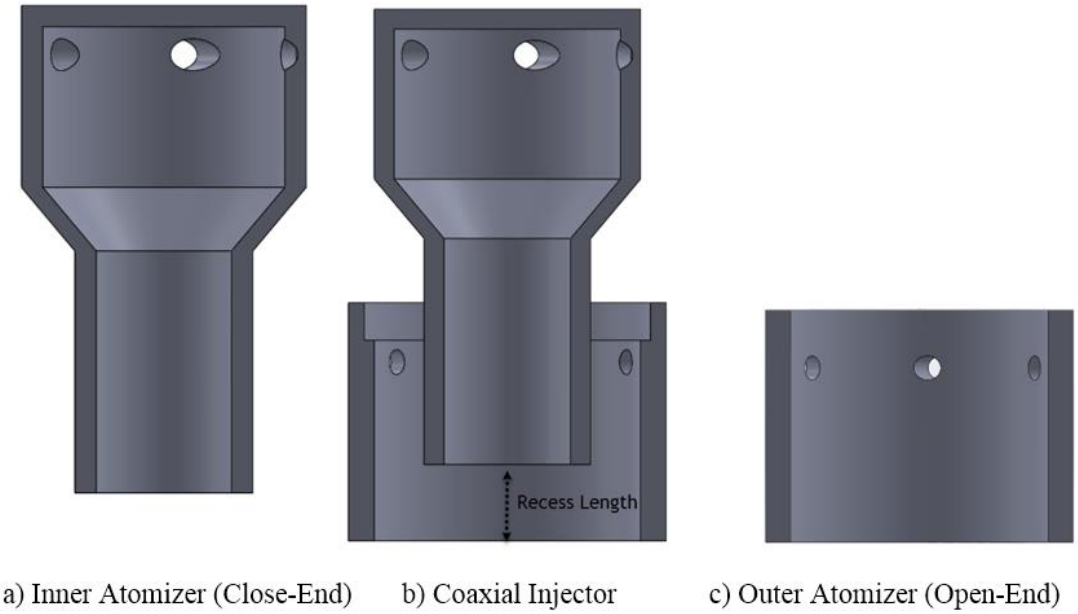

Figure 1.3: Coaxial Injector and Comprising Atomizers.

There are distinct advantages of using coaxial pressure swirl injectors in aerospace applications. Firstly, they reduce combustion instabilities. Secondly, they provide uniform mixing of oxidizer and fuel, which increases the combustion performance. Lastly, it reduces the required injector plate diameter since oxidizer and fuel are injected from the same injector [13]. Therefore, this study focused on coaxial pressure swirl injectors.

Coaxial pressure swirl injector can be divided into two main types. The first type is the gas-liquid pressure swirl injectors in which one propellant is in the gas phase while the other is in the liquid phase. The second type is the liquid-liquid pressure swirl

injectors in which two of the propellants are in the liquid phase. There are a vast number of researches in the literature on pressure swirl injectors whereas research on coaxial pressure swirl injectors, especially on the liquid-liquid ones are very limited, in this study the liquid-liquid type coaxial pressure swirl injectors were investigated.

Since the coaxial pressure swirl injectors were comprised of pressure swirl atomizers, atomization process in pressure swirl atomizers needs to be explained before moving on the coaxial injector atomization process.

The atomization process can be divided into three main parts as liquid film formation, primary atomization, and secondary atomization. In the atomization process in the pressure swirl atomizers, firstly, pressurized liquid enters the swirl chamber through the tangential inlets of the injector. Pressure decreases and the velocity of the flow increases in the tangential inlets. Thus, the flow goes out from tangential inlet to the swirl chamber with high velocity. Due to the positions of the tangential inlets, flow gains high angular velocity at the swirl chamber which forms a vortex. Because of the vortex, the velocity of the flow increases towards the center of the injector while pressure decreases. The pressure falls below the ambient pressure at the center of the atomizer and the ambient gas fills in from the nozzle, along the centerline of the injector, and forms a gas/air core and annular liquid film. The liquid film goes out of the atomizer nozzle and interacts with the surrounding gas, and it becomes unstable due to wave instabilities and getting thinner as it moves away from the atomizer exit. When the instabilities overcome the surface tension force, the liquid film spreads into ligaments, which is called primary breakup or primary atomization. Further down the flow, these ligaments breakup up into spray droplets and it is called secondary atomization. The exact physical explanation of the breakup has not been completely explained yet [14]. As a result of this process hollow cone spray forms. In hollow cone spray, most of the droplets present at the edges of the spray cone, as illustrated in Figure 1.4. The hollow cone pattern spray has smaller droplets in the narrow range [15].

Figure 1.4: Atomizer and Hollow Cone Spray.

The coaxial pressure swirl injector consists of two concentric pressure swirl atomizers. One of these atomizers supplies fuel while the other supplies oxidizer to the combustion chamber. Usually, the inner atomizer is used to supply oxidizer whereas outer atomizer is used to provide fuel. The inner atomizer is comprised of the swirl chamber (vortex chamber), the tangential inlets which deliver the propellant from oxidizer manifold to the swirl chamber and the discharge nozzle where the flow gets accelerated and leaves the injector [7]. The cross-section of the coaxial pressure swirl injector illustrated in Figure 1.5.

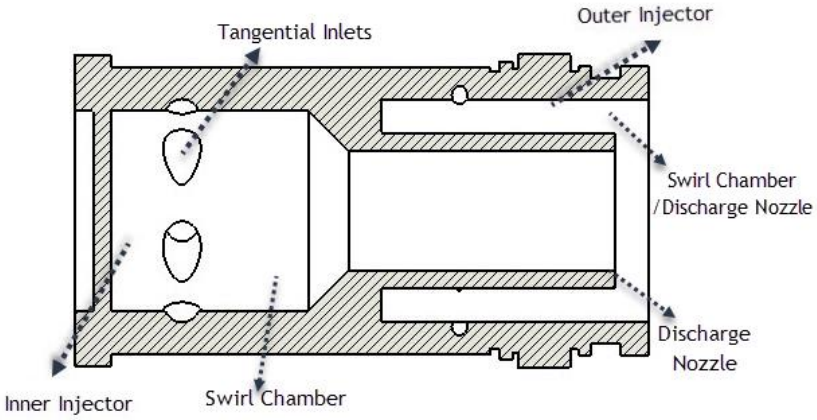

Figure 1.5: Cross section of Coaxial Pressure Swirl Injector [7].

Pressure swirl atomizers can be classified as open-end or close-end types. Close-end ones are typical pressure swirl atomizers which have swirl chamber with converging part and a discharge nozzle. However, open-end atomizers do not have separate swirl chamber and discharge nozzle. One-part works as both the swirl chamber and the discharge nozzle. In Figure 1.6, schematic of open-end pressure swirl atomizer was illustrated. D_s represents discharge nozzle and swirl chamber diameters, and their lengths were designated with L_s.

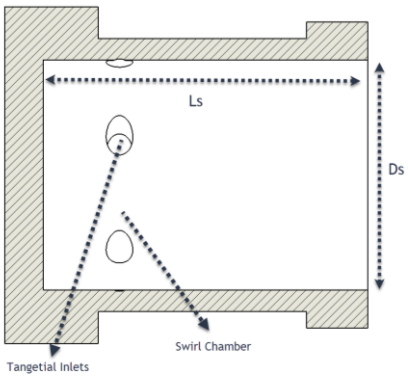

Figure 1.6: Schematic of Open-End Pressure Swirl Injector.

As in open-end type pressure swirl atomizer, the atomization process takes place similarly in the outer injector. High-pressure flow gets accelerated at tangential inlets, and the flow enters the swirl chamber with high velocity. The flow hits the wall of the swirl chamber with high velocity and moves to the outlet of the atomizer with swirling motion. Meanwhile, the pressure gets lower in the center of the atomizer due to the swirling movement. The pressure in the center axis of the atomizer becomes lower than the ambient pressure, and the ambient medium fills into the atomizer. The liquid flow comes out of the discharge nozzle and forms a conical sheet due to centrifugal force. The liquid sheet gets thinner as it moves in the ambient gas due to instabilities. These instabilities overcome surface tension force at some point, and then the liquid film spreads into ligaments, further down the ligaments breaks up into droplets.

Both atomizers form a uniform, and hollow cone shape sprays individually. When they operate as parts of the coaxial injector the resulting spray of inner and outer atomizers mix with each other. Mixing position and properties strongly depend on the recess length. In the coaxial pressure swirl injector, a swirling flow can be generated on one or both of the propellants. For the RD-0110 injector, both of the atomizers generate swirling flow. Swirling flow comes out of the atomizers nozzles forms conical sheets, and these conical sheets impinge with each other and forms a single conical sheet. Then, further the downstream of flow, the conical sheet gets thinner due to instabilities. As the instabilities overcome the surface forces, atomization takes place and droplets form. This process is illustrated in Figure 1.7.

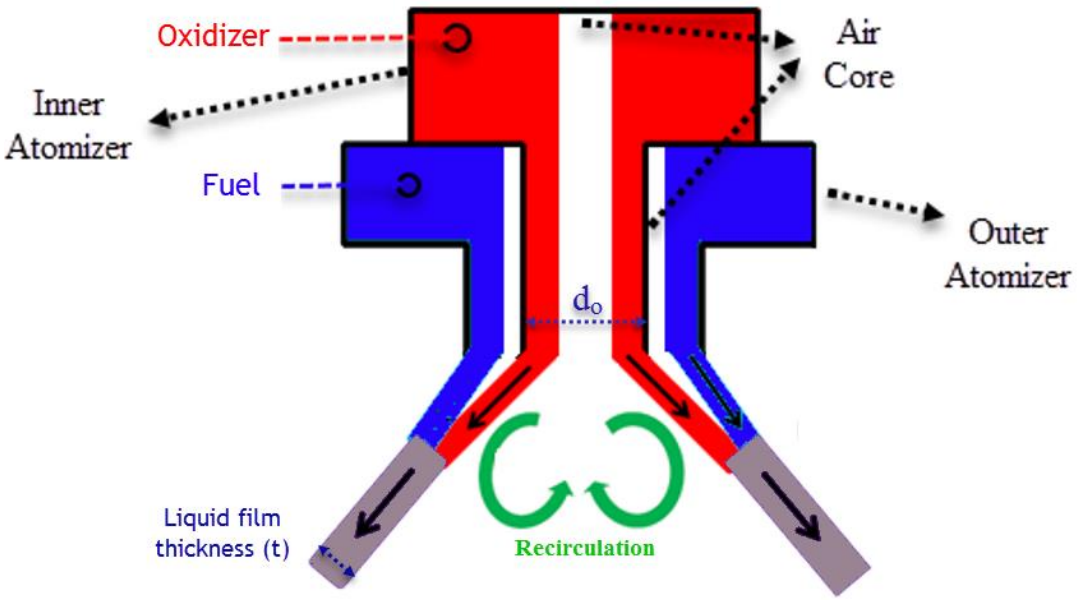

Figure 1.7: Diagram of Coaxial Pressure Swirl Injector [16].

The spray pattern of the pressure swirl atomizer is in the shape of a hollow cone which the droplets of the spray form a ringlike pattern, and there are very few droplets inside

the radius as illustrated by Figure 1.4. Cross section of the hollow cone spray and its cone angle was shown in Figure 1.8.

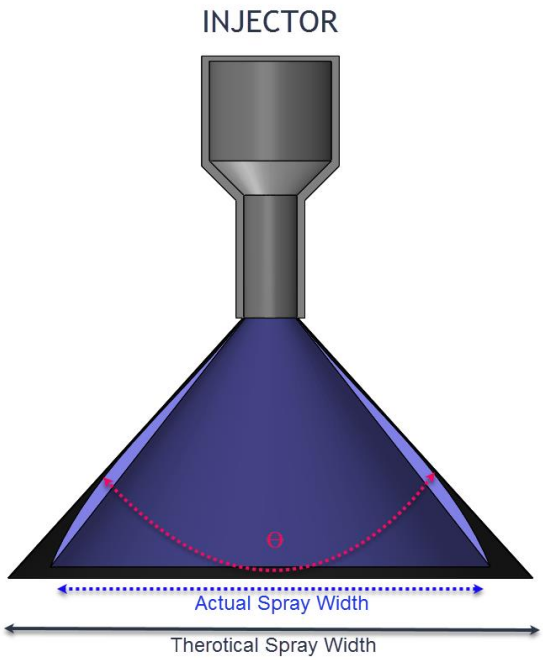

Figure 1.8: Spray Cone Angle.

Actual and theoretical spray patterns and so their widths are different due to the effect of the gravity, they are quite close at the near the nozzle exit, but while the spray moves away from the exit, it becomes slightly curved due to the effect of gravity in the actual case. Therefore, there is a small difference between the theoretical and actual spray cone angle. The spray cone angle is a significant property of a spray, and it should be considered along with the atomization performance of the injector in the design process [17].

1.2. Literature Survey

Previous studies presented in literature was summarized in this section. Along with the coaxial pressure swirl injector research, studies for the pressure swirl atomizer was also reviewed.

Since injectors are employed in a wide range of applications from combustion sprays to agricultural sprays, there are many studies on them in the literature. Spray properties of the injectors are the main interest point in researches. To define the spray properties numbers such as Weber and Sauter mean diameter (SMD) are frequently utilized. Weber number is a dimensionless number, and it is very useful to analyze fluid flows especially, when there is an interface between two different fluids. It is commonly used in literature to analyze the formation of droplets. Weber number was represented as follows;

$$We = \frac{\rho U_0^2 l}{\sigma} \qquad 1.1$$

Where ρ is the density of the fluid and l is the characteristic length (in this case it is the diameter of the droplet), U_0 is the relative velocity between the liquid and air and σ is the surface tension.

Sauter mean diameter (SMD) which is also named as volume-surface mean diameter is frequently used in spray characterization. Briefly, SMD is a representation of spherical objects in various diameters with an average diameter value [18]. It is a highly beneficial statistical method commonly used in the combustion area. SMD is explained in detail along with the other statistical methods used in section 2.3.1.

Discharge coefficient is another nondimensional number that used to define properties of the injectors. It is the ratio of theoretical discharge to real discharge. It indicates the required inlet pressure of the injector for the desired mass flow rate [19]. Discharge coefficient is a function of a passage area (A), mass flow rate ($\dot{m}$), density, and the pressure drop (ΔP) as represented in equation 1.2.

$$C_d = \frac{\dot{m}}{A\sqrt{2.\Delta P.\rho}} \quad 1.2$$

Many studies have been carried out to understand and model flow within the injectors. Almost all of these models, there are three main assumptions [20]. First, the flow is assumed incompressible and inviscid. Second, angular momentum is assumed as constant. Third, gravity and surface effects are neglected. Based on these assumptions the velocity of the spray is obtained as below:

$$V_{tot} = \sqrt{\frac{2\Delta P}{\rho}} \quad 1.3$$

$$V_{tot} = \sqrt{V_{tan}^2 + V_{axial+}^2 V_{rad}^2} \quad 1.4$$

The radial velocity component V_{rad} is ignored and the equation becomes:

$$V_{tot} = \sqrt{V_{tan}^2 + V_{axial}^2} \quad 1.5$$

$$rV_{tan} = c \quad 1.6$$

From tangential inlets to any point in the injector, tangential velocity is calculated as:

$$V_{in}R_{in} = rV_{tan} \quad 1.7$$

Also, Schmidt et al. [21] developed a model to make a connection between an internal injector and external spray. Their model mainly depends on observable external spray characteristic rather than the internal properties of the injector. To use this model, mass flow rate, pressure drop, and spray cone angle must be measured experimentally.

In this model, liquid film thickness (t) which is a crucial input parameter for any swirl spray atomization models, was calculated from exit velocity at the injector tip as in equation 1.8:

$$\dot{m} = \pi\rho ut(d_o - t) \quad 1.8$$

In the equation 1.8, mass flow rate ($\dot{m}$) and the injector exit diameter (d_o) are assumed to be known from experiment, and axial velocity at injector exit (u) is found using equation 1.9 and equation 1.10.

$$U = c\sqrt{\frac{2\Delta P}{\rho_l}} \quad 1.9$$

Velocity coefficient (c) is taken as 0.7 with an estimation and total velocity is found using equation 1.9.

$$U = ucos(\theta) \quad 1.10$$

Since the spray cone angle is known, axial velocity can be obtained from equation 1.10, and then the liquid film thickness can be found by using equation 1.8.

Atomizer models can be a useful tool to calculate main spray properties like spray cone angle, liquid film thickness, and the velocity of droplets. However, there is no analytical model to find spray properties of injectors in the literature due to the complex nature of atomization and empirical relations are generally case specific. So, using these relations can only give a rough forecast to injector designer. With the increase of computing power and development in experimental techniques, carrying

out CFD analysis and conducting experiments is a more reasonable option to investigate spray properties of the injectors. For these reasons, many experimental studies have been carried out on pressure atomizers and coaxial pressure swirl injectors.

Studies on closed-end type pressure swirl atomizers are prevalent. However, for the open types, there are few studies. Chen et al. [22] inspected the spray characteristic of an open-end type pressure swirl atomizer at various ambient pressure with different geometrical configurations by high-speed shadowgraphy technique. They carried out cold flow tests by changing the tangential inlet diameter and swirl chamber (discharge nozzle) length and the injection pressure with various ambient pressure. They concluded that with increasing ambient pressure, spray cone angle, and discharge coefficient decrease. And increasing tangential diameter leads to a reduction in spray cone angle and increase in discharge coefficient. Whereas, increasing discharge nozzle length leads to a decrease in spray cone angle and increase in discharge coefficient. Another research on open-end type pressure swirl atomizer was carried out by Fu [23]. He studied the effect of ambient pressure on the internal flow of open-end swirl injector. He performed the analysis from 1 to 100 bar, and he concluded that the velocity distribution rarely varies with ambient pressure. Based on his work, it can be concluded that although injectors typically operate at higher pressures than ambient pressure, the measured velocity distribution of injectors at ambient condition can be used for initial data for combustion analysis, since velocity distribution changes barely with ambient pressure.

Researches on coaxial swirl injectors are generally about gas-liquid types. Kang et al. [24] investigated the effects of gas/liquid ratio on the atomization performance of the gas-liquid coaxial swirl injectors with experiments in their research. High-speed camera with back-lighting technique photography phase Doppler anemometry (PDA) was utilized to measure the diameter and the velocity of the droplets. Images of the high-speed camera were used to calculate the spray cone angle along with the image processing tool. In the tests, the flow rate of the liquid was kept constant, and the flow

rate of gas was changed in each test. The results of the tests showed that gas/liquid ratio has a strong effect on the atomization performance of the gas-liquid coaxial. Increasing gas/liquid ratio lowers the SMD, whereas it negatively affects the uniformity of the spray distribution.

Chad et al. [25] designed a liquid-liquid swirl coaxial injector and performed cold flow tests at different mass flow rates to characterize atomization regions of the spray and to measure spray cone angles. They used backlit imaging and a two-dimensional PDPA system for measurement. As a result of their work, they found that the mass flow rate has a little influence on spray the cone angle.

Soltani et al. [26] investigated a liquid-liquid coaxial pressure swirl injector spray characteristic in a non-combusting environment. Velocity and drop size distribution at different locations were measured by PDPA. In their study, water was used as a test fluid, and it was supplied to both inner and outer swirl atomizers from different pressurized tanks. Their test setup was comprised of a water supply system, which includes two water tanks, pressurized nitrogen bottles, pressure regulators, flow meters, water filters, and PDPA system and data acquisition devices. From the test results, they concluded that inner atomizer has more impact on the coaxial injector spray than the outer atomizer and smaller droplets move more slowly than the larger ones since they have higher momentum.

Since recess length is a very critical parameter which directly affects the mixing of the fuel and the oxidizer, various researches have been conducted to investigate the effects of it on both gas-liquid and liquid-liquid coaxial pressure swirl injectors.

Yang et al. [27] studied the characteristic of gas-liquid type recessed coaxial swirl injector. They investigated the recess length effect on the spray characteristic experimentally and numerically. In the experiments, they illuminated spray with copper-vapor laser and recorded the images with the high-speed camera at 4500 frames per second rate. Image processing was utilized to calculate the SMD values of the spray. Water and air were used as test liquids to simulate propellants. From the

test results, they found that without recess length or with little recess length (0 to 1.5 mm) SMD values are high and there is certain recess length that corresponds to minimum SMD value for each test condition. And due to insufficiencies of the analytical models, tests need to be performed to find this recess length value.

The literature review has shown that pressure swirl atomizers were investigated from many aspects owing to the wide range of their applications. There are many studies conducted the effect of liquid properties, the geometry of the atomizer, injection and ambient pressure on the spray characteristic of the pressure swirl atomizer. Nevertheless, there are very few studies on the liquid-liquid coaxial pressure swirl injectors, especially experimental ones which shows the characteristic of the spray in all aspects. So, more research is need on liquid-liquid coaxial pressure swirl injectors. In this thesis, it is aimed to investigate this type of coaxial pressure swirl injector both numerically and experimentally to understand its nature and performance parameters.

This study is different from the ones presented in the literature. Firstly, the comparison of numerical and experimental results was presented in detail. Secondly, along with the coaxial pressure swirl injector, its compromising atomizers were also investigated. Tests and analyses were carried out for a broad range of flow rate. Thirdly, oxidizer/fuel ratio and the recess length effect on the coaxial injector spray were investigated. Two-dimensional axisymmetric and three-dimensional analysis were carried out and compared with each other, and the experiment results in order to show the validity of analyses. Lastly, unlike the researches in literature, all test results were presented in detail.

1.3. Scope of the Thesis

The parameters that affect the performance of the coaxial injector can be divided into two main groups. The first group is the injection conditions of the injector such as fuel and oxidizer properties, mass flow rates, and injection pressures. The second group is the geometric properties of the injectors, such as swirl chamber and nozzle lengths, number and positions of tangential inlets, diameters of nozzles and recess length.

The prediction of the spray cone angle, droplet size, and velocity distribution are crucial for injector design, so the parameters that affect these properties must be well understood to design high-performance injector. In this work, it is aimed to investigate some of these parameters to understand the effect of them on the atomization performance of coaxial pressure swirl injector.

For this study, as the baseline injector geometry, the Russian rocket engine RD-0110's injector, which is used in the third stage of Soyuz space vehicle was chosen. It is a coaxial pressure swirl injector comprising of two concentric pressure swirl atomizers. The inner one is a closed-end type atomizer, and the outer one is an open-end type atomizer, as illustrated in Figure 1.5. The inner atomizer supplies liquid oxygen (LOX) whereas the outer one supplies kerosene.

As aforementioned, recess length is the distance between the tips of the oxidizer injector and the fuel injector of coaxial pressure injectors. When the oxidizer injector is inward with respect to fuel injector this configuration named an internal recess. The configuration which their tips are at the same level is designated as zero recess configuration.

In this thesis, coaxial pressure swirl injectors and their comprising atomizers were numerically and experimentally investigated. The tests were carried out for the inner and the outer atomizers standalone operations in addition to coaxial injector configuration at various flow rates. Two different recess length and three different oxidizer/fuel ratio were investigated. A high-speed shadowgraphy technique was used to find the spray cone angles and a phase Doppler particle analyzer (PDPA or PDA) was employed to characterize spray by obtaining two-dimensional velocity field and SMD values. However, PDPA measurements could not be performed for the outer one due to the high spray cone angle.

Along with the experimental work, two-dimensional axisymmetric swirl and three-dimensional CFD analyses were carried out for the inner and outer atomizers and the

coaxial injector for different conditions. The results of the experimental and numerical work were presented and compared in detail.

CHAPTER 2

EXPERIMENTAL INVESTIGATION

2.1. Introduction

Cold flow injector tests are frequently used as a preliminary test prior to hot flow tests to predict the performance of injectors in LRE. Spray cone angle, the pressure drop through the injector, size and the velocity of droplets indicates the performance of the injector. Before the injector performs in the combustion chamber, these properties which can be measured by cold flow tests, provide very beneficial preliminary information. In cold flow injector tests, various spray measurement techniques can be used such as particle velocity measurement (PIV), phase Doppler particle analyzer (PDPA), and Malvern particle size analyzer.

PDPA is a very useful measurement method to investigate spray characteristic since axial, radial and swirl velocity components of droplets as well as droplet sizes and Sauter mean diameters (SMD) can be measured by PDPA. For this reason, two component PDPA system which is capable of measuring axial and radial velocity components and size of the droplets and SMD was used for the experimental investigation. The working principle and more detailed information about PDPA were presented in the following sections. Along with the PDPA measurements, the high-speed shadowgraphy technique was used in to observe macro properties of the spray such as spray cone angles and breakup length. The coaxial injector and its comprising atomizers were experimentally investigated and the results of the tests presented in this section.

2.2. Experimental Setup

The experiments were performed on the single element atmospheric cold flow injector test facility at TÜBİTAK SAGE. For safety reasons and ease of supply, water was

used to simulate the oxidizer and the fuel. The experimental system was shown in Figure 2.1.

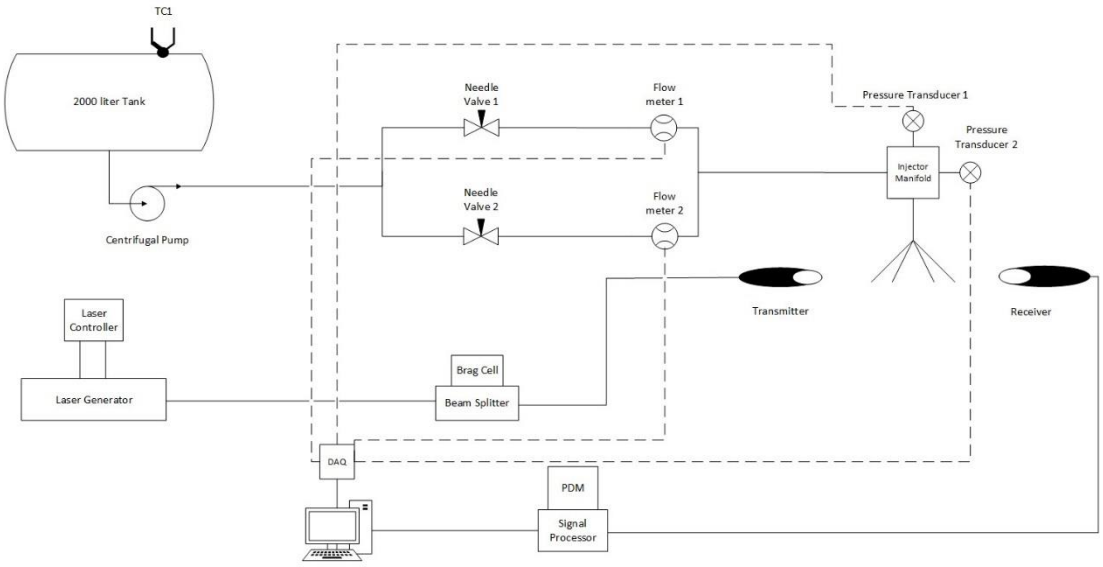

Figure 2.1: The Experimental Setup.

The experimental setup consists of a tank, a centrifugal pump, flow meters, needle valves, pressure transducers, a thermocouple, water filters, and the data acquisition system. The centrifugal pump was used to deliver the pressurized test liquids from the tank to the injectors at constant flow rates. The pressure transducer and the flow meters recorded pressure and flow rate data along with the data acquisition system. Water filters were employed to prevent possible contaminants in the supplied water since the tangential inlet diameter of the swirl injectors were around 1 mm, any contaminant may affect the resulting spray significantly. 2000 liters capacity tank was used which enabled to investigate many points on the spray without interrupting the test. The pressure transducers were placed in the reservoir inlets to measure the pressure drop through the reservoirs, and needle valves were used to adjust flow rates to the desired values. Two turbine type flow meters were used to measure incoming flow rates of inner and outer atomizers. The pressure transducers used in tests had a 0.5% error

margin, whereas the flow meters had a 1% error margin. The data from the flow meters and the pressure transducers were collected via the data acquisition system at 1000 Hz for both pressure and flow rate.

2.3. Phase Doppler Particle Analyzer

Phase Doppler particle analyzer (PDPA) is a non-intrusive, optical measurement technique which use Doppler effect phenomenon to measure instantaneous velocity and the size of the particles within a flow field. PDPA can measure the volume and velocity of the particles simultaneously with high accuracy, so it is an important measurement method for spray characterization.

The PDPA system mainly consists of a laser source, beam splitters, transmitter, receiver data acquisition system, and traverse. The laser beam created by a laser source goes through a beam splitter and splits into two parts of equal intensity. The laser beams are transmitted to transmitter lens by fiber cables. By virtue of transmitter lens, the two beams of the same color intersect and form the interference patterns which are a series of light and dark fringes. The point which intersects patterns occur is called measurement volume and properties of the particles are measured within that volume.

The PDPA system used in this work is two component PDPA which enables to measure axial and radial velocities of particles. Green laser beams measure axial velocity whereas the blue laser measure radial velocity, the interference patterns for green and blue laser beams were shown in Figure 2.2.

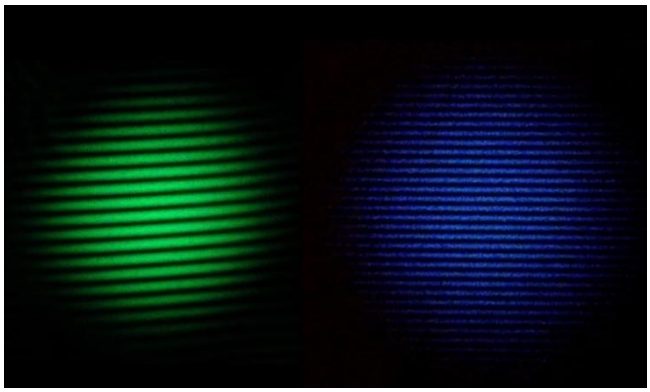

Figure 2.2: Interference Patterns of Green and Blue Laser Beams [28].

The particle passes through the fringes. The particle scatters light while crossing bright fringe however, it does not spread any light while crossing dark fringe. Thus, as the particle passes through the measurement volume, fluctuating scattered light intensity pattern is obtained as in Figure 2.3.

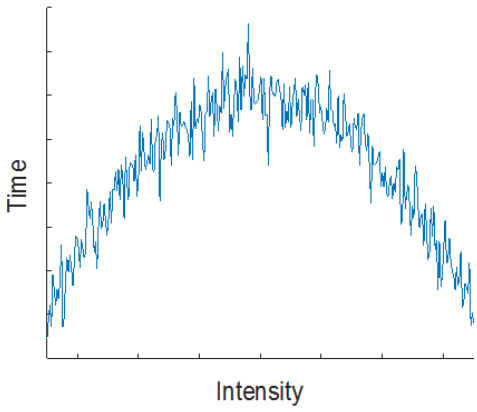

Figure 2.3: Scattered Light Intensity-Time Graph.

The scattered light is collected with Photomultiplier Tubes (PMT) and converted to electrical signals. The frequency of the signal which is also named as Doppler

frequency is measured. Since the distance between fringes is known, the velocity of the particles is obtained from 2.2.

$$U = \delta_f f_D \qquad 2.1$$

There are three different detectors within the PMT which named as A, B and C respectively, and each of these detectors measures the velocities of the particles independently. Diameter is measured by the time difference between signals (phases). The phase difference between A and B detectors is called AB phase, whereas the difference between the A and C detector is called AC phase. Two different diameter measurement takes place simultaneously from phase AB and phase AC. These two independent size measurements are used to increase measurement accuracy which is explained in detail in measurement the validation section.

In the placement of the PDPA system, forward scatter refraction with 37 degrees was used. Since the positive flow direction is from the unshifted laser beam to shifted one, the transmitter and the receiver were placed taking in to account the positive flow direction of the forming spray as can be seen from Figure 2.4.

Figure 2.4: Transmitter- Receiver Position.

2.3.1. Particle Size Analysis

Due to the nature of spray formation, many particles with various sizes are present in the flow field. To interpret the obtained data from the experiment results and to compare different test results with each other the diameters of particles are usually represented by mean values. Diameter statistics methods are used to find these mean values. Diameter statistics were calculated using equation 2.2.

$$D_{mn} = \left(\frac{\sum_{i=1}^{N} n_i D_i^p}{\sum_{i=1}^{N} n_i D_i^q} \right)^{\frac{1}{p-q}} \qquad 2.2$$

The names for the diameter statistics were given in Table 2.1.

Table 2.1: Diameter Statistics Table.

D_{10}	Diameter Mean
D_{20}	Surface Mean
D_{30}	Volume Mean
D_{32}	Sauter Mean
D_{43}	De Brouckere Mean

Surface area moment mean (D_{32}) also named as the Sauter Mean Diameter is the most commonly used mean in measuring the quality of sprays. For this reason, in the comparison of experimental results, SMD values were used.

2.3.2. Validation of PDPA Measurements

Before conducting the injector tests, validation tests were performed to obtain reliable data. The PDPA measurements were validated as explained in this section. Although the PDPA has some self-validation method in post-processing such as phase validation, intensity validation and setting diameter difference limit, an additional validation setup was used.

One of these self-validation methods is the setting diameter limit. Within the PDPA system, there are two different sensors, meaning that two independent size measurement takes place simultaneously. In other words, two different diameter values for one particle were measured by sensors. By setting the maximum diameter difference limit in the PDPA software, measured values which were outside the limit were not taken as valid data. The maximum allowable diameter difference limit was chosen as %7 recommended in the PDPA manufacturer manual [28].

Another self-validation method is checking the intensity values. When the particle passes through the measurement volume, the receiver gets light intensity as illustrated in Figure 2.3. When the particle is in the center of the measurement volume, a higher intensity value is obtained. If the particle is not entirely in the measurement volume, while it is crossing the measurement volume, the receiver gets lower intensity values. Thus, setting a threshold limit for the intensity value eliminates the incorrect measurement of the particle size. This threshold value needs to be different for each particle size because bigger particles have higher intensity values than the lower particles. For this reason, instead of defining a certain number that can reject correct measurement for smaller particles, the different limit is set for each particle diameter value. This is accomplished by setting a lower threshold curve for diameter versus intensity values, as illustrated in Figure 2.5.

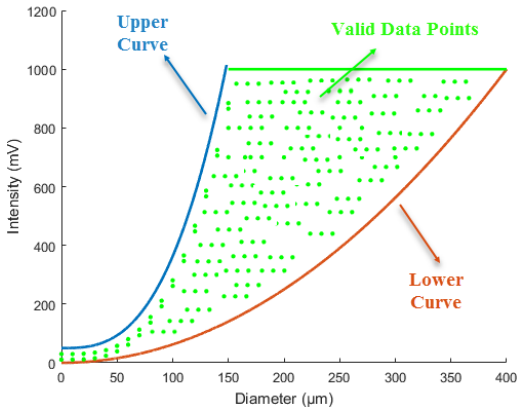

Figure 2.5: Validated Data Points Graph for PDPA Measurements.

In addition to the lower curve (threshold curve), also an upper curve was defined. The upper curve was set to prevent small particles from saturating the receiver. Slopes of the upper and the lower curves were set according to TSI Flowsizer software manual [28] by regarding the number of the validated particles, and the bigger particles should have the intensities (intensity of 1000 mv) near the saturation.

Along with these self-validation methods of post-processing, to validate the measurements of the PDPA, water particles with known diameter were formed with validation setup and measurements were performed. Then, the theoretical and measured results were compared in Table 2.2.

The validation setup used in this work is called Mono-size Droplet Generator (MDG), and it works on the principle of applying periodic excitation to a liquid reservoir which supplies a laminar jet. When the excitation frequency is adjusted to a resonant frequency; the laminar jet breaks up, and uniform droplets are formed at the excitation frequency. By knowing the flow rate and the excitation frequency, the size of the droplets can be calculated using equation 2.3 [29].

$$D = \left[\frac{6Q}{\pi f}\right]^{\frac{1}{3}} \qquad 2.3$$

Where Q is the liquid flow rate, f is excitation frequency, and D is the diameter of the droplet.

This validation setup consists of a function generator, a syringe with a pump, a traverse, and the drop generator head. The mono-size droplet generator setup is shown in Figure 2.6.

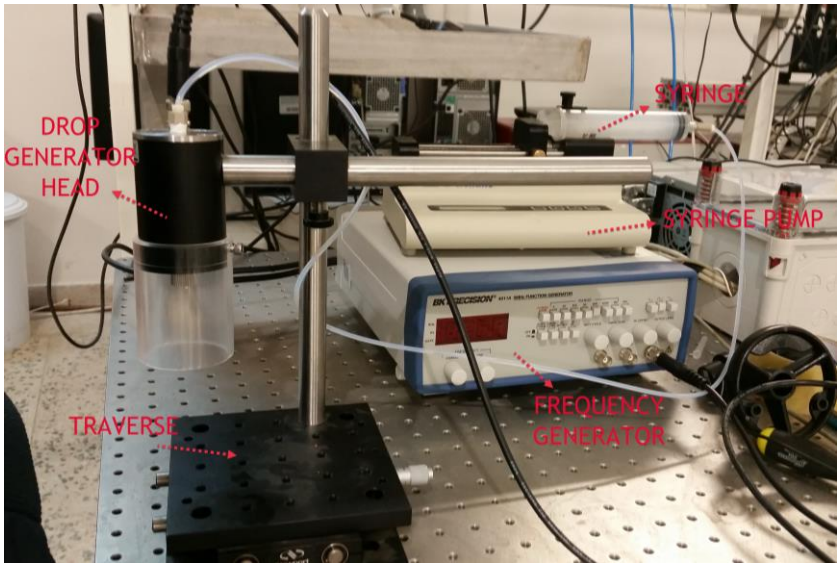

Figure 2.6: Mono-size Droplet Generator Setup.

A function generator (BK PRECISION 4011A) which is capable of producing wide range frequency sinus and square signals is connected to the drop generator head. Drop formation at the droplet head was shown in Figure 2.7. In this system, water is forced out of the syringe with an adjusted constant volumetric flow rate by the syringe pump. The forced water enters into the liquid reservoir part of the droplet head. The square wave signal is sent to the piezo-transducers from the frequency generator to disturb

the water in the liquid reservoir with the selected frequency. Water comes out of the orifice, and droplets with constant diameter are formed.

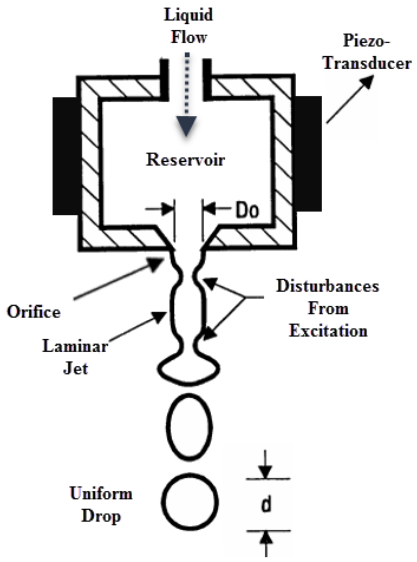

Figure 2.7: Drop Formation in Droplet Head [29].

By knowing the orifice diameter, frequency, and the flow rate were set at a certain value so the mono-size droplet generator forms 120-micrometer diameter droplets. To verify the measurement accuracy of the PDPA system, droplet size and the velocity of these formed droplets were measured by the PDPA system and the measured values compared with the theoretical values. The comparison results are displayed in Table 2.2.

Table 2.2: Comparison of Theoretical and Measured Values with MDG.

Properties	**Measured Value**	**Theroterical Value**	**Difference From Theorecial Value (%)**
Valid Count Data	49992	-	-
D_{10} [µm]	116.315	120	%3.0708
D_{20} [µm]	116.350	120	%3.0417
D_{30} [µm]	116.413	120	%2.9892
D_{32} [µm]	116.550	120	%2.8750
D_{43} [µm]	117.110	120	%2.4083

As can be seen in Table 2.2. the difference between the measured and theoretical value for diameter and SMDs is around 3% which is an acceptable error rate that does not affect the results of this research. The validation study proved that the PDPA system measurements were highly reliable.

2.3.3. Investigated Injectors Geometries

After ensuring the reliability of the PDPA measurements injectors were manufactured, and tests were performed. Injectors and reservoirs were designed in a way to be easily reassembled to try different geometric configurations with less effort. As aforementioned, the RD-0110 rocket injector was chosen as injector geometry. Dimensions of the injector were shown in Table 2.3.

Table 2.3: Geometric Properties of the RD-0110 Injector [8].

Type	Swirl Chamber Diameter [mm]	Swirl Chamber Length [mm]	Nozzle Diameter [mm]	Nozzle Length [mm]	Diameter of Tangential Inlets [mm]	Number of Tangential Inlets
Internal Injector (Oxidizer)	9.00	10.38	5.40	10.17	1.70	6
Outer Injector (Fuel)	10.00	10.50	10.00	10.50	0.70	6

The spray cone angle and the mass flow rates of the comprising part of the injector at design point were given in Table 2.4.

Table 2.4: Properties of the RD-0110 Injector at Design Point [8].

Type	Liquid	Mass Flow Rate [g/s]	Spray Cone Angle (°)
Inner Atomizer (Oxidizer)	LOX	172.9	80
Outer Atomizer (Fuel)	Kerosene	64.8	135

RD-0110 injector was manufactured with the designed reservoirs. RD-0110 injector geometry with 1.5 mm and 3.0 mm recess were produced. Firstly, the tests were carried out at the design point of the RD-0110 injector. Then, the tests with different flow rates at the same oxidizer/fuel ratio of the design point were performed. Lastly, tests at different oxidizer/fuel ratios for the different flow rates were conducted. As presented in Table 2.4, the inner atomizer of the RD-0110 injector operates with LOX, whereas the outer atomizer operates with kerosene. So, since the spray cone angle of the pressure swirl atomizers depends on the working fluid, the tests which carried out with water would not give the same spray cone angle value as in Table 2.4, but it would be very close.

2.4. Experiment Results

PDPA experiments were carried out at different mass flow rates for both the inner atomizer and the coaxial injector separately. Since the spray cone angle of the outer atomizer was quite high, the droplets of the spray fall on the lens of the receiver and blocks to the receiver's view so PDPA measurements could not be performed for the outer atomizer.

Along with the PDPA measurements, the flow rate and the pressure drop through the injector were recorded. The flow rate was measured with turbine type flow meter and

the data were collected at 1000 Hz frequency. Also, the pressure drop through the inner and outer atomizers was measured with a pressure transducer at a 1000 Hz frequency data rate. Discharge coefficients for the atomizers were calculated from the recorded pressure drop and the flow rates.

Similarly, Radke and Meyer [30] used PDPA to investigate the effect of injector geometry on atomization performance for the gas-liquid coaxial swirl injector. In the PDPA measurements, they collected a minimum of 2000 valid samples for each test point by using TSI Flowsizer software. In this work, 10000 valid points were collected for each measurement point. All measurements were taken from 10 mm away from the injector exit in order to compare the results within the same frame, but this leads that to measure relatively high SMD values near the injector exits because some parts of the measurement points were within the breakup region, especially for low flow rate tests. Measurement for the first 10 mm distance from the injector exit was not performed because the spray was optically very dense at this region and the data rates were low. The PDPA measurements were taken at more than 200 points for each test. The measured data points were shown with filled squares in Figure 2.8.

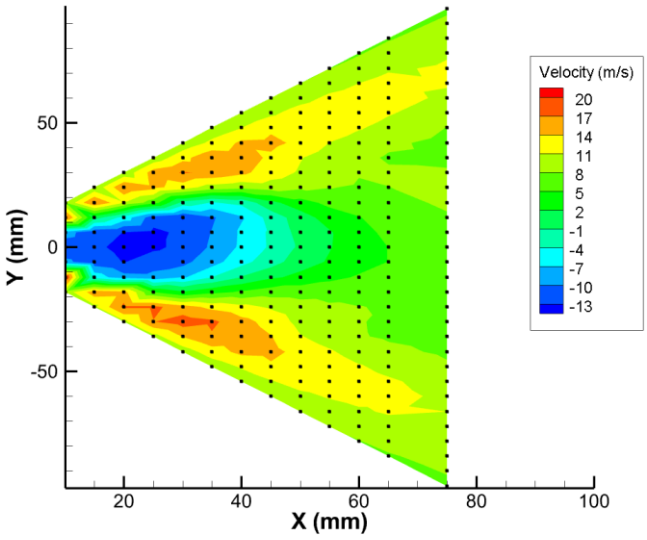

Figure 2.8: Measurement Points for the PDPA Measurements.

Also, the temperature of the water was measured in each experiment with calibrated T type thermocouple. The minimum water temperature recorded during the test was 13.2 ℃ while the maximum temperature was 19.3 ℃. Since properties of the water merely change in this range [31], the effect of the temperature was not taken into account while evaluating the results. Along with the PDPA measurements, spray cone angles were measured for all test conditions using the high-speed shadowgraphy technique. The results were presented in the next section.

2.4.1. Spray Cone Angle Measurements

standalone operations and the coaxial injector configuration at different flow rates. The high-speed shadowgraphy technique was used to measure the spray cone angle.

To use high-speed shadowgraphy method, a high-speed camera, a light source, and a screen was used along with the experimental setup presented in section 2.2. Experimental setup for the high-speed shadowgraphy technique was shown in Figure 2.9.

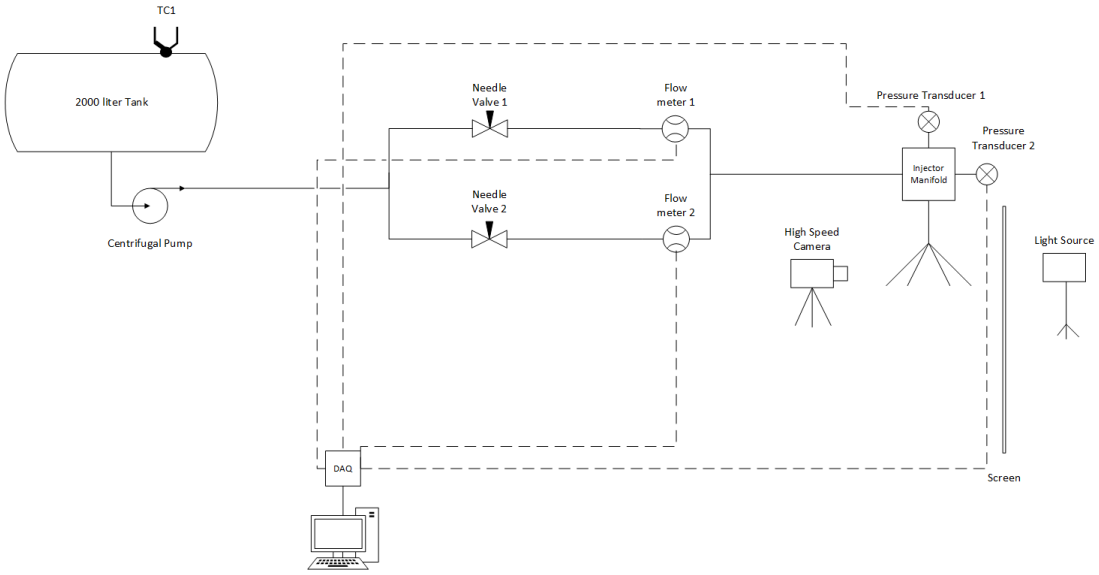

Figure 2.9:High-Speed Shadowgraphy Setup.

Images were recorded at 5000 frames per second rate to distinguish the fluctuations in the spray. The recorded images were used to find a spray cone angle with a developed image processing code.

The code uses the edge detecting method to find the spray cone angle, which was calculated for every frame. The average values were presented as a spray cone angle at that flow rate. Distance between two edges in the same vertical line was detected at first. Then, this process was repeated for another vertical line at a different axial position as illustrated in Figure 2.10. Using the distance between two edges of the spray at different axial locations, spray cone angle was measured from equation 2.4.

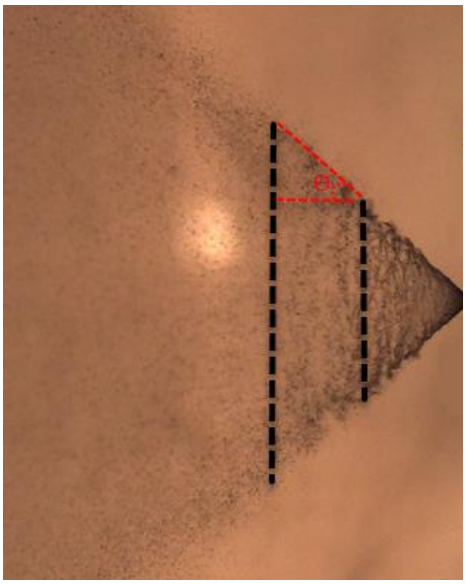

Figure 2.10:Spray Cone Angle Measurement.

Where Δy_1 is the distance between two edges of the vertical line 1, whereas Δy_2 is the distance between two edges of the vertical line 2, and Δx is the axial distance between two vertical lines and θ is the spray cone angle:

$$\theta = 2tan\left(\frac{\Delta y_2 - \Delta y_1}{2(\Delta x)}\right)^{-1} \qquad 2.4$$

Similarly, in the analysis phase fraction for the solution domain was captured at every millisecond. Spray cone angle was obtained for each frame with the developed image processing code. Then the average spray cone angle was calculated for each test. Also, the average spray cone angle was calculated for the analysis results.

2.4.2. Experiment Results of the Inner Atomizer

Before the coaxial swirl tests were performed, tests for the inner atomizer at different mass flow rates were carried out and the axial-radial velocities of the droplets, as well as the SMD (D_{32}) and diameter means (D_{10}) were obtained with the PDPA

measurement. Spray cone angle was measured by means of a high-speed camera. The flow rate and the pressure drop through the atomizer were also measured and recorded by the flow meter and the pressure transducer respectively. Discharge coefficient for the inner atomizer was calculated from the recorded pressure drop and flow rate values. Pressure drop through the inner atomizer versus mass flow rate graph is plotted in Figure 2.11. The test points were marked with circled points on the graph, and the curve was obtained by interpolating the test points.

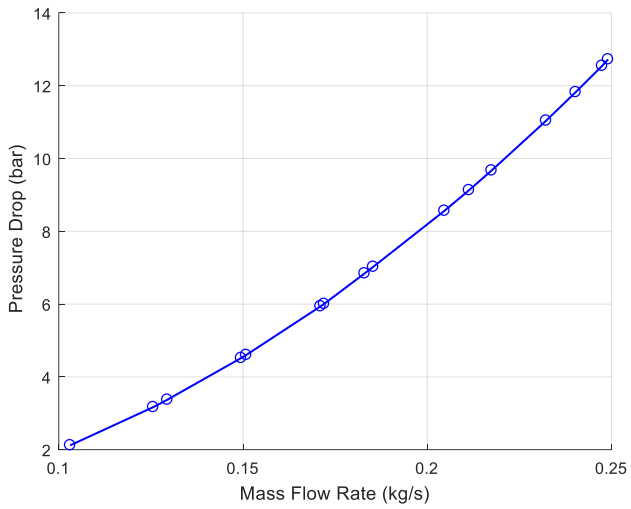

Figure 2.11: Pressure Drop vs Mass Flow Rate of Inner Atomizer.

The discharge coefficient of inner atomizer was calculated using the recorded mass flow rate and the pressure drop data from equation 1.2 [32]. The discharge coefficient versus mass flow rate for the inner atomizer was shown in Figure 2.12. The marked points on the graph were test points, and the curve was obtained by interpolating the test points.

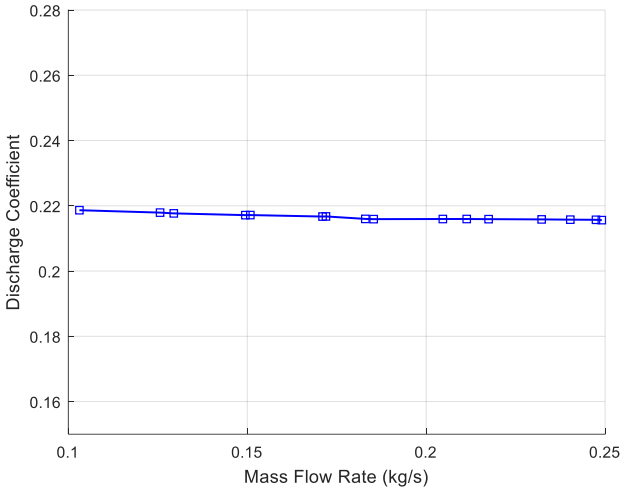

Figure 2.12: Mass Flow Rate vs Discharge Coefficient for the Inner Atomizer.

Spray cone angles for the inner atomizer at three different flow rates were presented together in Figure 2.13 to show the change in the spray with increasing injection pressure.

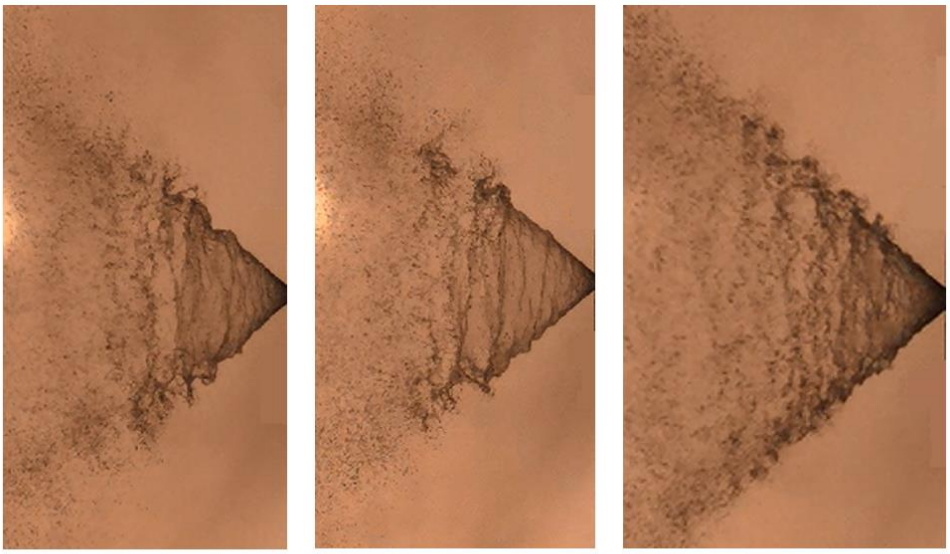

a) 4.7 lpm **b)** 6.0 lpm **c)** 9.0 lpm

Figure 2.13: Spray Cone Angle of the Inner Atomizer at Three Different Flow Rates.

Also, the temperature of the water was measured in each experiment with calibrated T type thermocouple. The minimum water temperature recorded during the test was 13.2 ℃ while the maximum temperature was 19.3 ℃. Since properties of the water merely change in this range [31], the effect of the temperature was not taken into account while evaluating the results. Along with the PDPA measurements, spray cone angles were measured for all test conditions using the high-speed shadowgraphy technique. The results were presented in the next section.

2.4.1. Spray Cone Angle Measurements

standalone operations and the coaxial injector configuration at different flow rates. The high-speed shadowgraphy technique was used to measure the spray cone angle.

To use high-speed shadowgraphy method, a high-speed camera, a light source, and a screen was used along with the experimental setup presented in section 2.2. Experimental setup for the high-speed shadowgraphy technique was shown in Figure 2.9.

results for the different flow rates were given together to make the comparison simpler.

The droplet size of the particles has a crucial influence on combustion efficiency. The smaller the drop size the less ignition energy is needed for the combustion. Therefore, a high surface to volume ratio particles is desired in the combustion chamber. In other words, a particle with low SMD value is desirable in combustion applications.

For 6 l/m flow rate axial velocity with streamlines was plotted in Figure 2.15, and the radial velocity field was shown in Figure 2.16.

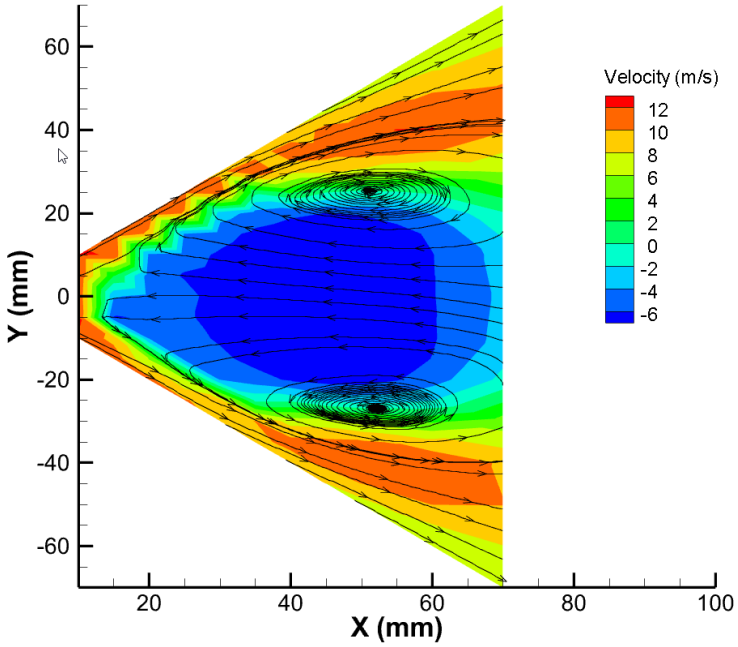

Figure 2.15: Axial Velocity of Inner Atomizer with Streamlines at 6 l/m Flow Rate.

As can be seen from Figure 2.15, vortex-like structures occur in the spray and positions of these structures are symmetric with respect to the x-axis.

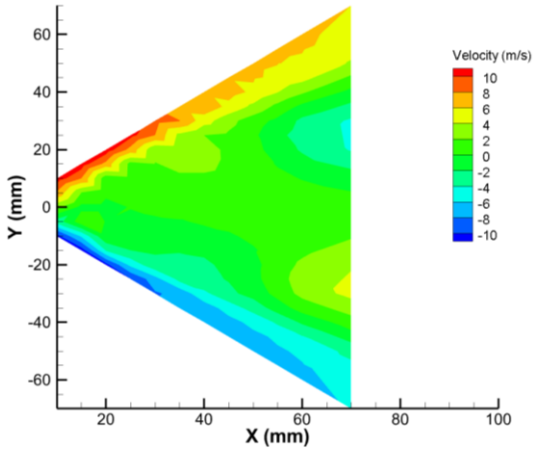

Figure 2.16: Radial Velocity of Inner Atomizer at 6 l/m Flow Rate.

The axial and the radial velocities of the droplets for flow rates of 6 l/m, 9 l/m, and 10.3 l/m were illustrated in Figure 2.17 and Figure 2.18. For the same flow rates, the SMD and diameter distributions were shown in Figure 2.19 and Figure 2.20 respectively.

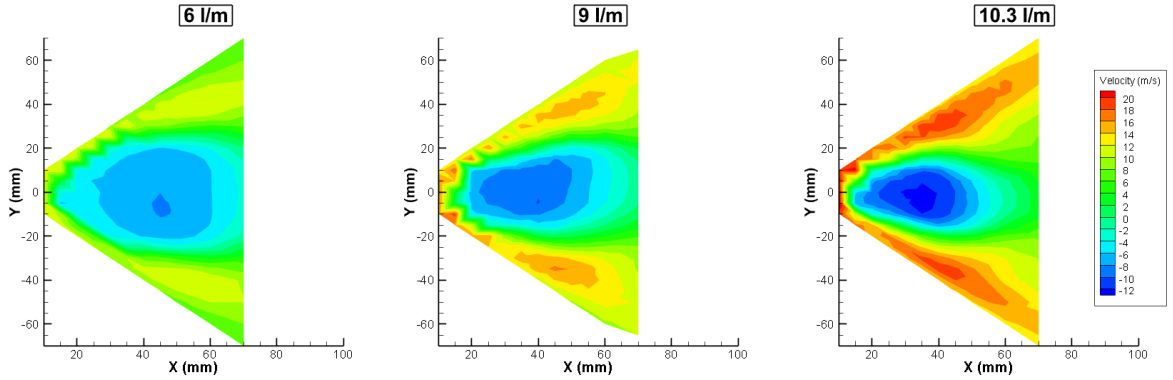

Figure 2.17

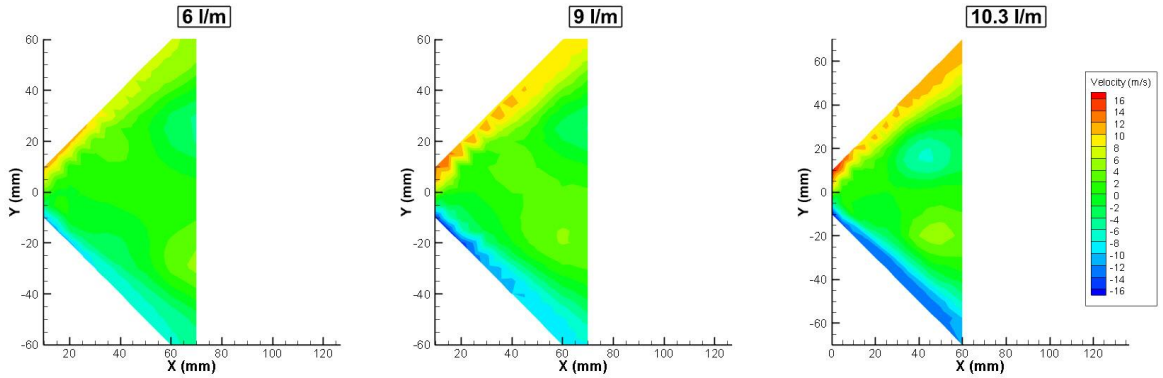

Figure 2.18:

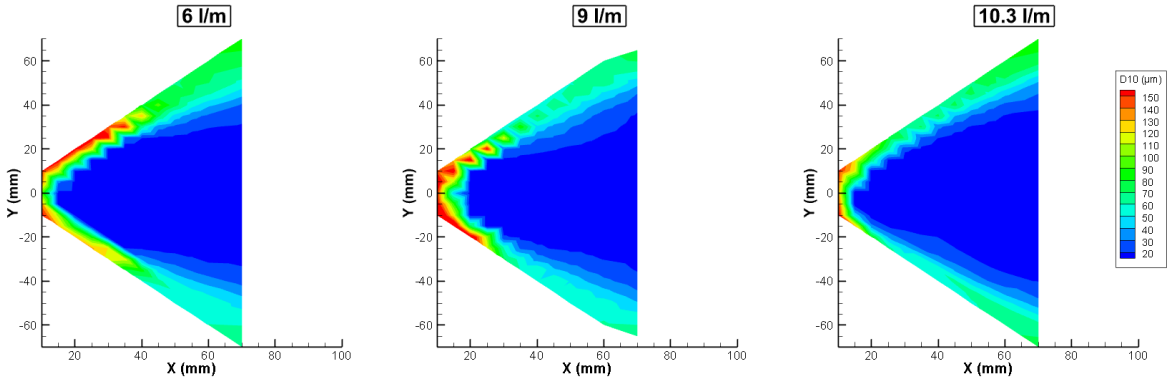

Figure 2.19: D10 Distribution of Inner Atomizer at Different Flow Rates.

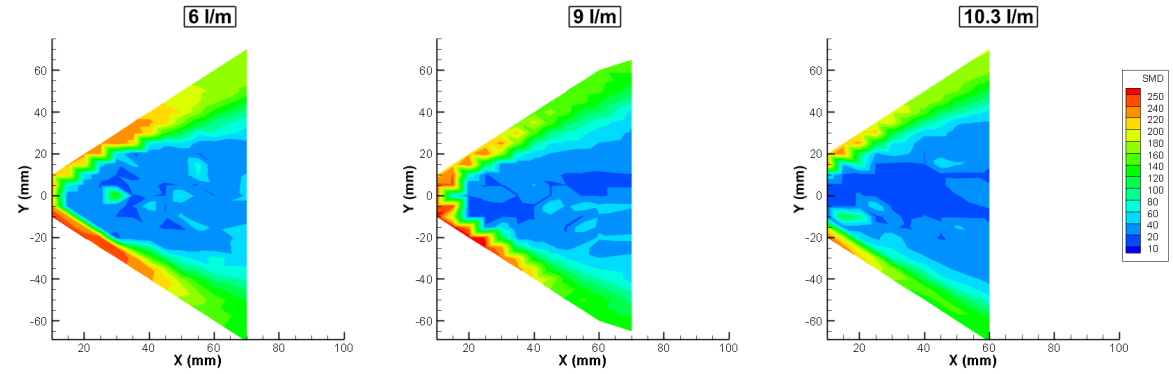

Figure 2.20: SMD Distribution of Inner Atomizer at Different Flow Rates.

As can be seen from Figure 2.19 and Figure 2.20, after the breakup droplets size gets smaller. Within the breakup region, relatively larger droplets are formed. Also, during the tests, it was observed that data rates increase dramatically after the breakup. Similarly, Radke and Meyer [30] have seen the same effect in their research.

For 6 l/m and 15 l/m flow rate tests, axial velocity of the droplets with the streamlines was shown together in Figure 2.21.

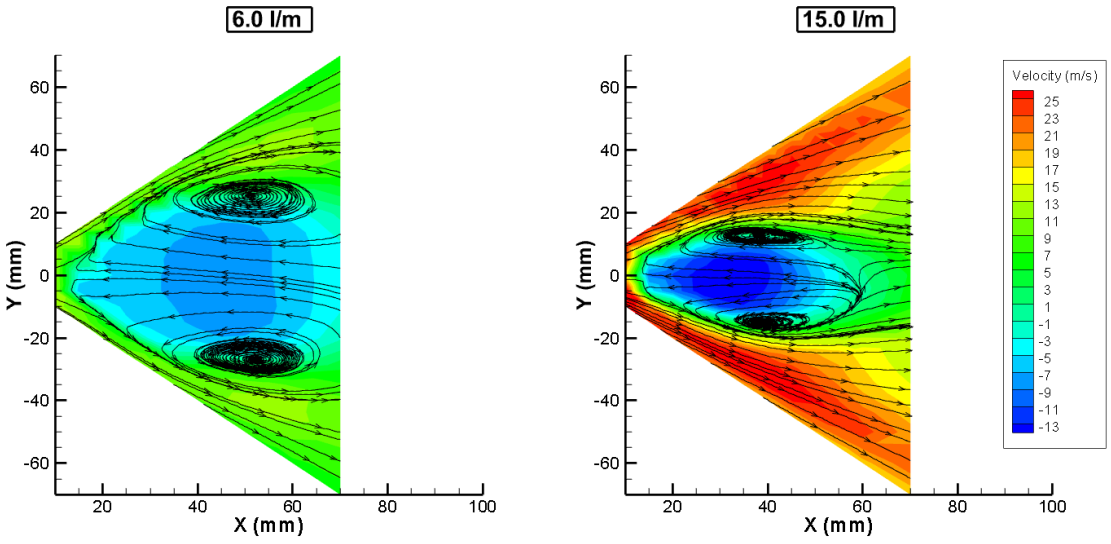

Figure 2.21:Comparison of Axial Velocities with Streamlines.

Comparing the 6 l/m and 15 l/m flow rates tests with the same contour, the effect of the increase in flow rate becomes more apparent. Figure 2.21 indicates that the magnitude of the axial velocities of the droplets for the 15 l/m flow rate is almost twice as big as the 6 l/m flow rate. Also, as the flow rate increases, the position of the vortex moves towards the injector exit.

2.4.3. Experiment Results of the Outer Atomizer

The spray cone angle and the pressure drop at different mass flow rates were measured, and the discharge coefficient was calculated for the outer atomizer as done for the inner atomizer. However, the PDPA measurement could not be performed due to reason beforementioned. Pressure drop through the inner atomizer versus mass flow rate graph was shown in Figure 2.22. The circled points on the graph are the test points, and the curve was obtained by interpolating the test points. The discharge coefficient of inner atomizer was calculated using the recorded mass flow rate and the pressure drop data from equation 1.2. Discharge coefficient versus mass flow rate for the outer atomizer was plotted as shown by Figure 2.23. The marked points on the graph are test points, and the curve was obtained by interpolating the test points.

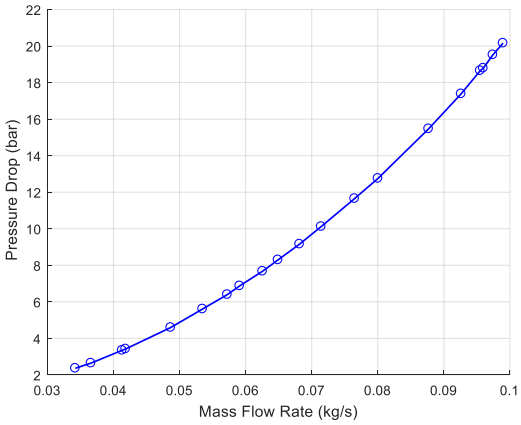

Figure 2.22: Pressure Drop vs Mass Flow Rate of the Outer Injector.

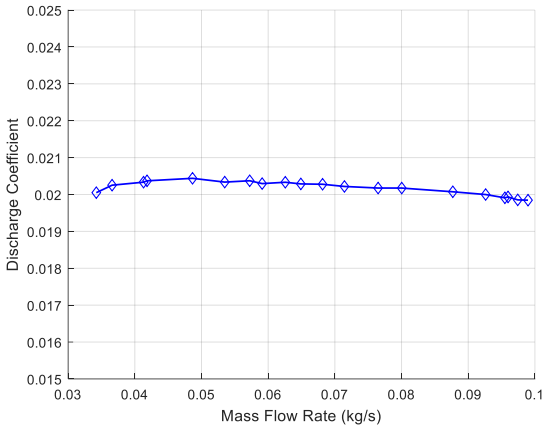

Figure 2.23: Discharge Coefficient vs Mass Flow Rate of the Outer Atomizer.

As can be seen from Figure 2.11 and Figure 2.22, pressure drop for the outer atomizer is higher than the inner atomizer since its tangential inlets area is smaller than the inner atomizer. Spray cone angle for the outer atomizer were measured for the flow rates of 2.1 l/m, 2.9 l/m, 3.6 l/m, and 4 l/m and 4.6 l/m. For the three different flow rate spray of the outer atomizer were presented in Figure 2.24 to show the change in spray cone angle.

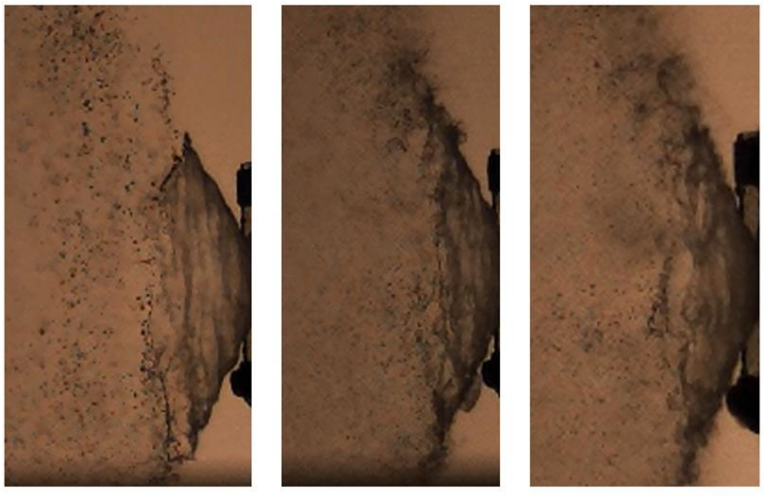

a) 2.1 lpm **b)** 3.6 lpm **c)** 4.6 lpm

Figure 2.24: Spray Cone Angle of the Outer Atomizer at Three Different Flow Rates.

As can be conducted from Figure 2.24, as the flow rate increases, breakup length decreases, and spray cone angle increases. Spray cone angles for the outer atomizer at different flow rates were measured and presented in Figure 2.25. The marked points on the graph were test points, and the curve was obtained by interpolating the test points.

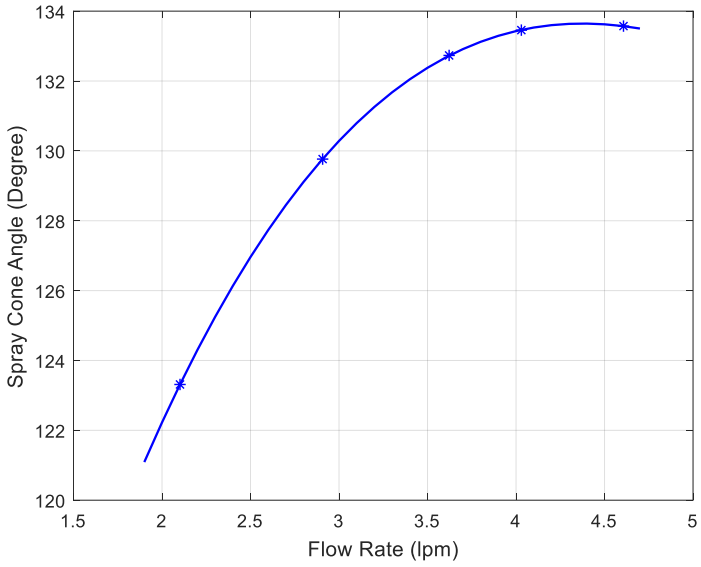

Figure 2.25: Flow Rate vs Spray Cone Angle for the Outer Atomizer.

Comparing the test results of the inner and the outer atomizer revealed that the spray cone angle of the outer atomizer is considerably higher than the inner atomizer's spray cone angle even for the lower flow rates. Like in the inner atomizer, as the flow rates increases spray cone angle increases up to a certain point after that point spray cone angle does not change much, even though the flow rate increases.

2.4.4. Experiment Results of the Coaxial Injector

For the coaxial injector, the same properties as in the inner and the outer atomizers were measured. Coaxial injectors with two different recess lengths were examined. Also, several oxidizer/fuel (o/f) ratios were tested to investigate the effect of the o/f ratio on the spray properties. Since several parameters investigated for the coaxial injector tests, the conducted tests were presented in Table 2.5 with details. The recess length of the tested coaxial injector, flow rates of the inner and the outer atomizers, and the o/f ratios were indicated in the table.

Table 2.5: Details of the Conducted Coaxial Injector Tests.

Test Name	Recess Length [mm]	Inner Atomizer Q [l/m]	Outer Atomizer Q [l/m]	O/F Ratio
Test 1	1.5	7.5	2.9	2.6
Test 2	1.5	9.0	3.5	2.6
Test 3	1.5	10.3	4.0	2.6
Test 4	1.5	12.0	4.6	2.6
Test 5	1.5	15.0	5.8	2.6
Test 6	1.5	7.5	4.7	1.6
Test 7	1.5	10.3	6.4	1.6
Test 8	1.5	7.5	2.1	3.6
Test 9	1.5	10.3	2.9	3.6
Test 10	3.0	7.5	2.1	3.6
Test 11	3.0	10.3	2.9	3.6

Spray cone angles of the coaxial injector configuration were measured as done previously for the comprising atomizers. All test results were presented in this section.

In the graphs, tests were labeled according to the flow rate of the inner atomizer (oxidizer rate). Firstly, the axial velocities for the 2.6 o/f ratio were presented. The comparison is made for the same o/f ratio to investigate the effect of the increase in flow rate. Axial velocities for the 2.6 o/f ratio, test 1, test 2, test 4 and test 5 were presented in Figure 2.8. Radial velocities for the same tests were shown in Figure 2.27. D10 and SMD values for the same tests were presented in Figure 2.28 and Figure 2.29.

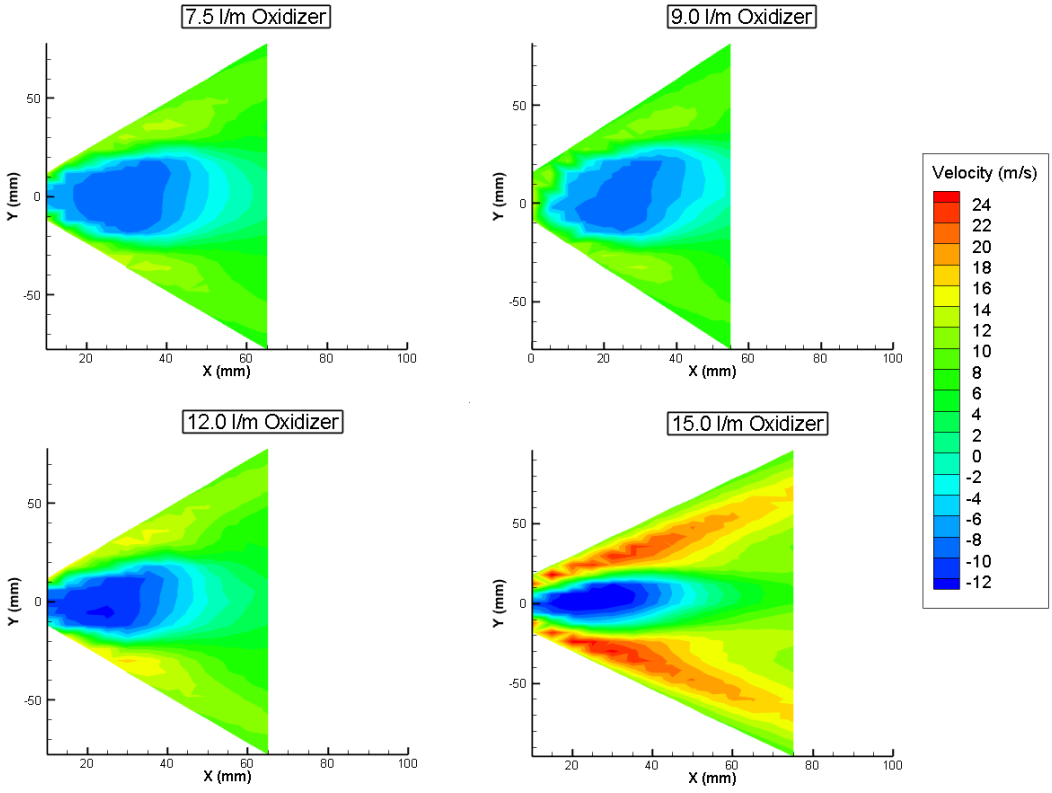

Figure 2.26:Axial Velocities at Different Flow Rates for 2.6 O/F Ratio.

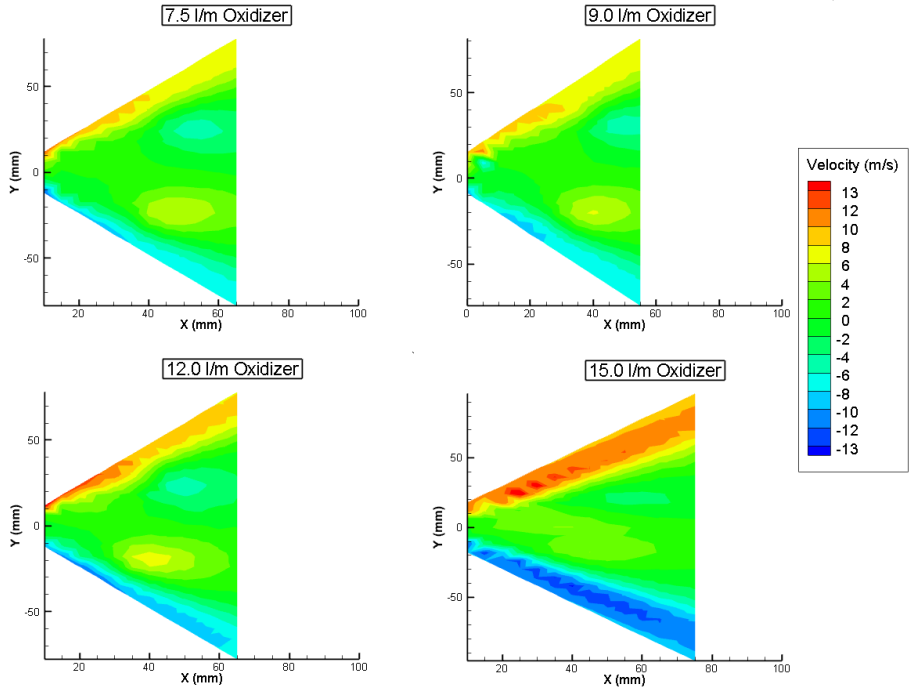

Figure 2.27: Radial Velocities at Different Flow Rates for 2.6 O/F Ratio.

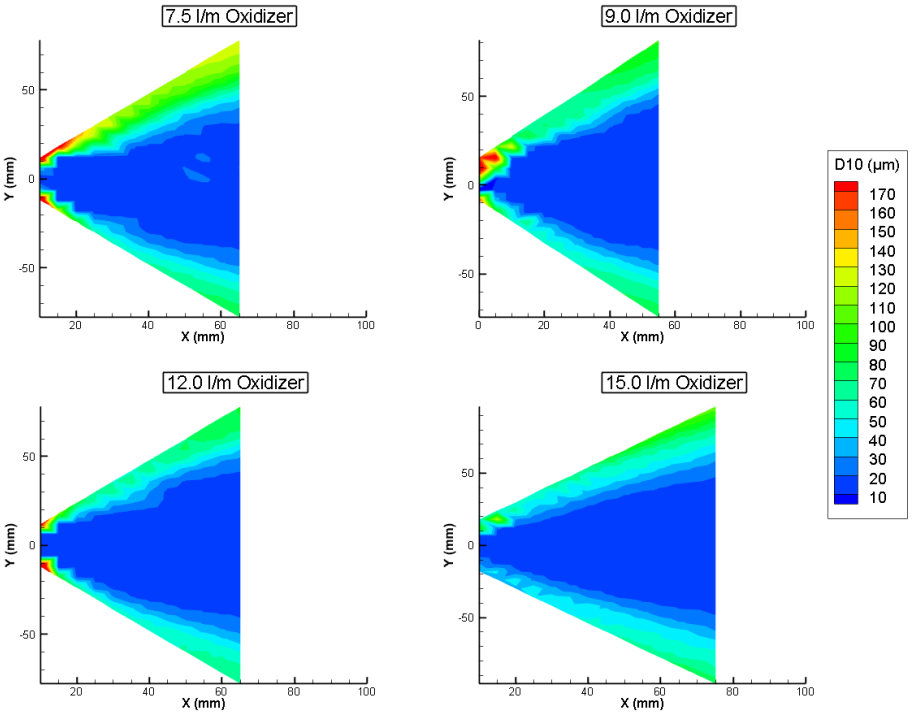

Figure 2.28:D10 Distribution at Different Flow Rates for 2.6 O/F Ratio.

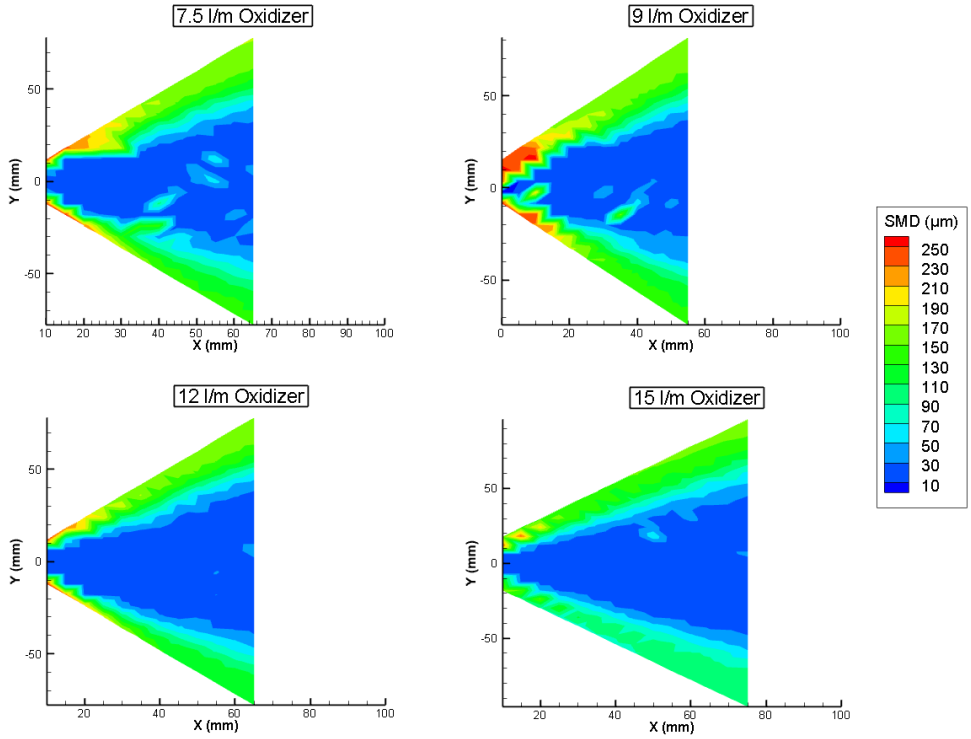

Figure 2.29:D32 Distribution at Different Flow Rates for 2.6 O/F Ratio.

Comparing the different flow rates shows that increasing flow rate leads to an increase in velocity magnitudes of the droplets in every direction. As the flow rate increases the breakup length decreases, atomization improves, and the size of the droplets becomes smaller. The results show that the effects of the increase in flow rate (for fixed o/f ratio) are similar for coaxial injector and the inner atomizer.

To examine the effect of change in o/f ratio the coaxial injector was tested at three different oxidizer/fuel ratios as 1.6, 2.6 and 3.6 for the 7.5 l/m and 10.3 l/m inner atomizer flow rates. For the 7.5 l/m inner atomizer flow rate, at three different o/f ratio test results (test 6, test 1, test 8) were presented together in Figure 2.30, Figure 2.31, Figure 2.32, and Figure 2.33. For the 10.3 l/m inner atomizer flow rate, at three different o/f ratio test results (test 7, test 3, test 9) were presented in Figure 2.34, Figure 2.35, Figure 2.36, and Figure 2.37. The o/f ratios of the tests were labeled in the figures.

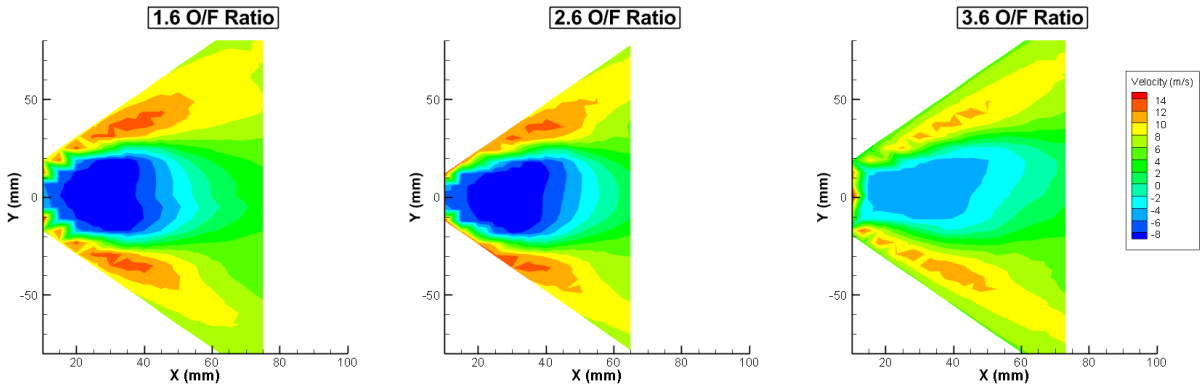

Figure 2.30: Axial Velocities for 3 O/F Ratio at 7.5 l/m Inner Atomizer Flow Rate.

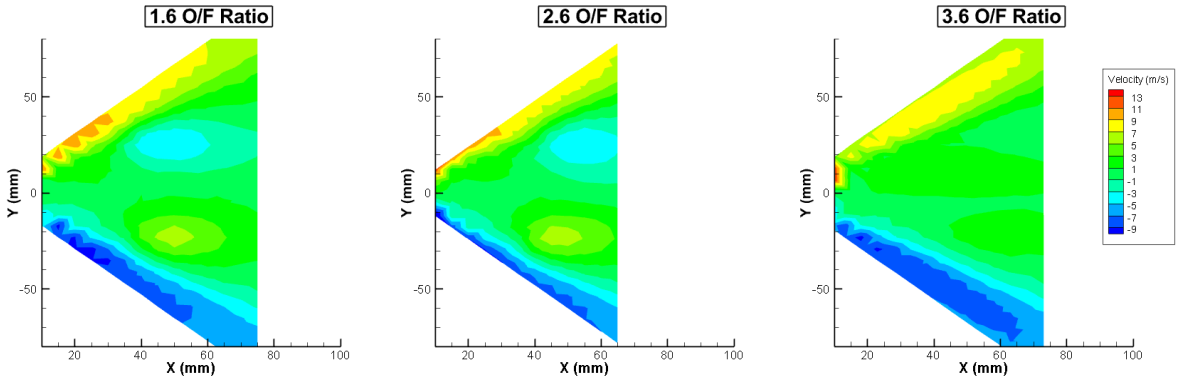

Figure 2.31: Radial Velocities for 3 O/F Ratio at 7.5 l/m Inner Atomizer Flow Rate.

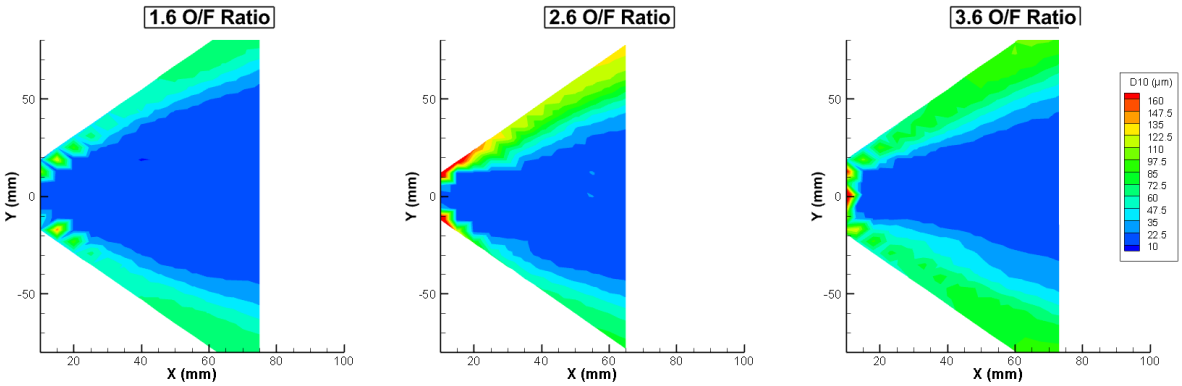

Figure 2.32: D10s for 3 O/F Ratio at 7.5 l/m Inner Atomizer Flow Rate.

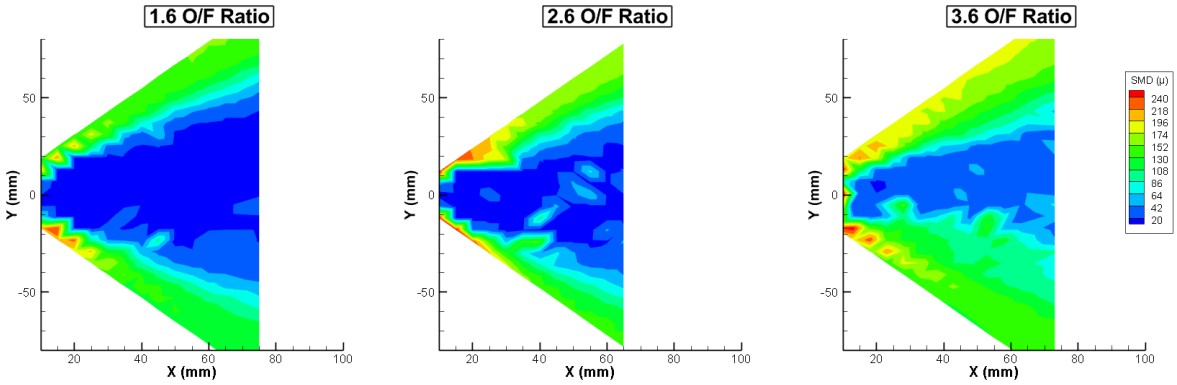

Figure 2.33: SMDs for 3 O/F Ratio at 7.5 l/m Inner Atomizer Flow Rate.

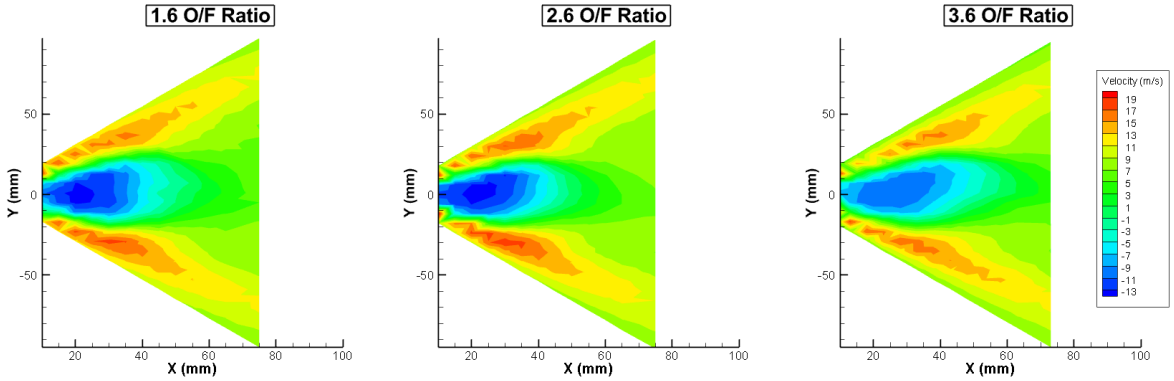

Figure 2.34: Axial Velocities for 3 O/F Ratio at 10.3 l/m Inner Atomizer Flow Rate.

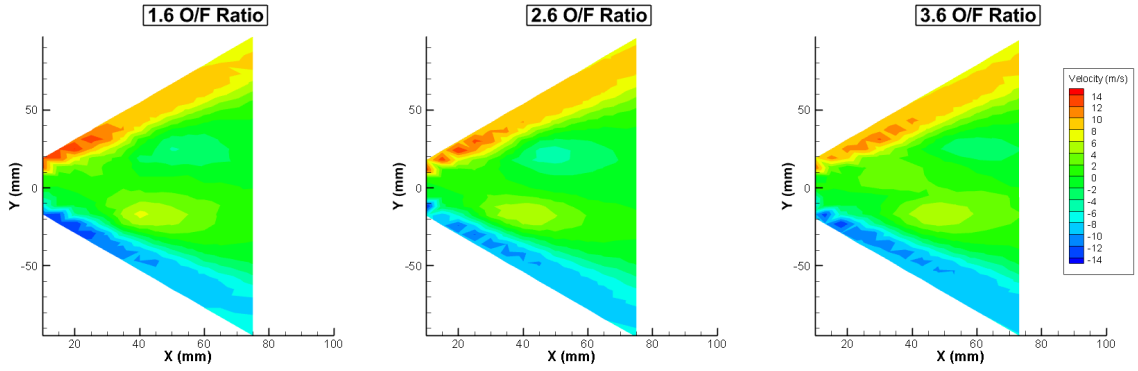

Figure 2.35: Radial Velocities for 3 O/F Ratio at 10.3 l/m Inner Atomizer Flow Rate.

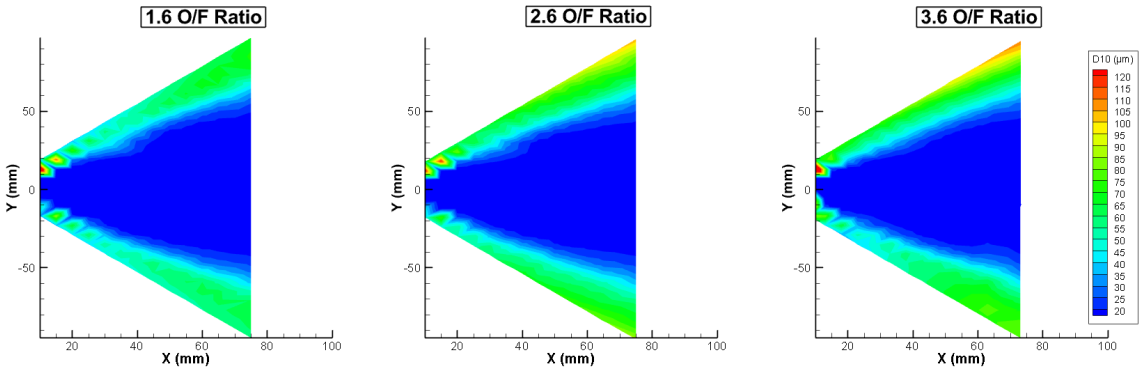

Figure 2.36: D10s for 3 O/F Ratio at 10.3 l/m Inner Atomizer Flow Rate.

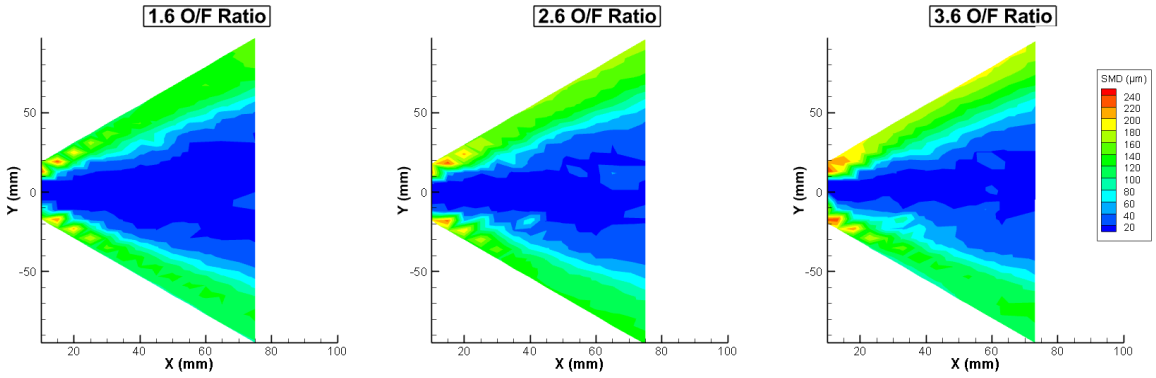

Figure 2.37: SMDs for 3 O/F Ratio at 10.3 l/m Inner Atomizer Flow Rate.

It was seen that for the 3.6 oxidizer/fuel ratio, the velocity of the droplets is smaller than the other two oxidizer/fuel ratios, whereas axial velocities of the 1.6 oxidizer/fuel ratio and 2.6 oxidizer/fuel ratio are close quite to each other. Velocities for the 1.6 o/f ratio is slightly higher than the 2.6 o/f ratio. For the lower o/f ratio, particles have a higher velocity, since the effect of the inner atomizer increases with the decrease of the o/f ratio.

To investigate the effect of the recess length tests with the same flow rates with different recess lengths were conducted. As indicated in Table 2.5, the inner atomizer flow rate is 10.3 l/m whereas, the outer atomizer flow rate is 2.9 l/m for test 9 and test

11 and recess lengths are 1.5 mm and 3 mm respectively. The axial velocities of the droplets for test 9 and test 11 were presented and compared in Figure 2.38.

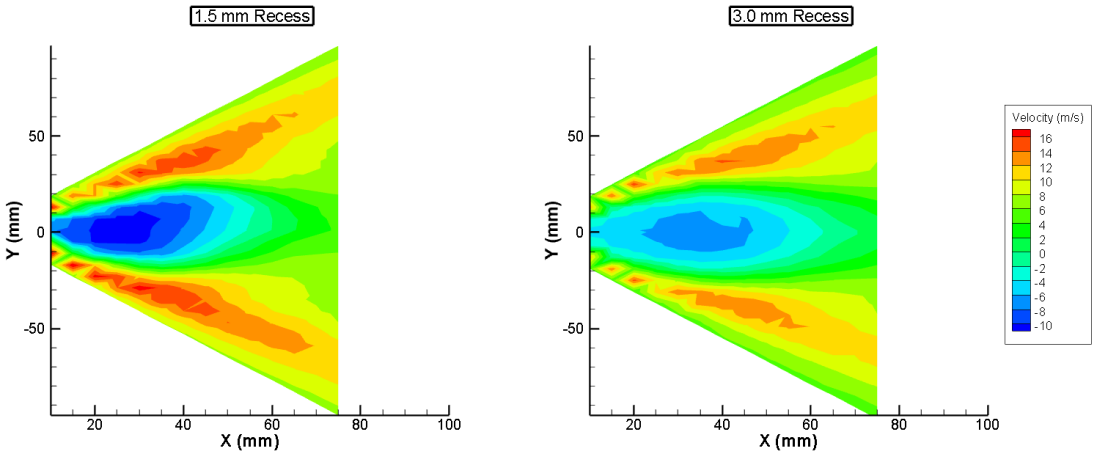

Figure 2.38: Comparison of Axial Velocities for Different Recess Lengths.

Velocity distributions of the droplets for two different recess are quite close to each other. Magnitudes of the velocities for 1.5 mm recess length are higher than 3 mm recess length. The SMD distribution of sprays for test 9 and test 11 were presented and compared in Figure 2.39.

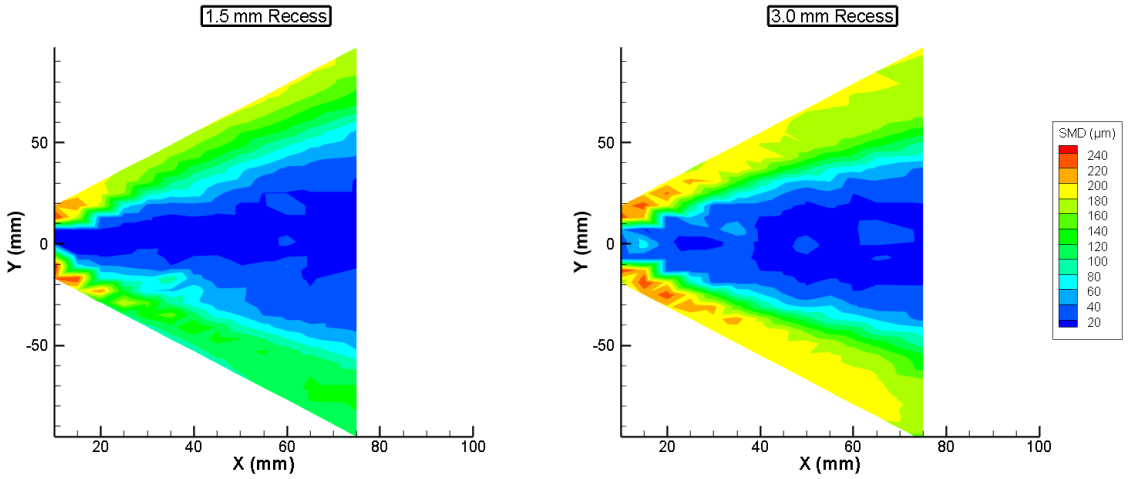

Figure 2.39: Comparison of SMDs for Different Recess Lengths.

Spray cone angle measurements were carried out for the coaxial injector as done to its comprising atomizers. Spray cone angles were measured for test 8, test 9, test 10, test 11. As indicated in Table 2.5, the inner atomizer flow rate for test 8 is 7.5 l/m whereas, the flow rate of the outer atomizer is 2.1 l/m and for test 9, the flow rate of the inner atomizer is 10.3 l/m whereas the flow rate of the outer atomizer is 2.9 l/m. The recess length is 1.5 mm for both tests. The other two measurements were carried out for 3 mm recess length. As indicated in Table 2.5, the inner atomizer flow rate for test 10 is 7.5 l/m whereas, the flow rate of the outer atomizer is 2.1 l/m. For test 11, the flow rate of the inner atomizer is 10.3 l/m whereas the flow rate of the outer atomizer is 2.9 l/m. Details of the conducted tests, and measured spray cone angles were given in Table 2.6.

Table 2.6: Measured Spray Cone Angles of Coaxial Injector.

Test Name	Recess Length [mm]	Inner Atomizer Q [l/m]	Outer Atomizer Q [l/m]	O/F Ratio	Spray Cone Angle (°)
Test 8	1.5	7.5	2.1	3.6	75.76
Test 9	1.5	10.3	2.9	3.6	85.82
Test 10	3.0	7.5	2.1	3.6	74.12
Test 11	3.0	10.3	2.9	3.6	79.59

As can be seen from Table 2.6, coaxial injector spray cone angle increases with increasing flow rate. Also, comparing the different recess lengths at the same flow rate shows that recess length has an essential impact on the spray cone angle. For a lower recess length, the spray cone angles are larger. Spray images for test 8 and test 9 were illustrated in Figure 2.40.

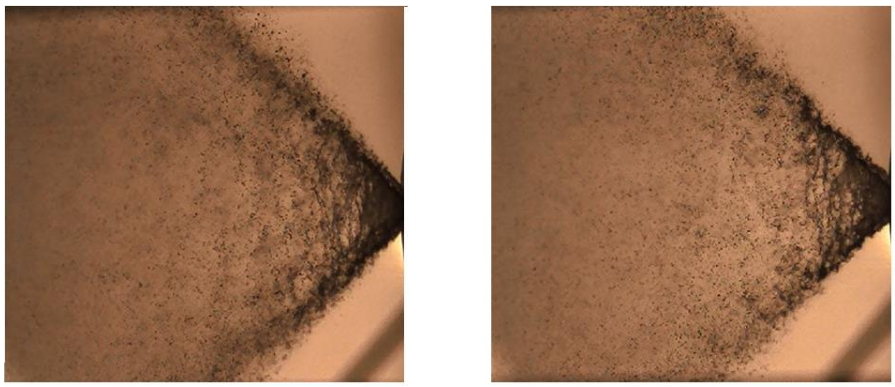

Figure 2.40: Comparison of the Sprays for Test 8 and Test 9.

Comparing the test 8 and test 9 shows that, similar to its comprising atomizers, as the injection pressure increases spray cone angle increases and breakup length decreases.

CHAPTER 3

NUMERICAL INVESTIGATION WITH COMPARISON TO MEASUREMENTS

3.1. Introduction

In this chapter, numerical analyses were conducted for the inner and the outer atomizer standalone and the coaxial injector configurations. Then, the numerical analyses results were compared with the experimental results, and the results were discussed. Firstly, the reservoirs which were designed to deliver uniform and the same amount flow to the tangential inlets of the atomizers were analyzed. The results of analyses were evaluated in terms of the uniformity of flow and the mass flow rate equivalency at the tangential inlets. Secondly, two-dimensional axisymmetric swirl analyses were performed for the inner and the outer standalone operations at various flow rate values. After that, three-dimensional VOF analyses were conducted for the same flow rates as axisymmetric analyses. All the calculations were done in a transient manner. Lastly, numerical analyses results and the experimental results were compared and discussed. The results were presented and examined in the following sections.

3.2. Governing Equations of the Analyses

In the numerical modeling of the reservoir analyses, two-dimensional axisymmetric analyses and three-dimensional analyses laminar, incompressible and steady Navier-Stokes equations were solved.

For the two-dimensional axisymmetric and three-dimensional analyses, Volume of Fluid (VOF) modeling technique was used to determine the interface between two phases. VOF is a free surface modeling method to track interaction between the multiple phase flows. So, for the two-dimensional axisymmetric and three-

dimensional analyses along with the Navier-Stokes equations, an additional equation was solved to find volume fraction of every cell of the solution domain.

Laminar, incompressible, and unsteady Navier-Stokes equations were solved in the analyses. For two-dimensional axisymmetric and three-dimensional analyses, the results shared for two phases. Conservation of mass flow is given in equation 3.1, and conservation of momentum is presented in equation 3.2.

$$\frac{\partial \rho}{\partial t} + \nabla.(\rho V) = 0 \qquad 3.1$$

$$\frac{\partial}{\partial t}\left(\rho \vec{V}\right) + \nabla.\left(\rho \vec{V}\vec{V}\right) = -\nabla(P) + \nabla.\left[\mu\left(\nabla \vec{V} + \nabla \vec{V}^{T}\right)\right] + \rho \vec{g} + \vec{F} \qquad 3.2$$

VOF shows the volume fraction of liquid to a total volume of liquid and gas by solving equation 3.3 for every cell in the solution domain.

$$a_l + a_g = 1 \qquad 3.3$$

When;

a_l=1 cell is full with liquid

a_l=0 cell is full with gas

0< a_l<1 cell partially filled with gas

The sum of the volume fraction of the two phases always equal to one. Phase fraction representation for the VOF was illustrated in Figure 3.1. The blue cell represents the liquid and, the red cells represent the gas phase. The volume fraction of the liquid was indicated in each cell.

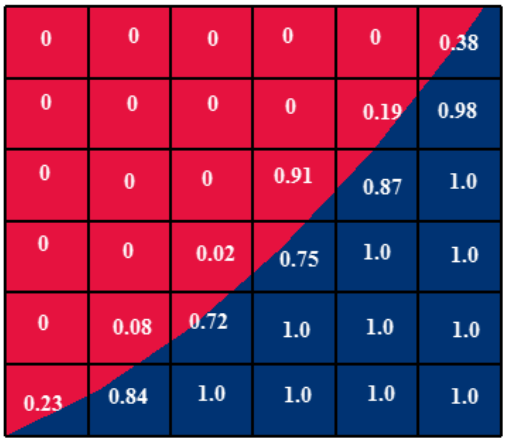

Figure 3.1: VOF Phase Representation.

3.3. Reservoir Analyses

In the RD-0110 rocket engine injector, the inner and the outer atomizers both have six tangential inlets. To ensure that the flow coming to these inlets was uniform and equally distributed, reservoirs at three different sizes were designed and analyzed both for the inner and outer atomizers.

In the analysis, the reservoir was assumed to be fully filled with water. Inlet and outlet of the reservoir were defined as the mass flow inlet and the pressure outlet respectively. Reynolds number at the tangential inlets was calculated for different mass flow rates, and laminar or SST k-omega turbulence model was solved according to the Reynolds number. Calculations were performed transiently with 10^{-6} second time step and mass flow rates through each of the tangential inlets were recorded at each time step. The results of the analysis for the inner and the outer atomizers were presented in the following sections.

3.3.1. Determination of the Reservoir Size for the Inner Atomizer

The designed reservoirs for the inner atomizer were shown in Figure 3.2. They were solved numerically to assess how well the mass flows were distributed to the tangential

inlets. The solutions were performed at a mass flow rate of 0.18 kg/s, using the ANSYS FLUENT software pressure-based solver with the k-omega SST turbulence model. Mass flow inlet and pressure outlet boundary conditions were applied at the inlets and outlets of the reservoirs, respectively as shown in Figure 3.3. In the analyses, a turbulence model was needed because the Reynolds number in the tangential inlets were above the critical level. All the calculations were done in a transient manner for 600 milliseconds, and then the mass flow rates to the inlets were plotted as shown in Figure 3.4 for the inner atomizer. In the figure, inlets were numbered from 1 to 6. For each inlet the mean mass flow rate was then computed from the transient results. The calculated mean values for "option 2" were shown in Figure 3.4. The results indicate that while the reservoir size increases the mass flow rates are distributed to tangential inlets more evenly. The maximum deviations between the mass flow rates of the tangential inlets do not exceed 2.1% for the evaluated reservoirs as indicated in Table 3.1. Therefore, for ease of placement of the injector in the test setup, the reservoir which was labeled as "option 2" in Figure 3.2 was chosen. Isometric view of the investigated reservoirs was shown in Figure 3.2.

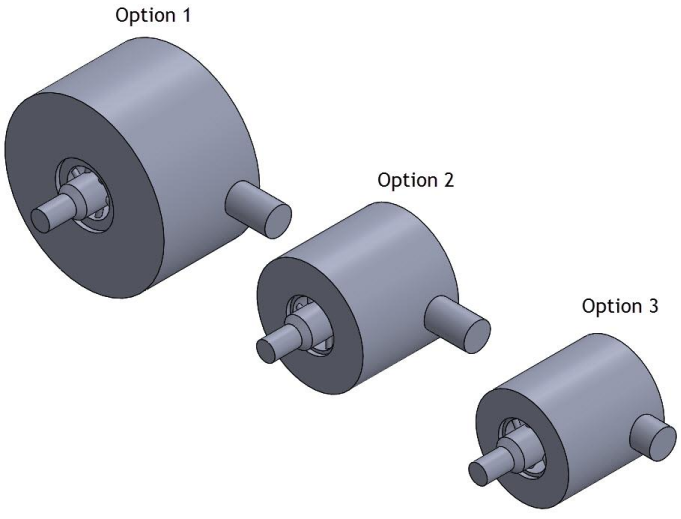

Figure 3.2: Isometric view of Different Size Reservoirs for the Inner Atomizer.

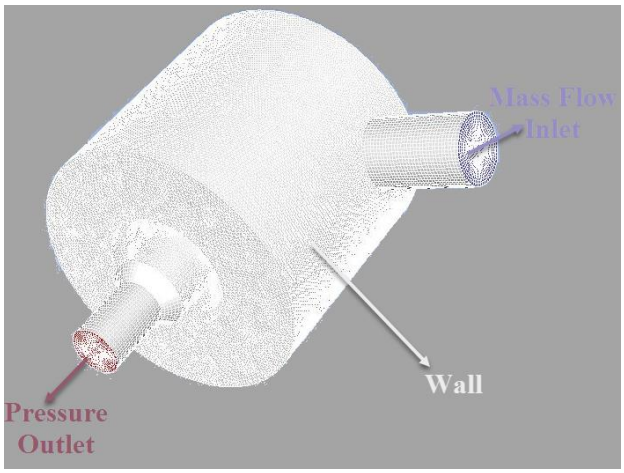

Figure 3.3: Applied Boundary Condition for the Inner Atomizer Reservoir.

Transient mass flow rates through the tangential inlets for the "option 2" were plotted as in Figure 3.4.

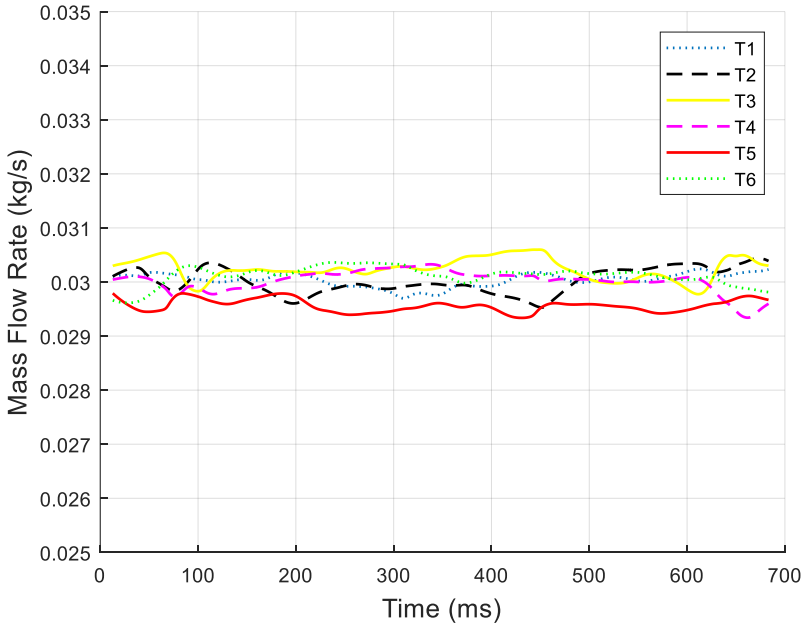

Figure 3.4: Mass Flow Rates through the Tangential Inlets for the Inner Atomizer Reservoir.

Volumes of the designed reservoirs and the mass flow rates equality through the tangential inlets for the reservoirs were tabulated in Table 3.1.

Table 3.1: Mass Flow Rates Equality through the Tangential Inlets for Different Reservoir Size.

	Volume (mm^3)	Max. Deviation from Mean Mass Flow Rate (%)
Option 1	94073	%1.12
Option 2	39418	%1.33
Option 3	28240	%2.10

For the selected reservoir size, mean mass flow rates through the tangential inlets and the deviation from mean values were tabulated in Table 3.2.

Table 3.2: Mass Flow Distribution through Tangential Inlets.

Tangential Inlet ID	Mean Mass Flow Rate (kg/s)	Deviation from Mean Mass Flow Rate (%)
T1	0.0300	> 0.1
T2	0.0300	> 0.1
T3	0.0302	0.81
T4	0.0300	> 0.1
T5	0.0296	1.33
T6	0.0301	0.37

3.3.2. Determination of Reservoir Size for the Outer Atomizer

Similar to the inner atomizer reservoir, reservoirs with different volumes were numerically investigated in terms of mass flow distribution equality for the outer atomizer as well. The isometric view of reservoirs with a different size was shown in Figure 3.5.

Figure 3.5: Isometric view of Different Size Reservoirs for Outer Atomizer.

As done in the inner atomizer reservoir, all reservoir options were calculated transiently at a flow rate of 0.06 kg/s mass flow rate. Similarly, as in the inner atomizer reservoir, as the size of the reservoir increases, the mass flow rate through the tangential inlets are closer to each other. Size of the evaluated reservoirs and the max deviation from the mean mass flow rate were presented in Table 3.3.

Table 3.3: Mass Flow Rates Equality for Outer Injector through the Tangential Inlets for Different Reservoir Sizes.

	Volume (mm^3)	Max. Deviation from Mean Mass Flow Rate (%)
Option 1	2596.31	2.6
Option 2	4316.26	1.9
Option 3	7915.18	1.7

For all the options evaluated, the maximum deviation from the mean mass flow rate is an allowable level. The reservoir was labeled as "option 2" in Table 3.3 was selected since deviation does not exceed 2% and it is easier to place in the test setup than a bigger option. Transient mass flow rates through the tangential inlets for the "option 2" were plotted in Figure 3.6.

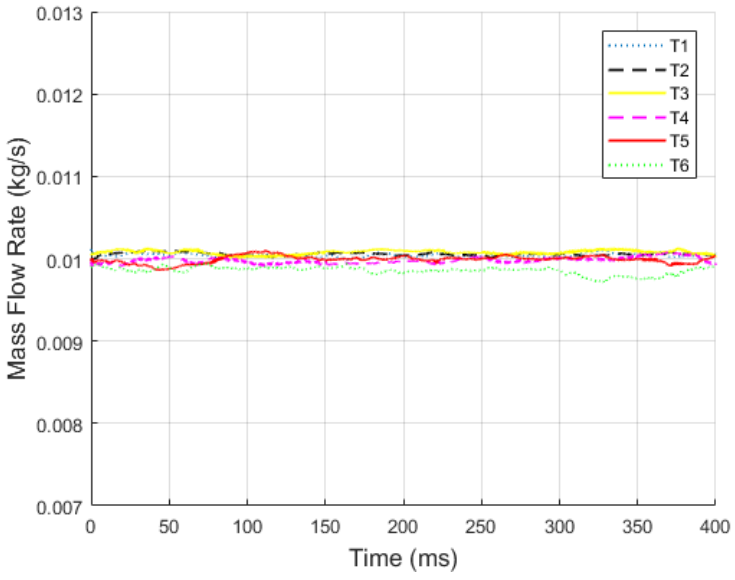

Figure 3.6: Mass Flow Rates through the Tangential Inlets for the Outer Atomizer Reservoir.

3.4. Two-Dimensional Axisymmetric Analyses

Flow inside and outside of the coaxial pressure swirl injectors are quite complicated due to the presence of liquid and gas phases in the flow. To model and investigate this multiphase flow, the VOF method was used in CFD analysis. Analyses were done via commercially available ANSYS FLUENT software. All the analyses were performed in a transient manner. The pressure-based solver was used as recommended in the software manual for VOF analysis. Pressure-velocity coupling was used as the solution method. In the model, the air was defined as an incompressible ideal gas, and the water was defined as an incompressible liquid.

The 2D axisymmetric swirl model was used in calculations to reduce the computing costs. In the analyses, the mass flow inlet and the pressure outlet boundary conditions were applied at the inlets and outlets of the atomizers respectively. The outside of the injector was defined as pressure outlet, and no-slip conditions were applied to the walls of the injector as shown in Figure 3.7.

Tangential and radial velocities through the slit (mass flow inlet) were defined by considering conservation of the mass and angular momentum [33],[34],[35]. Despite the fact that, Reynolds number of flow through the tangential inlet was from 11000 to 28000 for the mass flow rates which were tested, the solver was chosen laminar due to the laminarising effect of the swirling flow [36],[37]. Similarly, Borujerdi et al [38] solved the flow region inside the injector with both laminar and turbulent model, and their results demonstrated that laminar solution agrees better with experimental data although the Reynolds number is around 18000. Also, from the reservoir analysis, it was seen that although turbulence occurs within the tangential inlets of injectors at high mass flow rates, this turbulent flow does not maintain within the body of the atomizer since swirling forces inside the injector laminarise the flow as stated in Dash's study [36]. The Geo-Reconstruct method was used as a volume fraction representation method since it gives better results in phase interaction.

The mass flow rate through the slit was defined considering conservation of the mass and angular momentum as following [33]. Since there are six tangential inlets and these inlets are not axisymmetric in the real case, an equivalent annular inlet needs to be defined for the axisymmetric solution. Fu [23] used this annular inlet as the diameter of the tangential inlet. Similar to Fu's work, the annular inlet was taken as a diameter of the tangential inlet as shown in Figure 3.7. In addition to the atomizer's internal geometry, downstream of the atomizer was numerically investigated. As the downstream computational domain was extended 20 mm after the nozzle exit both in axial and radial directions. This distance roughly corresponds to 7.5 times the radius of the discharge nozzle (R_n). Similarly, Chen and Yang [33] used $10R_n$ in both axial and radial directions in their work. Edges of this extended solution domain were defined as the pressure outlet, and the x-axis was defined as the axis. Applied boundary conditions for analysis of the inner and the outer atomizers were shown in Figure 3.7 and Figure 3.8 respectively.

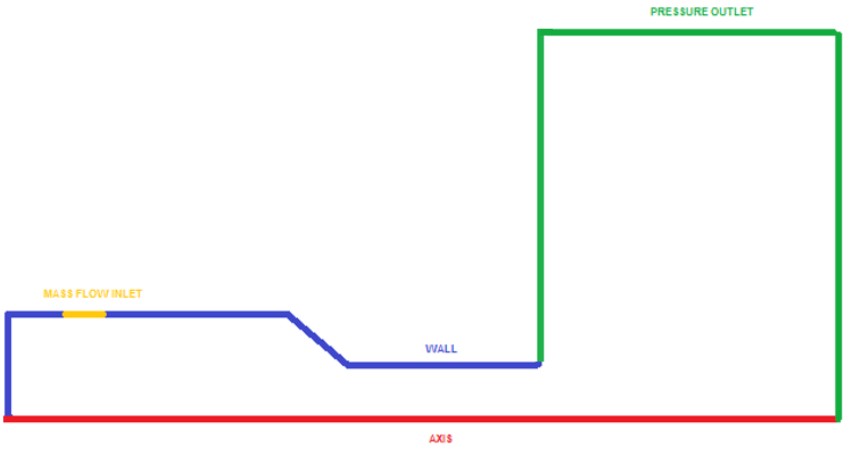

Figure 3.7: Applied Boundary Conditions of the Inner Atomizer Axisymmetric Analysis.

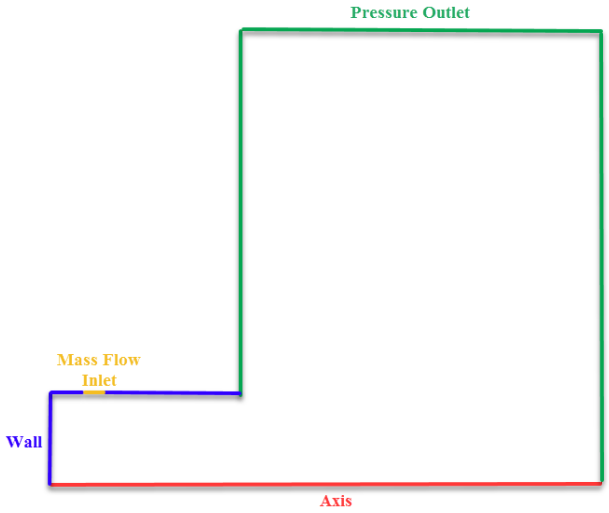

Figure 3.8: Applied Boundary Conditions of the Outer Atomizer Axisymmetric Analysis.

Conservation of mass and swirl strength were used similar to Similarly Wang's work to set the radial and tangential velocity of the flow at the mass flow inlet boundary. In the RD-0110 injector, the swirl directions of the inner and the outer atomizer sprays are in the clockwise direction due to the position of the tangential inlets. Path of the flow inside of the atomizer was illustrated in Figure 3.9. Top view of the swirl chamber cross was presented and flow directions were indicated with arrows.

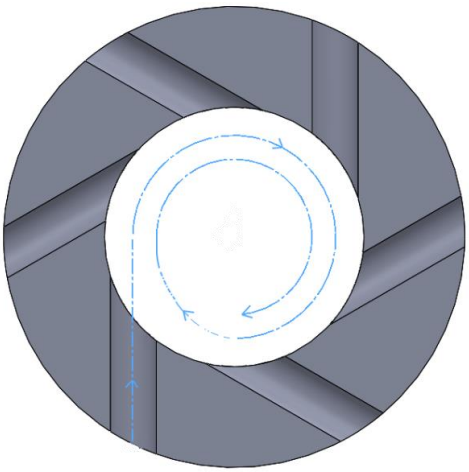

Figure 3.9: Rotation Direction of the Fluid in the Swirl Chamber.

Assuming that perfectly uniform liquid flow gets into the atomizer from all of the tangential inlets, the average velocity at the tangential inlets were calculated as below;

$$V_a = \frac{\dot{m}}{\rho_l A_t n_t} \tag{3.4}$$

Tangential velocity at the equivalent inlet was calculated as:

$$V_t = V_a \frac{r_s - r_t}{r_s} \tag{3.5}$$

Radial velocity at the equivalent inlet was calculated as:

$$V_r = \sqrt{{V_a}^2 - {V_t}^2} \tag{3.6}$$

Where $\dot{m}$ is the total mass flow through the swirl chamber of the injector, ρ_l is the density of the liquid, A_t is an area of the one tangential inlet, n_t is a number of tangential inlets r_s is the radius of the swirl chamber and r_t is the radius of the tangential inlet.

In the calculations, the surface tension of the water in the air was assumed to be constant and was taken as 0.072 N/m [39].

3.5. Three-Dimensional Analyses

Analyses for the inner and outer atomizer standalone operations as well as for the coaxial swirl injector were performed three-dimensionally at various flow rates. In the analyses, tangential inlets were defined as the velocity inlets, and all sides of the downstream domain were defined as the pressure outlet. No slip boundary condition

was applied to the walls. Boundary conditions applied for the inner atomizer, and the outer was shown by Figure 3.10 and Figure 3.11 respectively.

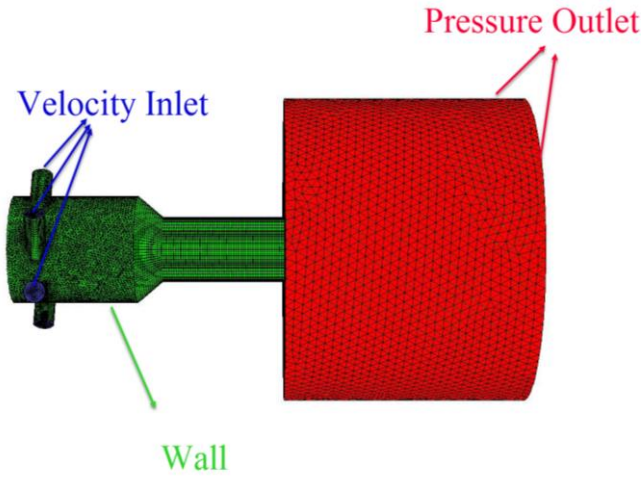

Figure 3.10: The Inner Atomizer Boundary Conditions for 3D Analysis.

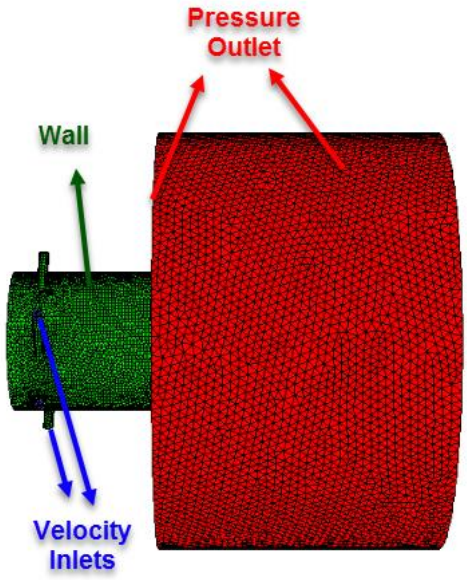

Figure 3.11: The Outer Atomizer Boundary Conditions for 3D Analysis.

The laminar solver was chosen for the analyses as in two-dimensional axisymmetric analyses. Geo-Reconstruct volume fraction method was used to represent the volume fraction in the solution domain. Calculations were performed transiently with a 10^{-6} second time. Spray cone angles were measured for all analysis result based on the volume fraction calculated in the downstream of the injector.

3.6. Results and Discussions

In this section, results of the analyses were presented and compared with the experimental results. Firstly, results for the two-dimensional axisymmetric and three-dimensional analyses were given for various flow rates. Then, the comparison of the analyses and test results for certain flow rates were presented.

3.6.1. Results of the Two-Dimensional Axisymmetric Analyses

Two-dimensional axisymmetric VOF analyses had been carried out for both inner and the outer atomizer at various flow rates. Analyses were performed in transiently with 2.10^{-6} second time step over 30 milliseconds for each case. Phase distribution and the velocity field of the spray were obtained from the analyses. Mean Axial, radial and the swirl velocity of the resulting spray was shown from the atomizer exit to 20 mm distance in both axial and radial directions. Analyses results of the inner and the outer atomizer were presented in the following sections. In the analyses' results graphs, the properties of this extended distance were shown.

3.6.1.1. Inner Atomizer Analyses Results

Results of the two-dimensional axisymmetric analysis for the inner atomizer were presented in this section. Analyses were performed for the flow rates of 6 l/m, 7.5 l/m,

9 l/m, and 10.3 l/m. Mean Axial, radial and swirl velocity distribution of the spray for the 9 l/m were presented in Figure 3.12, Figure 3.13 and Figure 3.14 respectively.

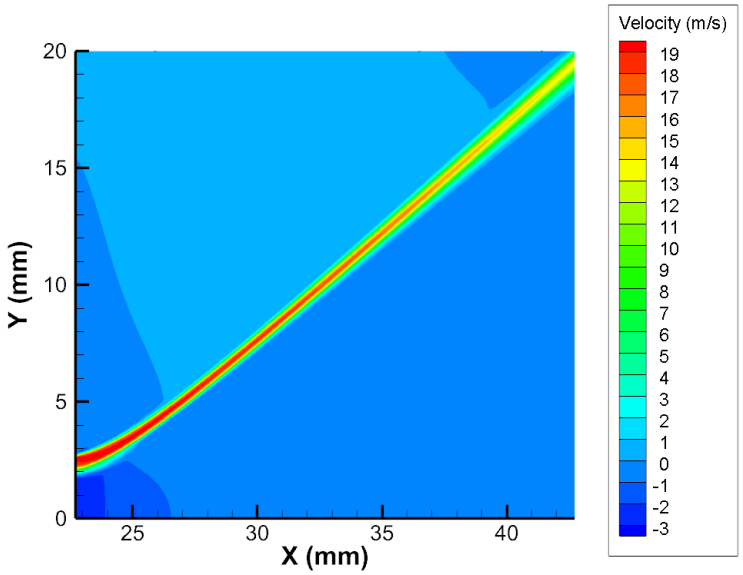

Figure 3.12: Mean Axial Velocity at 9 l/m.

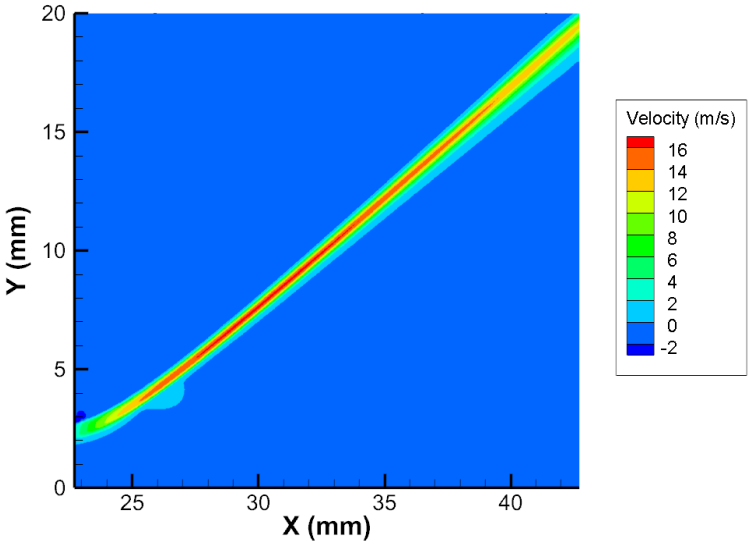

Figure 3.13: Mean Radial Velocity at 9 l/m.

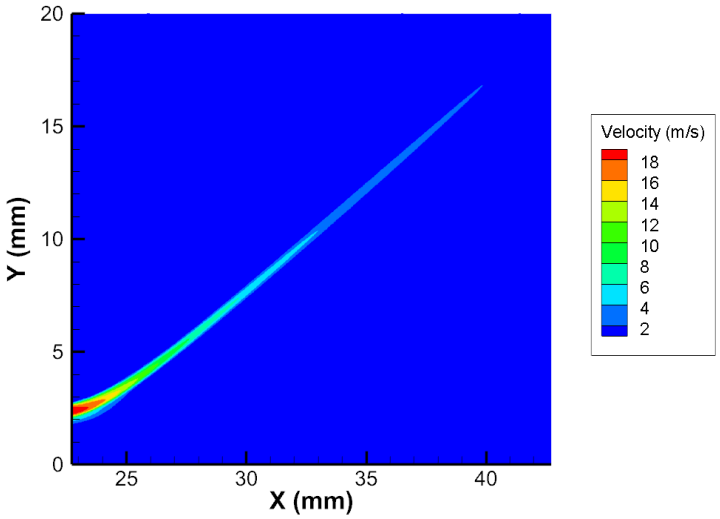

Figure 3.14: Mean Swirl Velocity at 9 l/m.

For 6.0 l/m, 7.5 l/m, 9.0 l/m and 10.3 l/m flow rates axial, radial and swirl velocities were presented in Figure 3.15, Figure 3.16, and Figure 3.17.

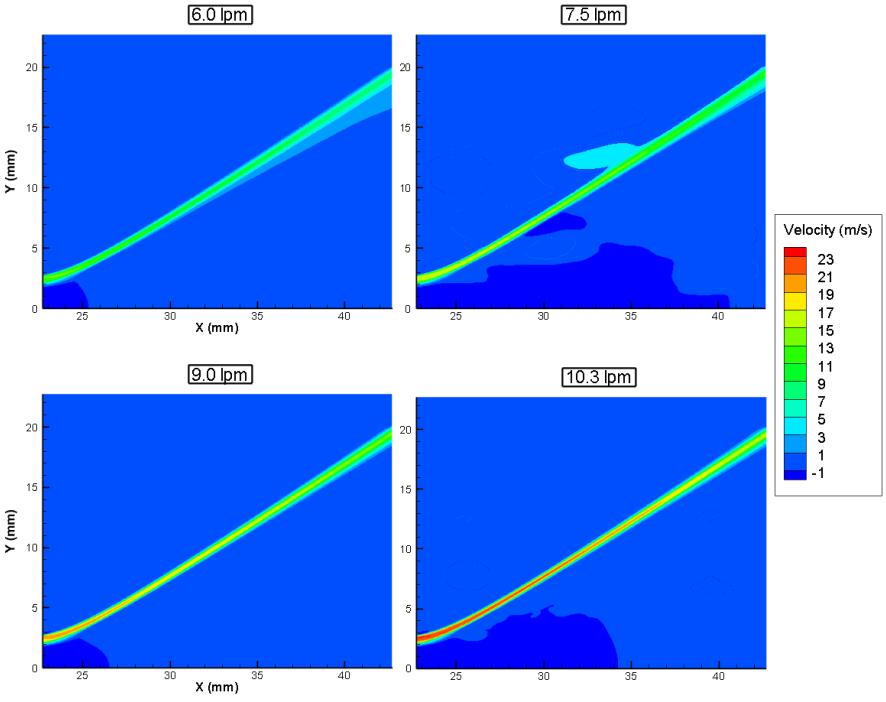

Figure 3.15: Mean Axial Velocity at Various Flow Rates.

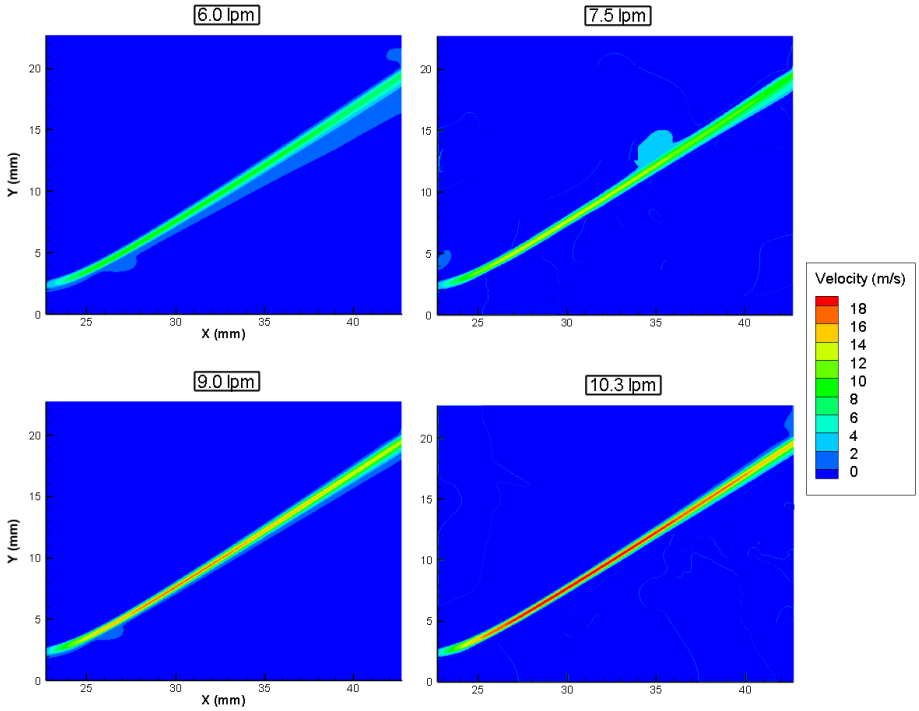

Figure 3.16: Mean Radial Velocity at Various Flow Rates.

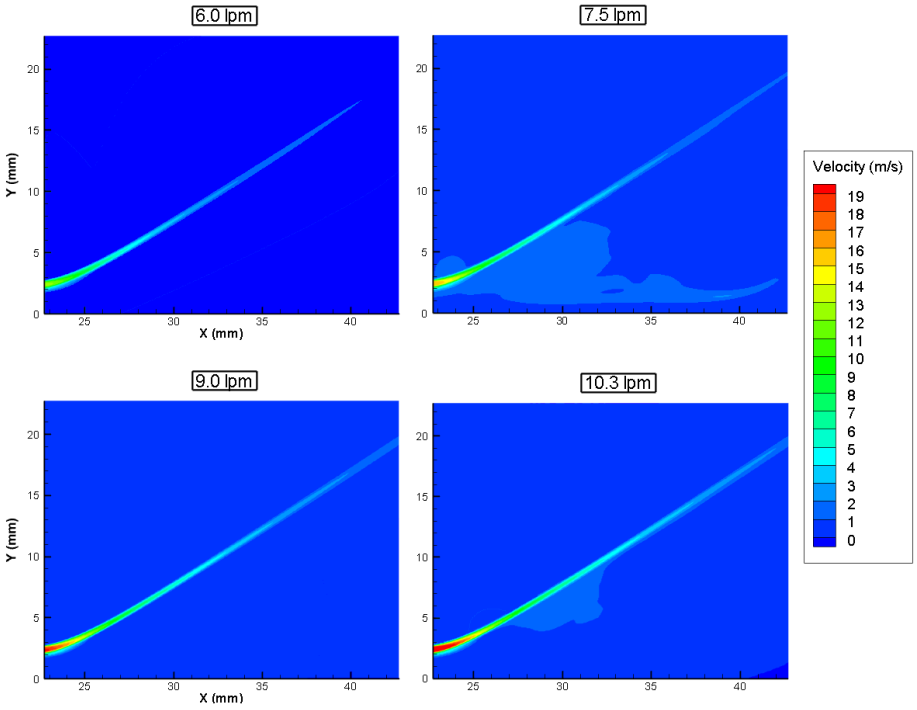

Figure 3.17: Mean Swirl Velocity at Various Flow Rates.

Comparing the analysis results, it can be seen that the velocity of the liquid sheet increases with the increasing flow rate for all the directions. Air moves towards the center of the atomizer and forms an air core. Moreover, the increase of the spray cone angle increases with increasing flow rate can be observed from the results.

Spray cone angles of the inner atomizer analyses were plotted as in Figure 3.18. The marked points on the plot were test points, and the curve was obtained by interpolating the test points.

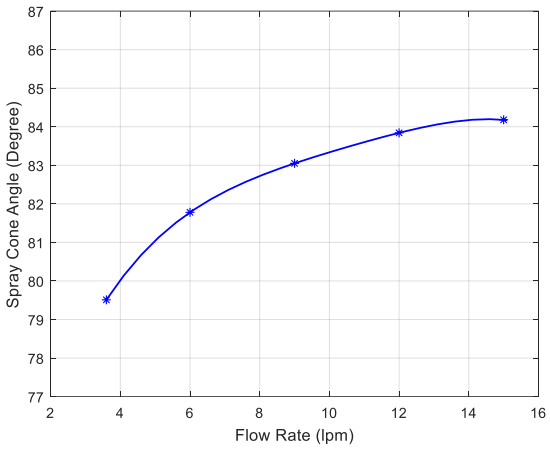

Figure 3.18: Inner Atomizer Spray Cone Angles.

While the flow rate increases spray cone angle increases up to a certain point after that point spray cone angle does not change much, even though the flow rate increases.

3.6.1.2. Outer Atomizer Analyses Results

Results of the two-dimensional axisymmetric analysis for the outer atomizer were presented in this section. Analyses were performed for the flow rates of 2.1 l/m, 2.8 l/m, and 3.5 l/m. Mean phase fractions of the solution domain for these flow rates were presented in Figure 3.19. Mean axial, radial and swirl velocities for these flow rates were presented in Figure 3.20, Figure 3.21, and Figure 3.22.

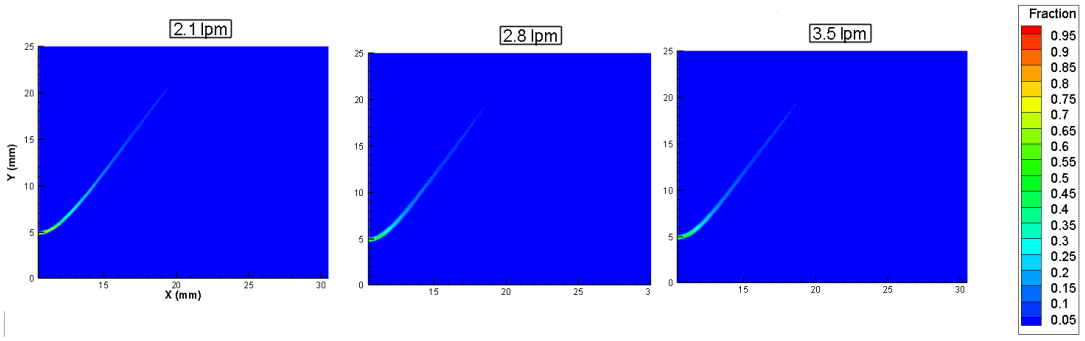

Figure 3.19:Mean Phase Fraction for Outer Atomizer Spray at Different Flow Rates.

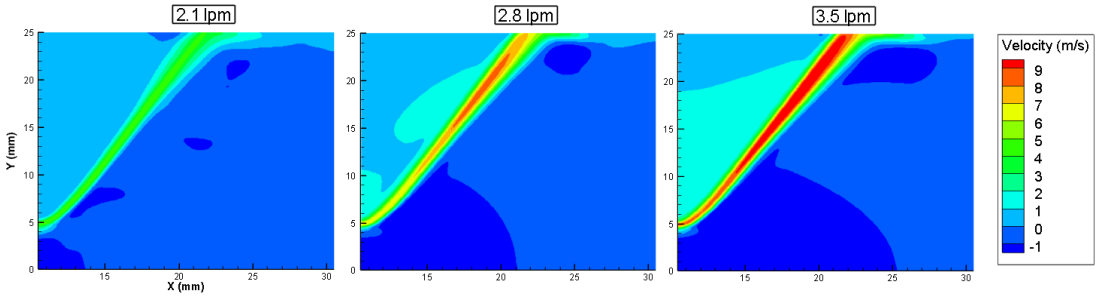

Figure 3.20: Mean Axial Velocity for Outer Atomizer Spray at Different Flow Rates.

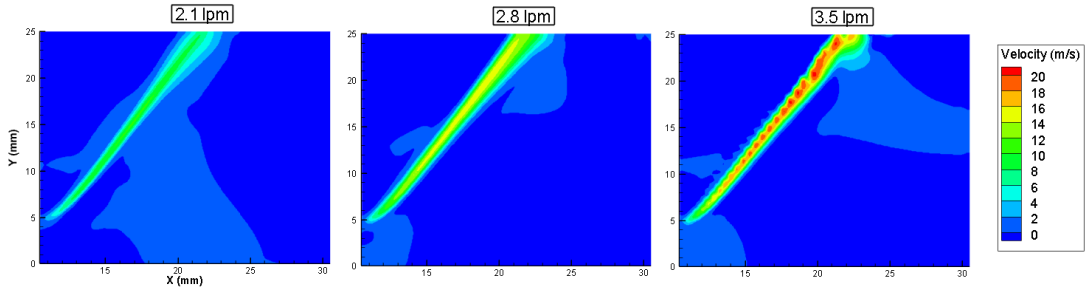

Figure 3.21: Mean Radial Velocity for Outer Atomizer Spray at Different Flow Rates.

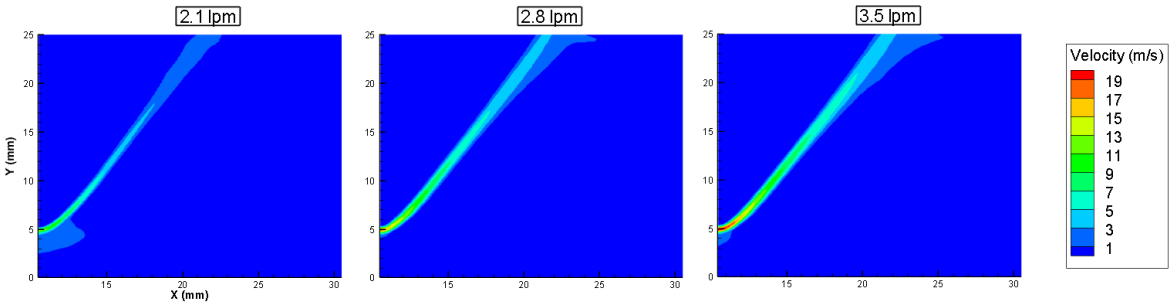

Figure 3.22: Mean Swirl Velocity for Outer Atomizer Spray at Different Flow Rates.

The velocity of the droplets in every direction increases with increasing flow rate as can be seen from the presented figures. Also, similar to the inner atomizer results, at the center of the atomizer air moves towards the atomizer center. Spray cone angles for several flow rates were plotted as shown in Figure 3.23. The marked points on the graph were analyses points, and the curve was obtained by interpolating these points.

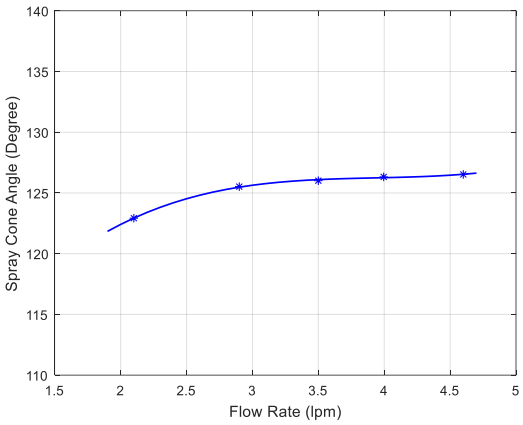

Figure 3.23:Outer Atomizer Spray Cone Angles.

As like inner atomizer spray cone angle of the outer atomizer increases with increasing flow rate up to some point, after that point, the spray cone angle almost become insensible to increase in flow rate.

3.6.2. Mesh Independency Study for 2D Axisymmetric Analyses

The analysis was repeated for three different mesh, and the axial velocity of the spray was compared to prove the obtained solution is independent of the mesh. Element and node numbers of the used meshes were presented in Table 3.4.

Table 3.4: Mesh Independency Study for 2D Axisymmetric VOF Analyses.

	Element Number	**Node Number**
Coarse Mesh	54280	53616
Medium Mesh	84628	83800
Fine Mesh	215465	214319

For the meshes presented in Table 3.4, the analysis is carried out for the 7.5 l/m flow rate. The mean axial velocities of these three different solutions were compared at the 5 mm, 10 mm and 15 mm away from the injector exit. The comparison was presented in Figure 3.24. In the figure y-axis represents mean axial velocity, whereas x axis shows the radial coordinates of the solutions for a fixed axial coordinate.

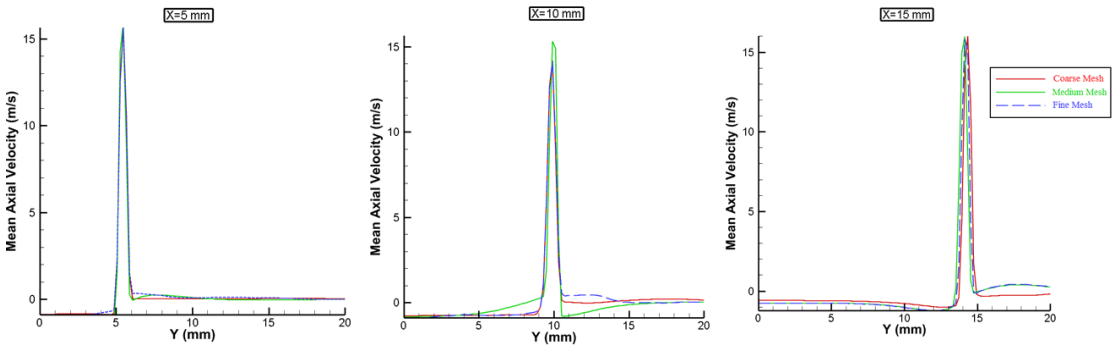

Figure 3.24: Mean Axial Velocity Distribution for Different Meshes.

As presented in Figure 3.24, the velocity distribution of spray barely changes with the changing mesh. So, the results have proved that solutions are independent of the mesh.

3.6.3. Results of the Three-Dimensional Analyses

In addition to two-dimensional axisymmetric analyses, three-dimensional VOF analyses were performed for the inner and the outer atomizer standalone operations and the coaxial injector. The results of the analyses were presented and compared in the following sections.

3.6.3.1. Inner Atomizer Analyses Results

Results of the three-dimensional analyses were presented in this section. Analyses were performed at various flow rates. Mean axial, radial and swirl velocities of the spray were presented for the flow rates of 6 l/m, 7.5 l/m, 9 l/m and 10.3 l/m in Figure 3.25, Figure 3.26 and Figure 3.27. The velocity distribution is obtained on the mid-plane of the downstream flow.

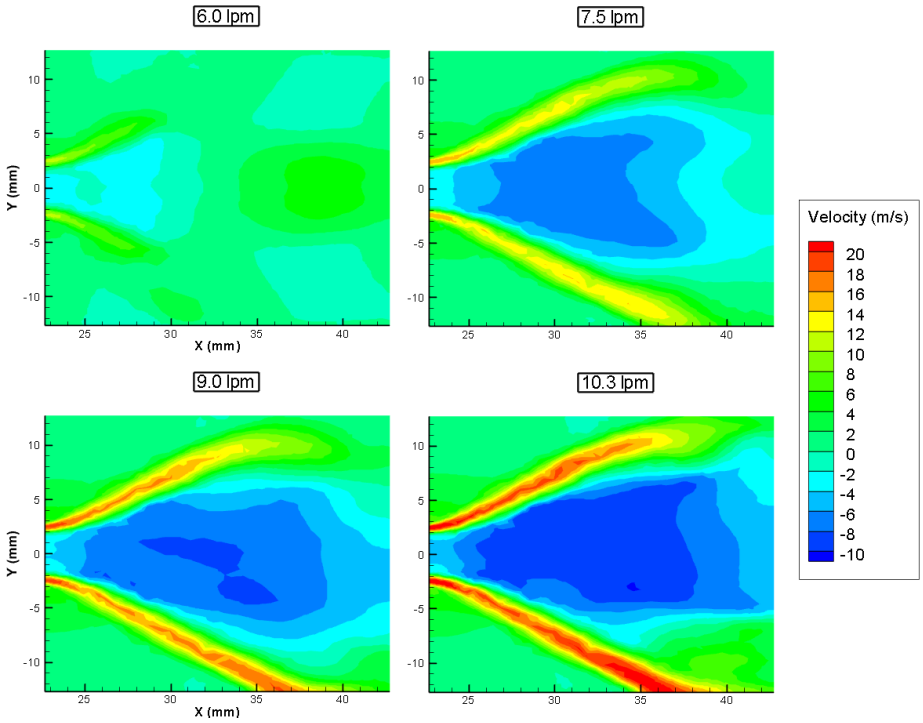

Figure 3.25: Mean Axial Velocity for Inner Atomizer Spray at Different Flow Rates.

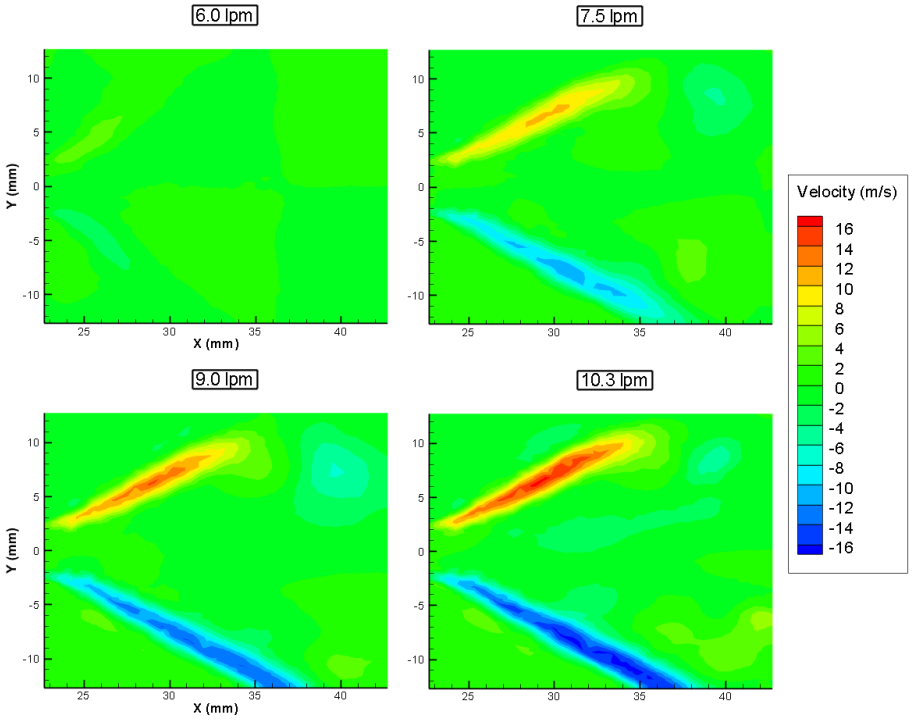

Figure 3.26: Mean Radial Velocity for Inner Atomizer Spray at Different Flow Rates.

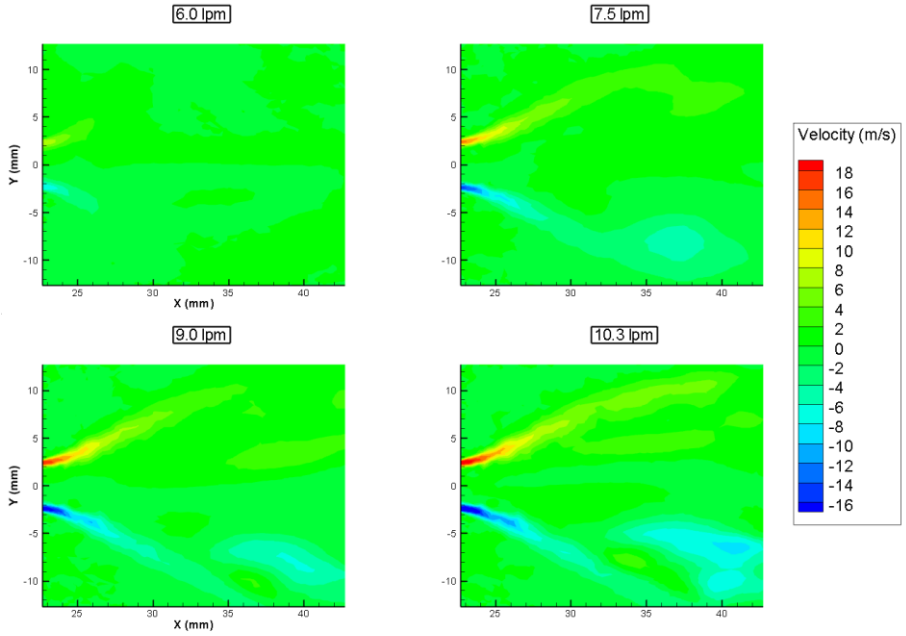

Figure 3.27: Mean Swirl Velocity for Inner Atomizer Spray at Different Flow Rates.

Phase distribution for the same flow rates was also shown in Figure 3.28. The blue color in the contour represents the air, whereas the red color represents the water. Phase fraction is indicated from 0 to 1.

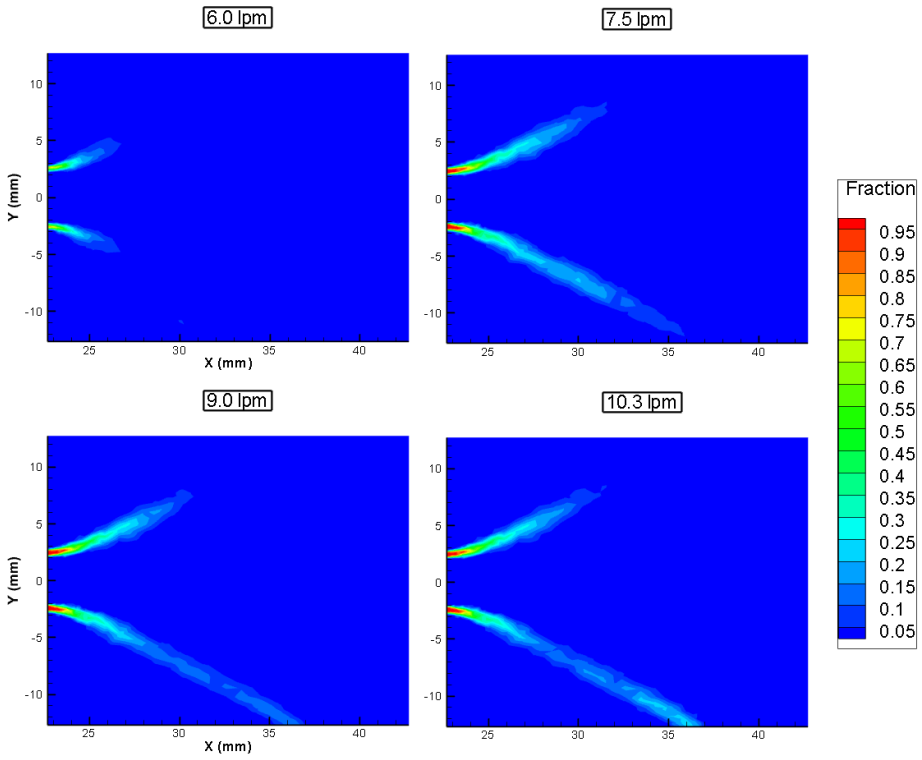

Figure 3.28: Phase Distribution for Different Flow Rates.

From the analyses, it was seen that the velocity of the liquid sheet increases with increasing flow rate, as expected. Also, as the flow rate increases, air penetrates the atomizer with higher velocity. From the test results and the analysis, it was proved that the spray is axisymmetric.

Spray cone angles of the inner atomizer analyses were presented in Figure 3.29. The marked points on the graph were analysis points, and the curve was obtained by interpolating these points.

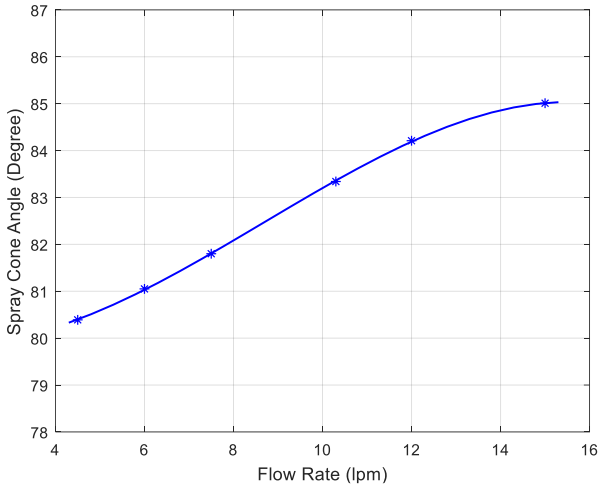

Figure 3.29: Inner Atomizer Spray Cone Angles.

Spray cone angle of the inner atomizer increase with increasing flow rate as like the two-dimensional axisymmetric analyses and the test results.

3.6.3.2. Outer Atomizer Analyses Results

Outer atomizer analyses were performed at various flow rates similar to the inner atomizer. Velocity profiles of the spray were compared for the different flow rates. Also, spray cone angles of the outer atomizer at various flow rates were calculated from the analysis results and plotted in Figure 3.33. For flow rates of 2.1 l/m, 2.8 l/m and 3.5 l/m, mean axial, radial and swirl velocity distributions were presented and compared in Figure 3.30, Figure 3.31, and Figure 3.32 respectively.

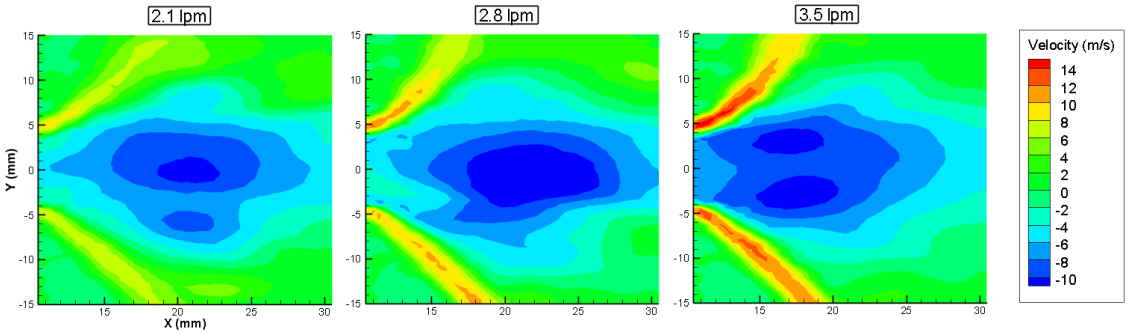

Figure 3.30: Mean Axial Velocity for Outer Atomizer Spray at Different Flow Rates.

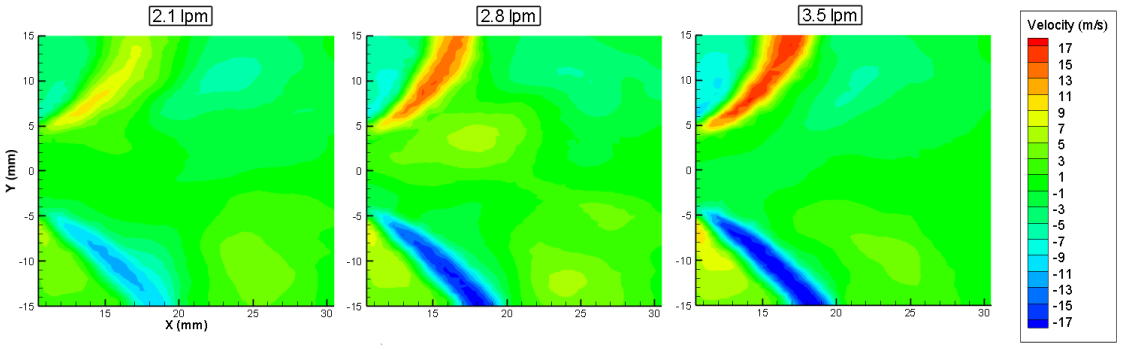

Figure 3.31: Mean Radial Velocity for Outer Atomizer Spray at Different Flow Rates.

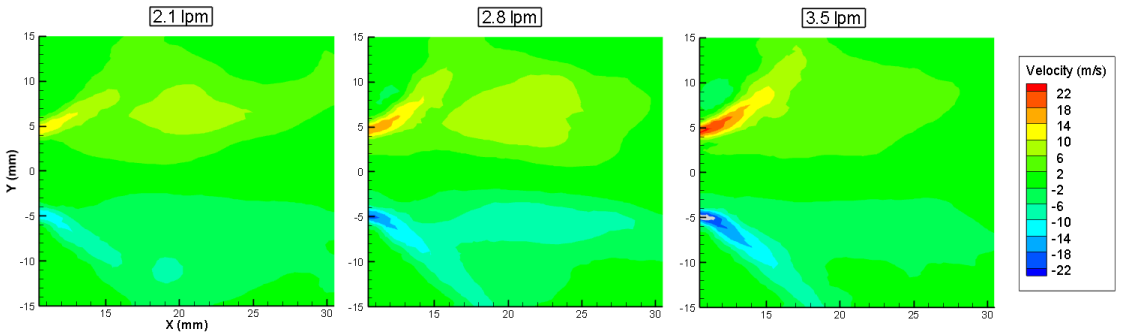

Figure 3.32: Mean Swirl Velocity for Outer Atomizer Spray at Different Flow Rates.

Spray cone angles of the outer atomizer analyses were presented in Figure 3.33. The marked points on the graph were analyses points, and the curve was obtained by interpolating the analyses points.

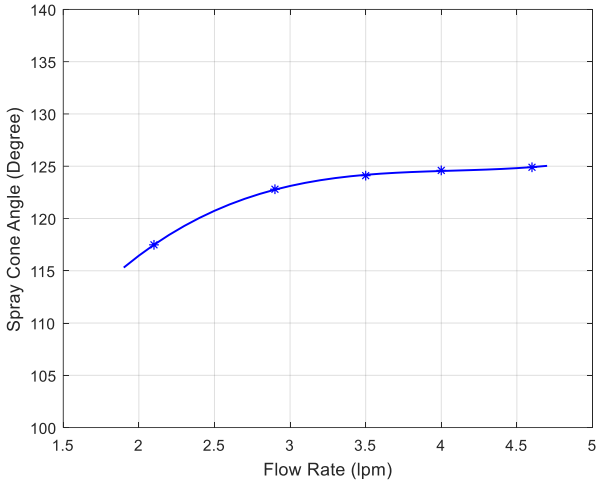

Figure 3.33: Outer Atomizer Spray Cone Angles.

3.6.3.3. Coaxial Injector Analyses Results

The coaxial injector was also analyzed similarly to its comprising atomizer. The result of the analysis for 7.5 l/m oxidizer and 4.68 l/m fuel flow rate, which was named as "test 6" in Table 2.5 were given. Phase fraction of the coaxial injector spray was given in Figure 3.34. The blue color represents the air fraction where the red indicates water. Axial, radial and swirl velocities of the coaxial injector spray were shown in Figure 3.35 and Figure 3.36, and Figure 3.37 respectively.

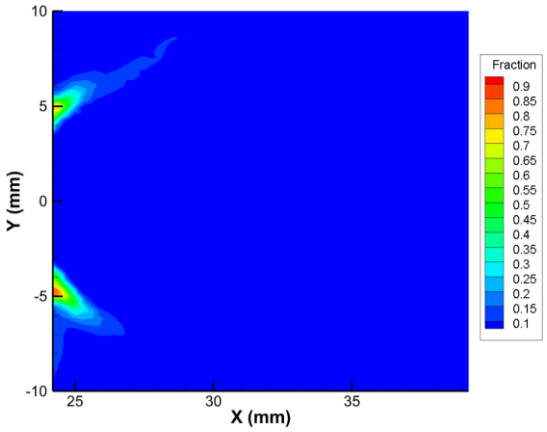

Figure 3.34: Phase Fraction of 7.5 l/m Inner Atomizer 1.6 O/F Rate.

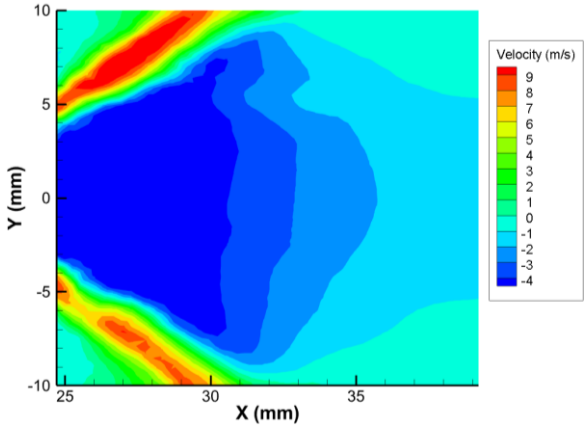

Figure 3.35: Axial Velocity of 7.5 l/m Inner Atomizer 1.6 O/F Rate.

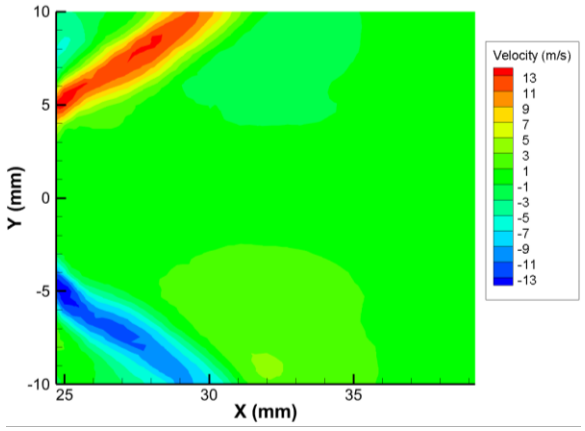

Figure 3.36: Radial Velocity of 7.5 l/m Inner Atomizer 1.6 O/F Rate.

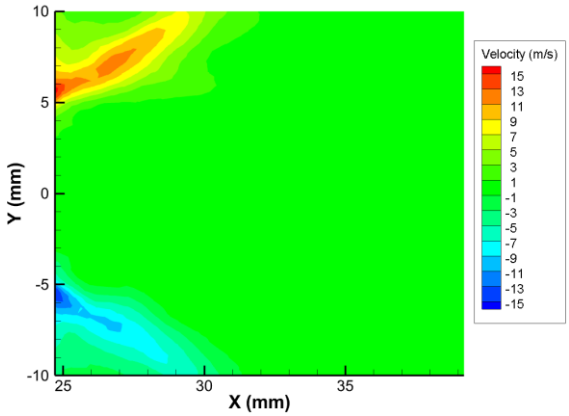

Figure 3.37: Swirl Velocity of 7.5 l/m Inner Atomizer 1.6 O/F Rate.

From the plotted velocity graphs, it can be seen that coaxial injector spray is symmetric with respect to the x-axis as inner atomizer spray. Also, the velocity profile of the coaxial injector is quite similar to the inner atomizer velocity profile.

3.6.4. Mesh Independency Study for Three-Dimensional Analyses

Mesh independency study has been performed to prove analyses results are independent of the mesh generated on the solution domain. Three different meshes were used, as indicated in Table 3.5.

Table 3.5: Mesh Independency Study for 3D VOF Analyses.

	Element Number	**Node Number**
Coarse Mesh	228891	42387
Medium Mesh	462017	84015
Fine Mesh	684451	125369

The analyses were performed for the 3.5 l/m flow rate with the three different meshes indicated in Table 3.5. Mean axial velocities of the spray for the three separate analyses were plotted together at the 5 mm, 10 mm and 15 mm away from the injector exit. The comparison was presented in Figure 3.38. In the figure y-axis represents mean axial velocity, whereas x axis shows the radial coordinates of the solutions for a fixed axial coordinate.

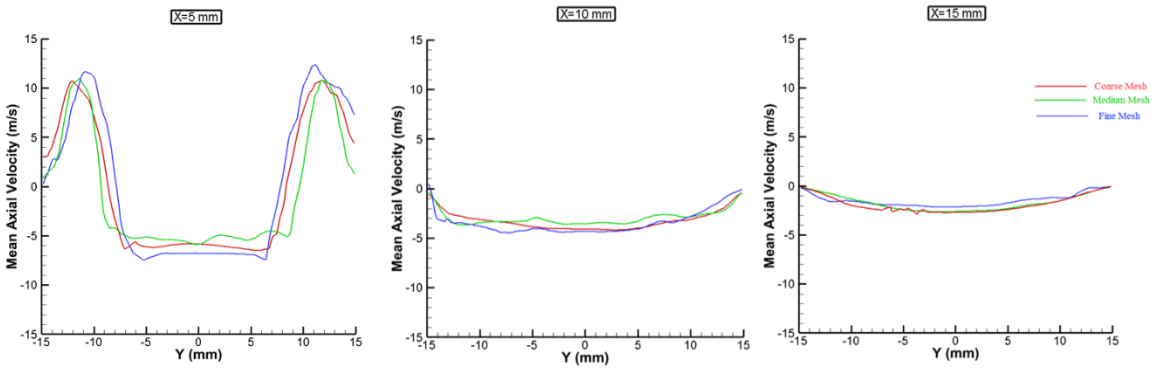

Figure 3.38: Mean Axial Velocity Distribution for Different Meshes.

The mean velocity distribution and the values were quite close to each other for each of the mesh used. The results have proved that solutions are independent of the mesh.

3.6.5. Comparison of Analyses and Test Results

In this section, two-dimensional axisymmetric analyses, three-dimensional analyses, and test results were compared and discussed in detail. In the comparison, axial and radial velocities of the spray were presented for two-dimensional axisymmetric analyses, three-dimensional analyses, and test results. However, for swirl velocity two-dimensional axisymmetric analyses and three-dimensional analyses were compared. Because the PDPA system used is two-dimensional and swirl velocities could not be obtained.

Firstly, numerical and test results of inner atomizer were presented. The comparison was made for the flow rates of 9 l/m and 10.3 l/m flow rates. In the graphs, the analyses results were given with the same distance for both axial and radial directions. However, for the tests, the length is different than the analyses. Since the measurements were carried out 10 mm away from the injector exit as explained previously.

Axial, radial and swirl velocity comparisons for the 9 l/m were presented in Figure 3.39, Figure 3.40, and Figure 3.41.

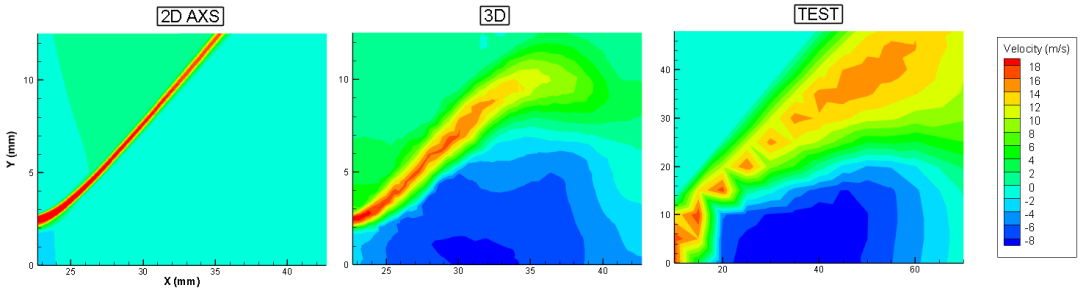

Figure 3.39: Axial Velocity Comparison of Test and Analyses at 9 l/m Flow Rate.

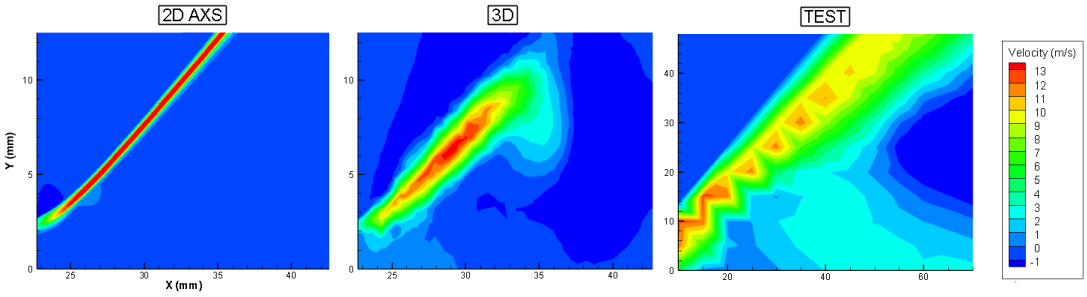

Figure 3.40: Radial Velocity Comparison of Test and Analyses at 9 l/m Flow Rate.

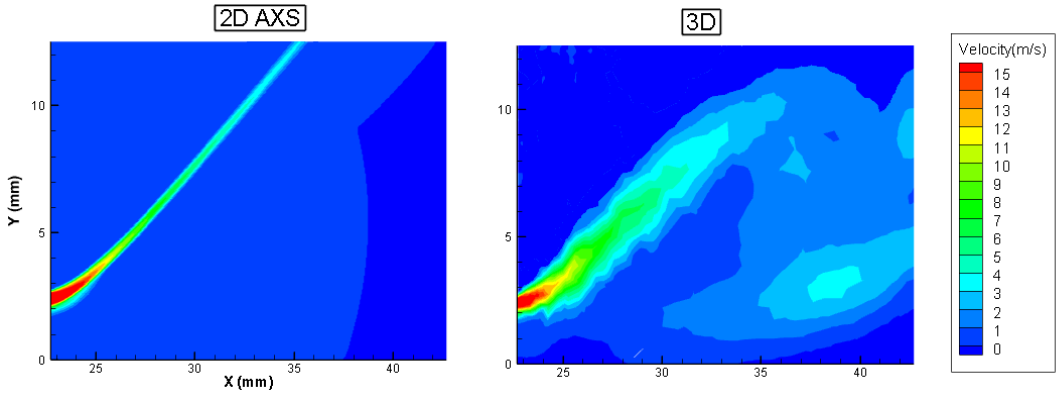

Figure 3.41: Swirl Velocity Comparison of Analyses at 9 l/m Flow Rate.

Axial, radial and swirl velocity comparisons for the 10.3 l/m were presented in Figure 3.42, Figure 3.43, and Figure 3.44.

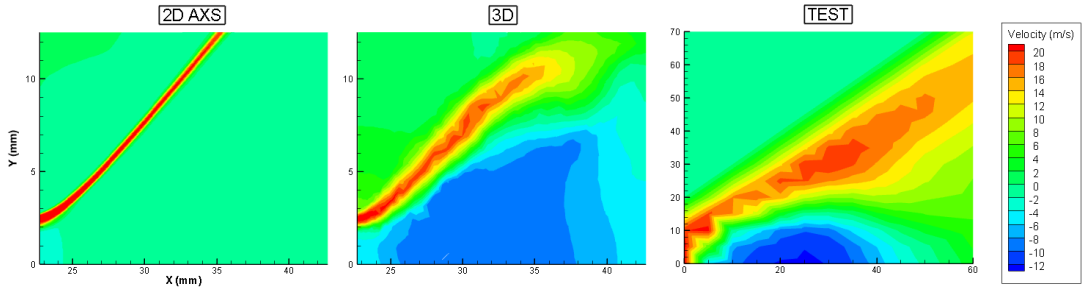

Figure 3.42: Axial Velocity Comparison of Test and Analyses at 10.3 l/m Flow Rate

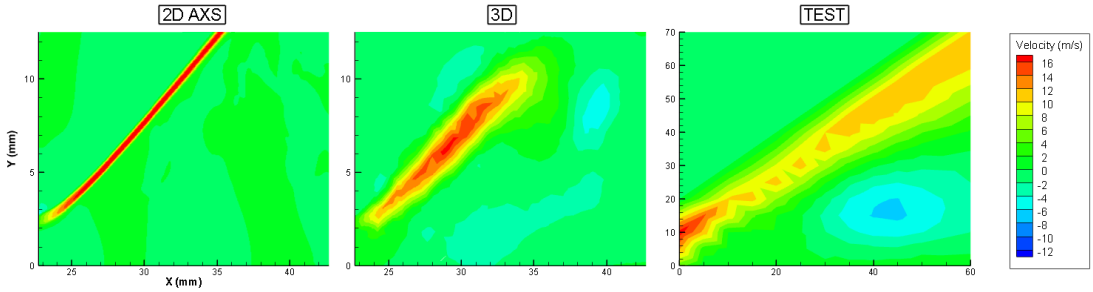

Figure 3.43: Radial Velocity Comparison of Test and Analyses at 10.3 l/m Flow Rate.

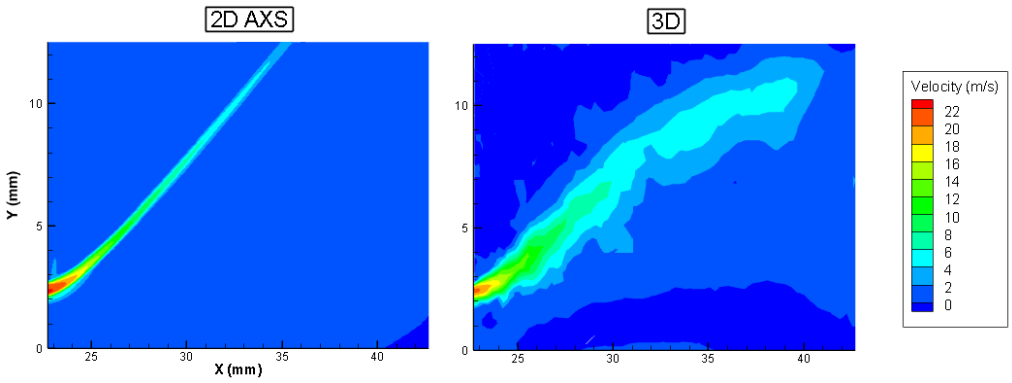

Figure 3.44: Swirl Velocity Comparison of Test and Analyses at 10.3 l/m Flow Rate.

As can be deducted from the presented figures, both two-dimensional axisymmetric and three-dimensional analyses give very close results to experiments and each other. Specifically, three-dimensional analysis is better to capture the velocity of the air. As can be seen from axial velocity comparisons figures (Figure 3.39 and Figure 3.42) negative velocity values in the center of the injector exit are very close for three-dimensional analyses and test results.

Also, the measured spray cone angles of inner atomizer spray for the tests and analyses at different flow rates were compared in Figure 3.45.

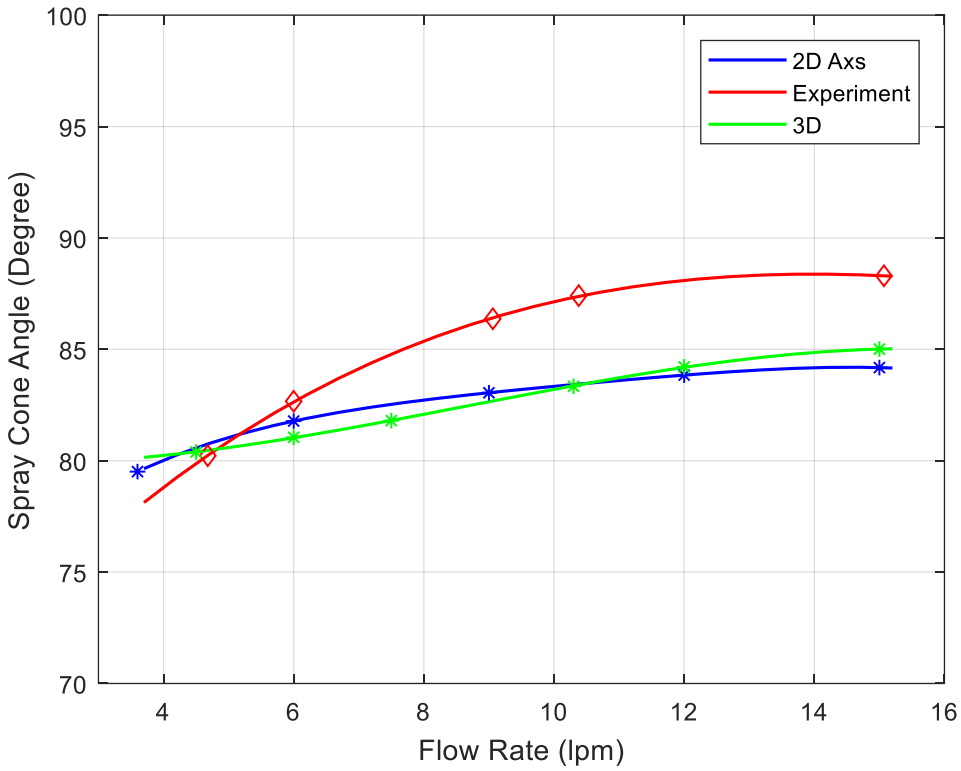

Figure 3.45: Comparison of Spray Cone Angles for the Inner Atomizer.

Comparing the spray cone angles for the inner atomizer it was seen that the calculated spray cone angles and test results are quite close to each other for the investigated flow rate range. Moreover, the curves of the test and analyses results show similar manner. The spray cone angle increases with increasing flow rate up to a certain point. After that point, the spray cone angle almost become insensible to increase in flow rate.

Similar to the inner atomizer, the comparison was also made for the outer atomizer. Two-dimensional axisymmetric and three-dimensional analyses results were compared for a flow are of 2.8 l/m as presented in the following figures.

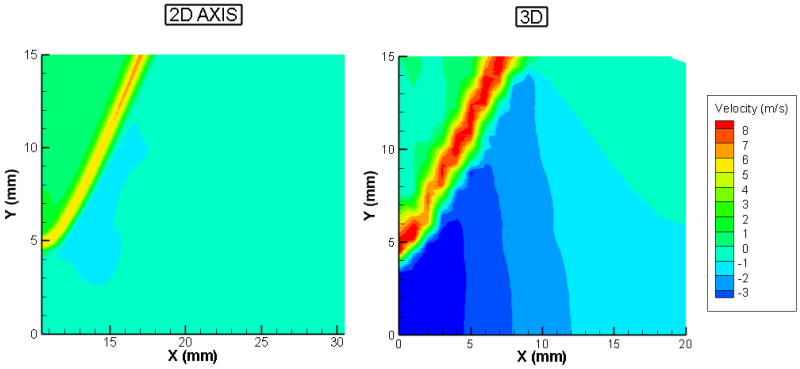

Figure 3.46: Comparison of Axial Velocity for 2.8 l/m Flow Rate.

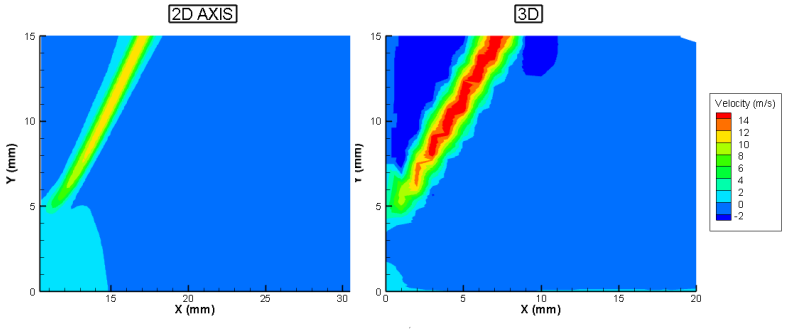

Figure 3.47:Comparison of Radial Velocity for 2.8 l/m Flow Rate.

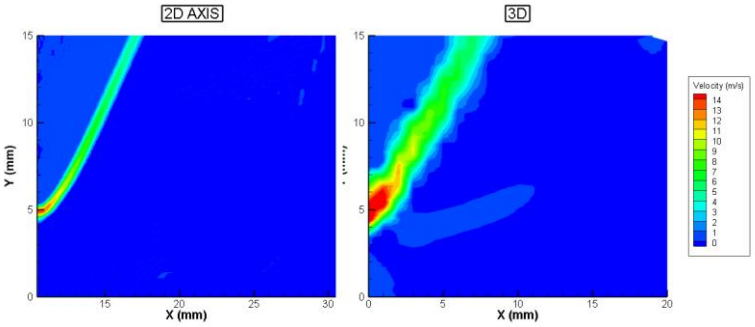

Figure 3.48: Comparison of Swirl Velocity for 2.8 l/m Flow Rate.

From the comparison of the velocities, it can be seen that results are close to each other. Velocities magnitudes of three-dimensional analysis are slightly higher than the

two-dimensional axisymmetric analyses. There are differences between the two solutions because atomizer is not entirely axisymmetric.

In addition to the velocity comparison, spray cone angles were compared. Calculated spray cone angles of two-dimensional analyses, three-dimensional analyses and tests were given in Figure 3.49.

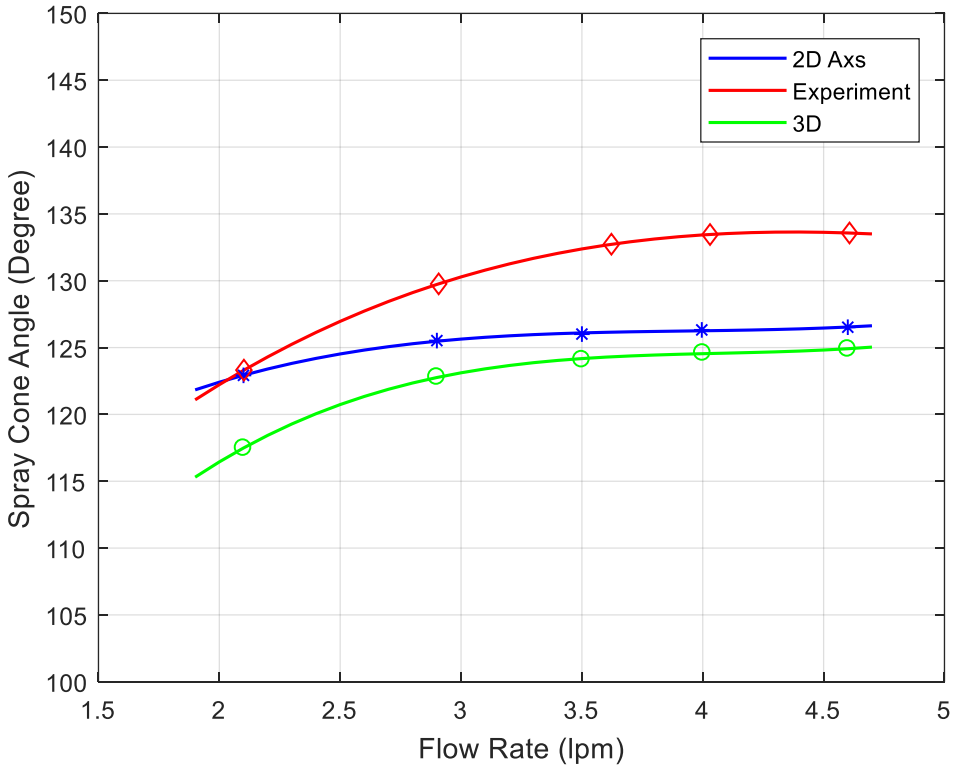

Figure 3.49: Comparison of Spray Cone Angles for the Outer Atomizer

Similar to the inner atomizer, the trend of the curves for test and analyses results are quite close to each other. The difference between the analyses and tests results are not significant considering the application area.

Analyses and test results also compared for the coaxial injector. The result of the three-dimensional analysis and experiment for 7.5 l/m oxidizer and 4.68 l/m fuel flow rate which was named as “test 6” in Table 2.5 were presented together. Comparisons of the axial and radial velocity profile were shown in Figure 3.50 and Figure 3.51.

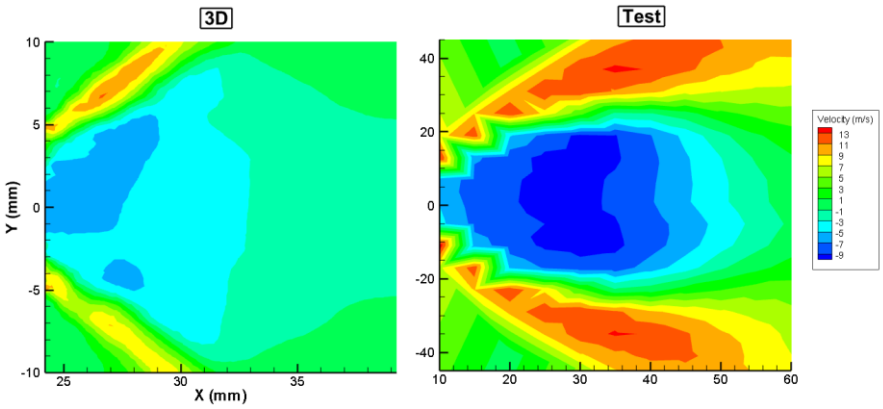

Figure 3.50: Comparison of Axial Velocity for 7.5 l/m Inner Atomizer 1.6 O/F Rate.

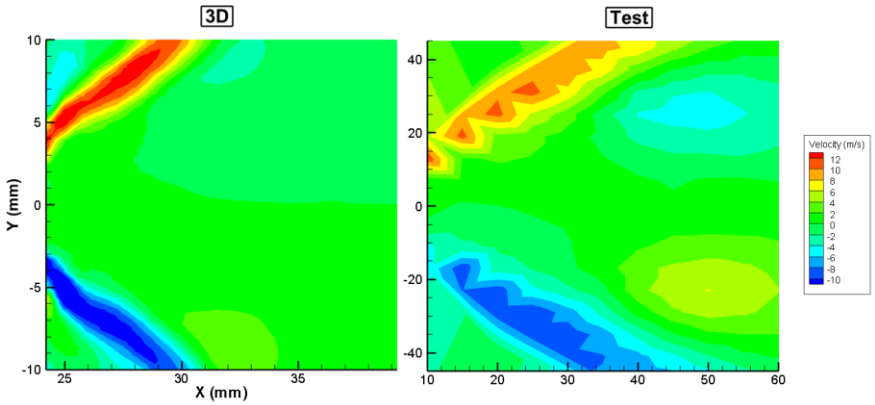

Figure 3.51: Comparison of Radial Velocity for 7.5 l/m Inner Atomizer 1.6 O/F Rate.

CHAPTER 4

CONCLUSION

In this study, coaxial pressure swirl injector and its comprising atomizers were investigated experimentally and numerically. The spray of the coaxial injector and the atomizers were measured with a high-speed shadowgraphy technique for a wide range of flow rates. Two-dimensional velocity profile and particle size distribution were obtained for the coaxial injector and inner atomizer at different flow rates by PDPA measurements. Coaxial injector tests were carried out with two different recess length and different oxidizer/fuel ratios. Along with experiments, numerical analyses were carried out for the coaxial injector and its comprising parts. The deductions from this work were presented in this chapter.

Comparing the sprays of the inner atomizer and the coaxial injector for the same flow rate of inner atomizer it was seen that coaxial spray properties are quite close to the inner atomizer's spray. This indicates that inner atomizer has more effect on the spray of the coaxial injector than the outer atomizer. Spray cone angles of the outer and inner atomizer changed when they operated together. The spray cone angle of the outer atomizer decreased whereas the spray cone angle of the inner atomizer increased and they merged at some point and forms one spray.

Spray cone angle measurements were performed for the inner and outer atomizer standalone operations and the coaxial injector configuration at different flow rates. It was seen that as the injection pressure increases spray cone angle also increases up to a certain point. After that point spray cone angle is almost insensitive to increase in injection pressure. Test and analyses results revealed that the spray of the investigated injector is uniform and axisymmetric. As anticipated, higher injection pressure leads to higher spray droplet velocities and lower droplet diameters. PDPA measurements

revealed that bigger droplets which are near the edge of the spray move with the liquid film, whereas the smaller droplets move with the air. Bigger droplets present at the edges of the spray, whereas the smaller droplets are usually at the center of the hollow cone.

Discharge coefficient, spray cone angles, and pressure drops of the inner and outer atomizers were obtained for a broad range of flow rates. Main spray characteristic of the open-end type outer atomizer and the closed-end type inner atomizer were also obtained.

Also, coaxial injector spray characteristics at various o/f ratio were presented and compared. It was seen the inner atomizer has more effect on the spray of the coaxial injector than the outer atomizer. Comparing two different recess length reveals the effects of recess length on the spray properties.

Two-dimensional axisymmetric and three-dimensional analyses were carried out, and the results were compared with each other and the experiment results. It was seen that both numerical models are highly successful in calculating the spray cone angle of the spray and the velocity field of the droplets. The results of the three-dimensional analyses and two-dimensional axisymmetric analyses are quite close to the experimental results. As expected, three-dimensional analyses results are closer to the experimental results than the axisymmetric analyses results. Regarding the computing time for the axisymmetric solution is considerably lower than three-dimensional analyses, conducting two-dimensional axisymmetric analysis can be very useful for preliminary investigation of an injector. This study shows that using numerical model enables to obtain highly close results to the real case for pressure swirl atomizers and coaxial pressure swirl injectors. Therefore, numerical models can be utilized to obtain the spray cone angle and velocity profile of the sprays of pressure swirl atomizers and coaxial pressure swirl injectors. By this means, efforts on conducting time-consuming tests can be reduced, and the points that cannot be tested with available test setup could be investigated.

REFERENCES

[1] G. P. Sutton, "Merits of Liquid Propellant Rocket Engines and Their Applications," in *History of Liquid Propellant Rocket Engines*, 2006, pp. 5–22.

[2] "Liquid Rocket Engine," *National Aeronautics and Space Administration*, 2011. [Online]. Available: https://www.grc.nasa.gov/www/k-12/rocket/lrockth.html.

[3] P. P. Popov, W. A. Sirignano, and A. Sideris, "Propellant Injector Influence on Liquid-Propellant Rocket Engine Instability," *J. Propuls. Power*, vol. 31, no. 1, pp. 320–331, 2015.

[4] D. R. Kirk, "Rocket Combustion Chambers." Mechanical and Aerospace Engineering Department Florida Institute of Technology.

[5] A. H. Lefebvre, "Fifty Years of Gas Turbine Fuel Injection.pdf." pp. 251–276, 2000.

[6] V. Bazarov, *Design and Dynamics of Jet and Swirl Injectors*. 2004.

[7] V. Y. M. H. J. H. M. Popp, *Liquid Rocket Thrust Chambers: Aspects of Modeling, Analysis, and Design*. American Instute of Aeronautics and Astronautics, 2004.

[8] V. Yang and E. A. William, *Liquid Rocket Engine Combustion Instability*. 1993.

[9] S. Soller, R. Wagner, H.-P. Kau, P. Martin, and C. Mäding, "Combustion Stability Characteristics of Coax-Swirl- Injectors for Oxygen/Kerosene," *AIAA/ASME/SAE/ASEE Jt. Propuls. Conf. Exhib.*, vol. 43, no. July, p. 22, 2007.

[10] V. R. Rubinsky, "Combustion Instability in the RD-0110 Engine," 1994.

[11] R. Woodward, K. Miller, V. Bazarov, G. Guerin, S. Pal, and R. Santoro,

"Injector research for Shuttle OMS upgrade using LOX/ethanol propellants," *34th AIAA/ASME/SAE/ASEE Jt. Propuls. Conf. Exhib.*, no. 1, pp. 1–5, 1998.

[12] J. H. Seol, P. G. Han, W. H. Jeong, and Y. Yoon, "Recess Effects on Spray Characteristics of Swirl Coaxial Injectors," *KSAS International Journal*, vol. 4, no. 1. pp. 26–33, 2003.

[13] F. Ommi, K. Nekofar, A. Kargar, and E. Movahed, "Experimental Investigation of Characteristics of a Double-Base Swirl Injec- tor in a Liquid Rocket Propellant Engine," *Sci. York*, vol. 10, no. 14, pp. 92–111, 2009.

[14] D. Version, *Aalborg Universitet Computational and Experimental Study of Sprays from the Breakup of Water Sheets Madsen, Jesper*. 2007.

[15] Y. Sun, Z. Guan, and K. Hooman, "A review on the performance evaluation of natural draft dry cooling towers and possible improvements via inlet air spray cooling," *Renew. Sustain. Energy Rev.*, vol. 79, no. May, pp. 618–637, 2017.

[16] C. Bostwick, "Liquid Oxygen / Liquid Methane Co-axial Swirl Injector Development," *Architecture*, no. July, pp. 1–15, 2010.

[17] Y. Hardalupas and J. H. Whitelaw, "The characteristics of sprays produced by coaxial airblast atomisers," *J. Propuls. Power*, vol. 10, no. 4, pp. 453–460, 1994.

[18] P. B. Kowalczuk and J. Drzymala, "Physical Meaning of the Sauter Mean Diameter of Spherical Particulate Matter Physical Meaning of the Sauter Mean Diameter of Spherical Particulate Matter," vol. 6351, no. October, 2015.

[19] A. Mandal, M. A. Jog, J. Xue, and A. A. Ibrahim, "Flow of power-law fluids in simplex atomizers," *Int. J. Heat Fluid Flow*, vol. 29, no. 5, pp. 1494–1503, 2008.

[20] B. B. Vasques, M. T. de Mendonca, W. M. D. Dourado, and Asme, "Numerical and Experimental Study of Swirl Atomizers for Liquid Propellant Rocket

Engines," *Proc. Asme Int. Mech. Eng. Congr. Expo. 2011, Vol 1*, pp. 951–957, 2012.

[21] D. P. Schmidt *et al.*, "Pressure-Swirl Atomization in the Near Field," *SAE Tech. Pap.*, vol. 1999, no. 1999-1–496, 1999.

[22] Q.-F. Fu, L.-J. Yang, W. Zhang, and K.-D. Cui, "Spray Characteristics of an Open-End Swirl Injector," *At. Sprays*, vol. 22, no. 5, pp. 431–445, 2012.

[23] Q. Fu, "Numerical simulation of the internal flow of swirl atomizer under ambient pressure," *Proc. Inst. Mech. Eng. Part C J. Mech. Eng. Sci.*, vol. 230, no. 15, pp. 2650–2659, 2016.

[24] Z. Kang, Q. Li, J. Zhang, and P. Cheng, "Effects of gas liquid ratio on the atomization characteristics of gas-liquid swirl coaxial injectors," *Acta Astronaut.*, vol. 146, pp. 24–32, 2018.

[25] C. J. Eberhart, D. M. Lineberry, and M. D. Moser, "Experimental Characterization of a Swirl Coaxial Injector Element," no. August, pp. 1–14, 2009.

[26] M. R. Soltani, K. Ghorbanian, M. Ashjaee, and M. R. Morad, "Spray characteristics of a liquid-liquid coaxial swirl atomizer at different mass flow rates," *Aerosp. Sci. Technol.*, vol. 9, no. 7, pp. 592–604, 2005.

[27] L.-J. Yang, M.-H. Ge, M.-Z. Zhang, Q.-F. Fu, and G.-B. Cai, "Spray Characteristics of Recessed Gas-Liquid Coaxial Swirl Injector," *J. Propuls. Power*, vol. 24, no. 6, pp. 1332–1339, 2008.

[28] TSI, "Analyzer (PDPA)/ Laser Doppler Velocimeter (LDV) Operations Manual," 2006.

[29] TSI, "MDG-100 Monosize Droplet Generator Operation and Service Manual," 2010.

[30] C. R. Radke and T. R. Meyer, "Effect of Injector Geometry on Atomization of

a Liquid-Liquid Double Swirl Coaxial Injector using Non-Invasive Laser , Optical and X-ray Techniques," pp. 1–6, 2014.

[31] Y. Cengel, "Heat Transfer: A Pratical Approach," in *McGraw - Hill*, 2002.

[32] Y. Li-jun, "OPEN-END LIQUID SWIRL INJECTOR," vol. 2.

[33] X. Chen and V. Yang, "Effect of Ambient Pressure on Liquid Swirl Injector Flow Dynamics," *Phys. Fluids A Fluid Dyn.*, vol. 26, no. 10, p. 102104, 2014.

[34] Q. Fu, "Numerical simulation of the internal flow of swirl atomizer under ambient pressure," vol. 0, no. 0, pp. 1–10, 2015.

[35] B. Sümer, "Experimental and Numerical Investigation of Pressure Swirl Atomizer," Middle East Technical University, 2014.

[36] S. K. Dash, M. R. Halder, M. Peric, and S. K. Som, "Formation of Air Core in Nozzles With Tangential Entry," *J. Fluids Eng.*, vol. 123, no. 4, p. 829, 2001.

[37] J. J. Chinn, A. J. Yule, and H. J. K. De Keukelaere, "Swirl Atomizer Internal Flow: A Computational and Experimental Study," *12th Annual Conference of ILASS-Europe*. pp. 41–46, 1996.

[38] A. Nouri-Borujerdi and A. Kebriaee, "Numerical Simulation of Laminar and Turbulent Two-Phase Flow in Pressure-Swirl Atomizers," *AIAA J.*, vol. 50, no. 10, pp. 2091–2101, 2012.

[39] A. W. Adamson and A. P. Gast, *Physical Chemistry of Surfaces*, 6th ed. Wiley, 1997.